# Vibrotactile Processing in Rodents: Perceptual and Neuronal Stability of Whisker Stimulation

---

**Dissertation**

zur

**Erlangung der naturwissenschaftlichen Doktorwürde**

**(Dr. sc. nat.)**

vorgelegt der

**Mathematisch-naturwissenschaftlichen Fakultät**

der

**Universität Zürich**

von

**Johannes Maria Mayrhofer**

aus

Österreich

Promotionskomitee

**Prof. Dr. Fritjof Helmchen** (Vorsitz)

**Prof. Dr. Bruno Weber** (Leitung der Dissertation)

**Prof. Dr. Richard Hahnloser**

Zürich, 2013

*Für Sandra*

# Table of contents

# List of figures

# 1 Summary

The analysis of cortical map plasticity in the context of experience and learning has been a research focus for many years (Diamond et al., 1994; Feldman, 2005; Margolis et al., 2012; Siucinska and Kossut, 1996). However, the stability of neuronal stimulus representation under constant conditions remains understudied and unclear (Lütcke et al., 2013). The need for a balance between these two processes is clear. On the one hand, plasticity enables us to learn new experiences and adapt to new stimulus conditions. On the other hand, stability of stimulus representation enables us to recognize familiar stimuli even under noisy conditions. The aim of my thesis was to study how an internal representation of a stimulus evolves over a long time period. Does perceptual stability or variability have a behavioral correlate? Ultimately, can we predict decisions based on neuronal signatures of these stimuli in the brain? I focused on a representation of vibrotactile stimuli in neuronal ensembles of the primary whisker cortex with the help of chronic two-photon calcium imaging. Since motor activity can influence the neuronal activity in the primary sensory areas (Petreanu et al., 2012) and vice versa (Chen et al., 2013a), stimuli were presented passively to the rodents. Additionally, the study was restricted to the supragranular layers of the barrel cortex primarily because of methodological reasons. The key question addressed was: What is the perceptual and neuronal stability of whisker stimulation? The work can be divided into three subprojects, each related to a specific question:

First, how constant is the somatosensory perception of animals performing a decision making task? Mice and rats were trained to tolerate head-fixation and perform a perceptual decision making task. Pairs of vibrotactile frequencies were simultaneously presented to single whiskers on the rodent's left and right snout. The animals were able to discriminate a target frequency (90 Hz) from a distractor frequency (0 Hz – 80 Hz). Hundreds of trials were performed per day and similar psychophysics was reached in mice and rats. After the learning phase the level of performance remained relatively constant. This suggested a stable sensory percept induced by the different stimulation frequencies. Likewise, similar psychophysical curves and thresholds across animals indicated the presence of similar sensory processing across animals.

Second, how permanent is the stimulus representation in individual cortical neurons and on a cortical network level? Using chronic two-photon calcium imaging in mice, we found a stable and stereotypic frequency representation in supragranular layers of somatosensory cortex, which was preserved over months. Stimulus evoked activity was tuned towards higher frequencies in almost all neurons (89%). In addition, the network activity patterns elicited by the different stimulus frequencies were relatively stable over time, with similar inter- and intra-day variability. Different stimulation frequencies did not activate orthogonal population activity patterns in cortex (Srivastava et al., 2008; Wick et al., 2009), indicative of similar representations of the different frequencies on the network level. Ipsilateral stimulation only evoked small responses and the influence on the contralaterally evoked response was weak. A small population of highly responsive neurons (~2%) was sufficient to decode the different frequencies.

Third, can we detect modulation of these stimulus representations depending on behavior response of the animal? Our two-alternative forced choice task allowed the animals to respond in three ways. They either chose one of two reward locations or indicated that they are not engaged in the task by not licking at the two waterspouts. Using these clearly defined behavioral response categories allowed us to compare response properties of layer 1-3 neurons in the respective conditions. Larger responses for the condition where the animal was engaged (correct and error responses) compared to the situation where the animal did not respond to the stimulus (miss condition) were observed. This suggested that the animal was in an alert state (attending; possibly a desynchronized state) in the engaged condition leading to an enhanced representation of repeated or temporally extended stimuli (less adaptation; (Castro-Alamancos, 2004; Harris and Thiele, 2011)). We also confirmed the results from the anaesthetized recordings in mice in the sense that ipsilateral responses were smaller and less frequent than contralateral responses in layer 2/3 neurons. Neuronal activity in the supargranular layers was sparse, and only few cells displayed high amplitude activation during tactile stimulation.

In conclusion, only a small population of neurons was reliably activated through vibrotactile stimulation. These neurons are most likely the building block for consistent and stable representation of sensory percepts.

# 2 Zusammenfassung

Die Anpassungsfähigkeit des Nervensystems an sich verändernde Umweltbedingungen (Plastizität) ist eine wesentliche Eigenschaft, die die Überlebensfähigkeit von Tieren gewährleistet. Gleichzeitig ist besonders bei Säugern das zentrale Nervensystem auf eine sehr hohe Stabilität und Konstanz ausgelegt, die u.a. Langzeiterinnerungen über viele Jahre hinweg ermöglicht. Diese beiden Eigenschaften, Plastizität und Konstanz befinden sich in einem Gleichgewicht, um sowohl Anpassung als auch Wiedererkennung zu gewährleisten. Das Studium der neuronalen Plastizität des zerebralen Kortex ist ein wichtiger Forschungsbereich der Neurowissenschaften (Diamond et al., 1994; Feldman, 2005; Margolis et al., 2012; Siucinska and Kossut, 1996). Die Stabilität der Reizverarbeitung hingegen wurde nur sehr wenig erforscht unter anderem wegen dem Fehlen von geeigneten Ableitungsverfahren vor allem auf der Ebene von identifizierten Neuronenpopulationen (Durelli et al., 1978; Thompson and Best, 1990).

Das Ziel meiner Arbeit war die Langzeit-Untersuchung der kortikalen Reizverarbeitung auf neuronaler Ebene. Die zentrale Frage dabei war, ob die neuronale Antwort auf einen gewissen Reiz über die Zeit stabil ist und ob sich dies im Verhalten widerspiegelt. Zudem wollte ich untersuchen, ob die beobachteten Aktivitätsmuster einer Neuronenpopulation eine Vorhersage über die Entscheidung des Tieres zulässt, wenn dieses Tier Reize unterscheiden muss. Der Fokus meiner Untersuchungen lag dabei auf der vibrotaktilen Reizverarbeitung in Gruppen von Neuronen im primären somatosensorischen Kortex von Nagern (Maus und Ratte, Schnurrhaar-Kortex). Dabei benutzte ich genetisch kodierte intrazelluläre Kalziumindikatoren in Kombination mit Zweiphotonen-Mikroskopie. Die neuronale Aktivität wird dabei als transiente Veränderung der interazellulären Kalziumkonzentration gemessen, die direkt mit der Entstehung von Aktionspotentialen korreliert (Helmchen et al., 1997; Lütcke, 2010). Diese Methode ermöglicht es erstmalig, grosse Neuronenpoplulationen (bis zu einigen 100 Zellen) über lange Zeiträume (Monate) zu messen und so die Langzeitdynamik und Interaktion einer Neuronenpopulation zu erfassen, die vermutlich der Plastizität und Stabilität zu Grunde liegt (Margolis et al., 2012).

In meiner Arbeit versuche ich drei Fragen zu beantworten, die unterschiedliche Aspekte der neuronalen und perzeptuellen Konstanz darstellen:

Erstens: Wie konstant ist das somatosensorische Perzept von Mäusen und Ratten?

Mäuse und Ratten wurden trainiert, eine Kopffixierung zu tolerieren und unterschiedliche Frequenzen der Schnurrhaarstimulationen zu unterscheiden. Während des Versuchs wurde ein Schnurrhaar der rechten und eines der linken Gesichtsseite gleichzeitig mit einem vibrotaktilen Reiz stimuliert, welche sich jedoch in der Frequenz unterschieden. Dabei zeigte sich, dass die Tiere die Zielfrequenz (90 Hz) von der Vergleichsfrequenz (0 Hz bis 80 Hz) unterscheiden können. Es wurden bei Ratten und Mäusen mehrere hundert Wiederholungen pro Sitzung durchgeführt und es konnten zwischen beiden Spezies keine qualitativen Unterschiede in der Unterscheidungsleistung (Psychophysik) nachgewiesen werden. Nach einer gewissen Lernphase war die Trefferquote individueller Tiere sehr konstant. Die Tiere konnten also die präsentierten Frequenzen mit gleichbleibender Trefferquote unterscheiden, was ein sehr starker Hinweis auf ein stabiles und konstantes Perzept der verschieden Frequenzen ist. Auch einzelne Tiere untereinander verglichen, wiesen sehr ähnliche psychometrische Kurven auf. Daraus kann man auf eine ähnliche Reizverarbeitung über einzelne Tiere hinweg schliessen.

Zweitens: Wie stabil ist das neuronale Aktivitätsmuster auf der Ebene einzelner Neuronen sowie auf der Ebene von Neuronen-Gruppen, das durch vibrotaktile Reize hervorgerufen wurde?

Mit Hilfe der Zweiphotonen-Mikroskopie konnte eine stabile und stereotype Reizverarbeitung von Frequenzen in den supragranulären Schichten des somatosensorischen Kortex nachgewiesen werden. Die Aktivität der neuronalen Netzwerke, welche durch verschiede Stimulusfrequenzen induziert wurde, blieb stabil über die Zeit und zeigte eine ähnliche Variabilität innerhalb einer Messsitzung und über Tage hinweg. Grundsätzlich war immer eine bestimmte Neuronenpopulation aktiv, die sich nur sehr wenig änderte und auf sehr unterschiedliche Stimulusfrequenzen antwortete (z.B. 10 und 90 Hz). Dieses Ergebnis deutet auf eine ähnliche Reizverarbeitung und -repräsentation der unterschiedlichen Stimulusfrequenzen innerhalb des neuronalen Netzwerkes hin. Die Stimulus-induzierte Antwortamplitude war generell höher bei höheren Stimulationsfrequenzen (89%). Davon abgesehen war eine sehr kleine Gruppe von stark antworteten Neuronen (2%) ausreichend, um die verschieden Frequenzen zu dekodieren.

Drittens: Kann die Entscheidung eines Tieres basierend auf der neuronalen Verarbeitung der Reize im primären somatosensorischen Kortex vorhergesagt werden?

In dem hier angewandten Verhaltensparadigma hat das Tier drei Antwortmöglichkeiten: Entweder es diskriminiert die Stimulusfrequenzen richtig, was zu einer Belohnung führt; es entscheidet falsch oder es verhält sich passiv und entscheidet sich nicht. Somit können neuronale Aktivitätsmuster von drei klar abgrenzbaren Verhaltenskategorien untersucht werden, was bei anderen Paradigmen schwieriger ist (z.B. im „Go-NoGo“ Paradigma). Die grössten Antwortamplituden traten im ersten und zweiten Fall auf, wenn das Tier geantwortet hat und somit angenommen werden kann, dass das Tier die Stimuli beachtet und auf seinen Frequenzgehalt in analysiert hat. Im dritten Fall, wenn das Tier den Stimulus ignoriert hat, waren die neuronalen Antwortamplituden kleiner. Es kann also vermutet werden, dass die Lösung der Aufgabe ein erhöhtes Aufmerksamkeitsniveau erfordert, was wiederum zu einem asynchronen Netzwerkzustand führt (Harris and Thiele, 2011). Eine Konsequenz eines solchen Zustandes kann die geringere Antwortadaptation sein (Castro-Alamancos, 2004; Harris and Thiele, 2011), die zu einer verbesserten Repräsentation und Unterscheidbarkeit von länger dauernden Stimuli führt. Generell war auch hier das gemessene neuronale Aktivitätsniveau in den supragranulären Schichten eher niedrig.

Zusammenfassend kann gesagt werden, dass nur eine geringe Anzahl von Neuronen auf vibrotaktile Reize reagieren, diese jedoch mit einer sehr hohen Antwortstärke. Diese kleine Neuronenpopulation könnte für die beständige Reizweiterverarbeitung ausreichen und die Grundlage für ein stabiles Perzept sein, da sie durch eine sehr geringe Variabilität gekennzeichnet ist, sowohl in den Antworten als auch in ihrer Zusammensetzung.

# 3 Introduction

## 3.1 Brain: from neurons to circuits

Since Santiago Ramón y Cajal and Camillo Golgi first portrayed the brain in great detail over 100 years ago, neuroscience has become an expansive field and we now understand more about brain organization at the anatomical, cellular/molecular and functional levels. At the anatomical level, the mammalian brain can be subdivided into the medulla, pons, cerebellum, midbrain, diencephalon (thalamus and hypothalamus), and cerebral hemispheres (or telencephalon: cerebral cortex, basal ganglia, the amygdala, and the hippocampal formation and corpus callosum) (Figure 1A; (Kandel, 2000)). These structures present a prominent difference between vertebrates, since the relative subdivision size varies between species. For example, the human brain has the highest cortical neuron density and cortical thickness, though not the largest cerebral cortex (neocortex; Figure 1B; (Roth and Dicke, 2005)). At the cellular and molecular level, thousands of different brain areas can be identified using fine distinctions of neural structure, chemistry, and connectivity. In total the human brain consists of about $10^{11}$ neurons of which $2x10^{10}$ are part of the neocortex and each neuron connects to about 7000 other neurons. Eighty percent are excitatory glutamatergic projecting neurons and 20% are inhibitory interneurons that use gamma-aminobutyric acid (GABA) as their main neurotransmitter. At the functional level, each brain region can be subdivided by its role in different types of information processing (e.g. sight, touch, sound, smell, taste). The functionally connected sub-regions are linked through identifiable pathways. These projections are highly organized, thus creating topographic maps and a hierarchical organization in functional systems. Another apparent functional property is that one side of the brain controls the other side of the body.

Many studies (including this thesis) have focused on the neocortex, as it is central to cognitive function (Munk, 1880). The cerebral cortex is anatomically divided into four lobes: occipital, parietal, temporal and frontal lobe. It can also be classified in functionally distinct regions e.g. visual, auditory, somatosensory, motor cortex. If the human cerebral cortex was flatten it would cover an area of about 0.22 $m^2$ (DeFelipe, 2010) (e.g. 22cm x 100 cm), and for this reason it has folded over evolution to fit in the

human skull. This cortical sheet has a thickness of 1.4 to 4.5 mm (DeFelipe, 2010) and consists of 6 layers (Figure 1C; (Brodmann, 1909)):

**Layer 1, molecular layer**: a-cellular layer with few neurons (mainly interneurons). Apical dendrites of these cells are located below and axons travel through or form connections in this layer.

**Layer 2, external granular cell layer:** small pyramidal neurons and numerous stellate neurons (interhemispheric corticocortical afferents and efferents).

**Layer 3, external pyramidal cell layer:** small and medium-size pyramidal neurons, interneurons (interhemispheric corticocortical afferents and efferents).

**Layer 4, internal granular cell layer:** different types of stellate (spiny and smooth) and pyramidal neurons (thalamocortical afferents and intra-hemispheric corticocortical afferents).

**Layer 5, internal pyramidal cell layer:** large pyramidal neurons and some interneurons (subcortical efferents and interhemispheric corticocortical afferents and efferents).

**Layer 6, polymorphic or multiform layer:** few large pyramidal neurons and many small spindle-like pyramidal and multiform neurons (thalamocortical efferents).

The layers organize inputs (afferents) and outputs (efferents) within the cortical area and have a characteristic connectivity pattern between layers and neuronal types. These cortical microcircuits show a column like organization (from layer 1 to 6). Since receptive fields and stimulus tuning of neurons is changed by moving along layers and less when moving perpendicular through layers (Hubel and Wiesel, 1968; Mountcastle, 1957), so called minicolumns or basic functional units of the cortex were proposed (Douglas and Martin, 2004; Mountcastle, 1997). These canonical microcircuits are based on the common excitatory pathways and inhibition within a column over the cortical sheet. They try to capture some common rules such as recurrent excitation and inhibition, the amplification of weak inputs from the thalamus or other cortical areas, and the balance of excitation and inhibition (Figure 1D; (da Costa and Martin, 2010)). Since there are only relatively weak inputs from the thalamus, it is important to note that the neocortex is modulated, but not driven by sensory input (Bruno, 2006).

The nervous system has a large range of spatial scales from atoms and molecules (1 nm), neurons (10 um), neuronal circuits (100 um – 1 mm), brain regions (1 cm), up to the brain (10 cm) and complete nervous system (1 m). Also, time scales vary from action

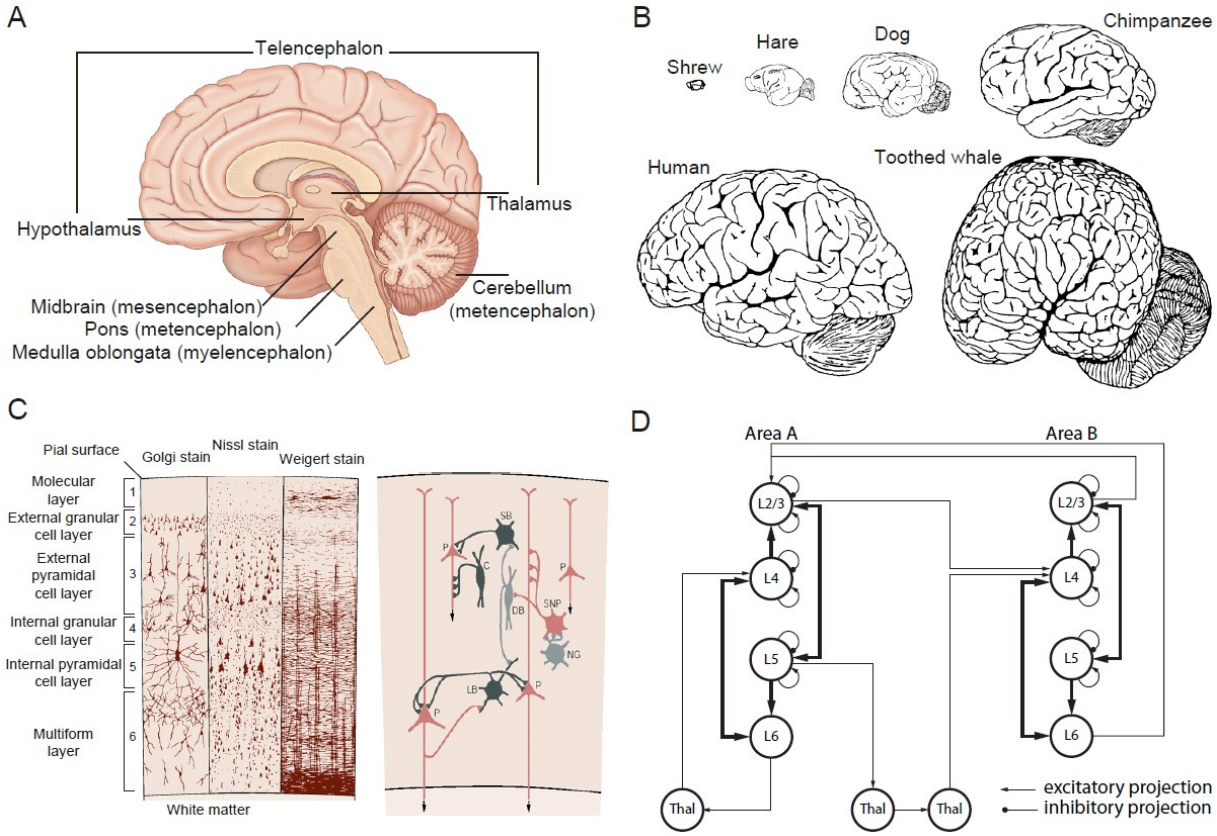


**Figure 1. Brain, neocortex and microcircuits.**

**(A)** Anatomical subdivision of the mammalian brain (sagittal section through the human brain, taken from (Drake, 2010)): medulla, pons, cerebellum, midbrain, diencephalon (thalamus and hypothalamus), and cerebral hemispheres (or telencephalon: cerebral cortex, basal ganglia, the amygdala, and the hippocampal formation and corpus callosum). **(B)** A series of mammalian brains (taken from (Roth and Dicke, 2005)). Humans do not have the largest brain in absolute terms and are exceeded in size by many cetaceans (whales, dolphins, porpoises and the elephants). They also do not have the most convoluted cortex. **(C)** The neurons of the cerebral cortex are organized in characteristic layers (adapted from (Kandel, 2000)). Left subpanel: The Golgi stain shows neuronal cell bodies and dendritic trees. The Nissl method displays cell bodies and proximal dendrites. A Weigert stain for myelinated fibers reveals the pattern of axonal distribution. Right subpanel: Different types of GABA-ergic neurons (dark gray) and putative GABA-ergic neurons (light gray) have different connections with pyramidal (P) and spiny non-pyramidal (SNP) cells in the neocortex. The GABA-ergic cells include chandelier cells (C), which terminate exclusively on the axons of other neurons, and the large and small basket cells (LB, SB), whose axons terminate mainly on other cell bodies. Double bouquet (DB) and neurogliaform cells (NG) may also be GABA-ergic. **(D)** Representation of the major connections in the canonical microcircuit (adapted from (da Costa and Martin, 2010)). Excitatory connections are represented by arrows and inhibitory ones as lines with round ends. Neurons from different cortical layers or brain structures are represented as circles. “Lx” labels the cortical layer where the cell body is located, “Thal” labels the thalamus and “Sub” labels other subcortical structures.

potentials (1 ms), neuromodulatory effects and short term plasticity (1 - 60 seconds), long term plasticity (1 – 60 minutes) up to structural changes (days to years). As a consequence, a large variety of different optical and electrical recording and stimulation techniques are needed to study brain dynamics.

## 3.2 Perceptual stability and perceptual discrimination

*Stimulus encoding: stable and changing*

The brain is thought to be flexible and associative, where sensory information about the environment is transformed into motor actions (goal-directed behavior). On the one hand, perceptual discrimination is needed to differentiate between previously acquired associations (meanings) and novel experiences. On the other hand, the ability to ignore some differences (noise) between sensory input patterns is required, otherwise all experiences would be unique (Shadlen and Newsome, 1994). Learning occurs at many levels of the brain from primary areas to higher areas and on multiple time scales (Feldman, 2005). Single synapses can act as coincident detectors of pre- and post-synaptic events and change their synaptic weight (Zucker, 1999). Neuromodulatory systems can temporarily change the network characteristic of defined regions up to the entire brain by shifting the balance of excitation and inhibition (Gentet et al., 2010; Lee and Dan, 2012). Primary sensory areas show a strong map plasticity when sensory input is withdrawn (Diamond et al., 1994; Margolis et al., 2012). These altered responses are evidence of enormous flexibility and the ability of the brain to adapt to an ever-changing environment. While this response is important, a certain persistency and stability is equally evident, and perceptual discrimination and perceptual stability must remain balanced (Lütcke et al., 2013). However, it is not entirely clear how this balance is maintained at the cellular level. For example, it remains unknown if visual recognition manifests as conservation of spiking activity or sub-threshold membrane fluctuations and the establishment of stable representations through single cells or small groups of neurons. Computational modeling and experimental data suggest that the balance between flexibility and stability could be established by network functions as pattern separation and pattern completion (Barnes et al., 2008; Hasselmo, 1999; Leutgeb et al., 2007; Niessing and Friedrich, 2010; O'Reilly and McClelland, 1994).

*Stimulus encoding in primary cortex: firing rate versus timing*

Neurons signal information through sequences of action potentials, but the neural code by which information is conveyed through the cortex remains elusive (Harris, 2005; Shadlen and Newsome, 1994). The inter spike interval is highly variable and shows Poisson-like statistics. Repeatedly stimulating a neuron within its receptive field with the same stimulus leads to different single trial spike patterns. When averaged over trials, spiking can show precise stimulus locking (Ahissar et al., 2001; Ewert et al., 2008). In recent decades, two coding schemes were put forward: the rate code (Shadlen and Newsome, 1994) and the temporal code scheme (König et al., 1996) (Figure 2A). In the case of the rate code, the information is encoded as firing rate in a certain time span. In contrast, the temporal code scheme puts more emphasis on the inter spike interval. In the second case, much more sequences exist to encode distinct information. In either way the information has to be "read" from some downstream neuron. In a first order approximation, neurons can be treated as "leaky integrators" (Figure 2A). When sufficient excitatory input (e.g. more excitation than inhibition) within a time window is received by a postsynaptic neuron, a spike is generated. This model can handle both frameworks but the temporal code would require shorter excitatory postsynaptic potentials (EPSP) as compared to the 10 - 30 ms spikes observed experimentally in adult pyramidal cells (Harris, 2005). It is still not clear which code is used or if both are implemented (for a subcortical structure involved in sound localization there is clear evidence that the exact timing of spike sequences is used) and how trial-to-trial variability in the spike pattern is compensated. One way of approaching this dilemma is to record from many neurons at the same time and observe how the neuronal population represents the stimulus.

*Population code, attractor state*

Since stimulus induced activity shows high trial-to-trial variability on the single neuron level it was hypothesized that the stimulus may be encoded by a population of neurons (about 100 neurons (Shadlen and Newsome, 1994)). More recently, evidence suggests that population states could exist (olfactory bulb of zebra fish (Niessing and Friedrich, 2010) and mouse auditory cortex (Bathellier et al., 2012)) supporting Hebb's cell assembly hypothesis (Hebb, 2002). According to a Hebbian rule, a network stores externally presented patterns through modification of recurrent excitatory synapses (learning phase). Whenever external input is given to the network, it evolves from this

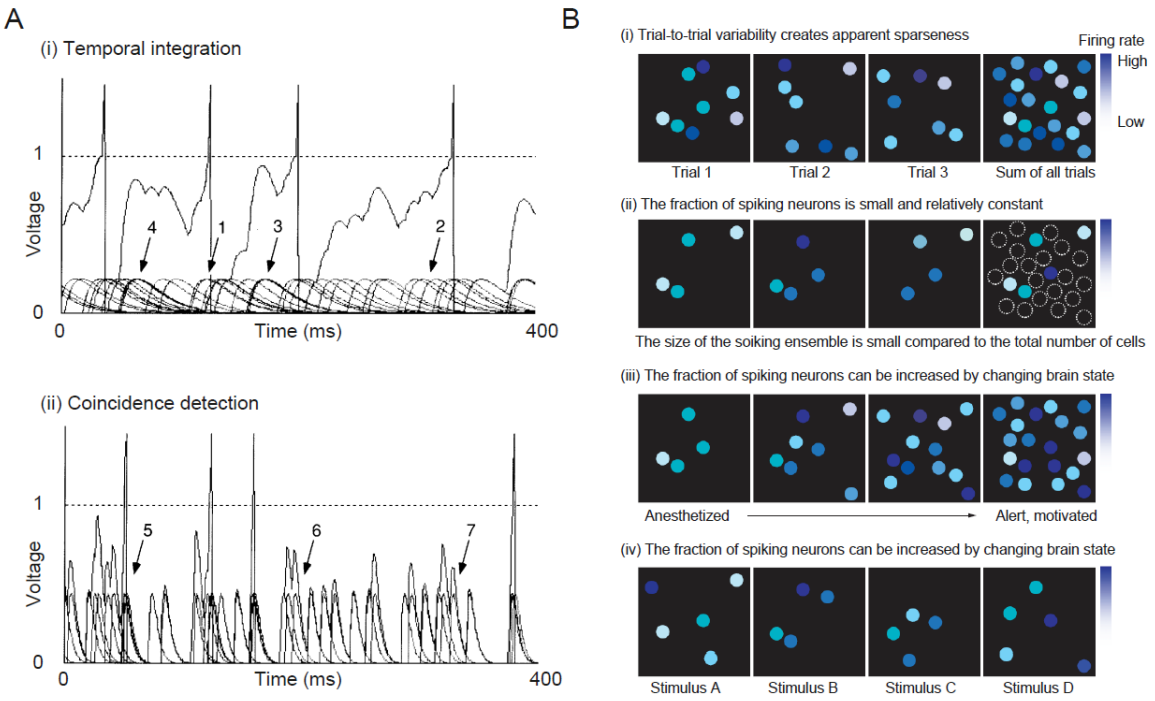


**Figure 2. Coding schemes: single neurons and population.**
**(A)** Postsynaptic potentials (PSPs) are processed differently in the coincidence-detection and the temporal integration schemes (taken from (König et al., 1996)). (i) Temporal integration of a train of excitatory PSPs by a simulated neuron. The excitatory PSPs were simulated by an alpha function with a time constant of 15 ms. When the membrane potential reaches threshold (broken line at value 1; arbitrary voltage scale), an action potential is triggered and the membrane potential undergoes reset. The majority (75%) of all PSPs contribute to a subsequent action potential. The remaining PSPs (25%) do not affect the output of the simulated neuron. In this regime, both nearly coincident PSPs (I) and temporally distributed PSPs (2) can trigger an action potential. However, simultaneously arriving PSPs do not necessarily trigger an action potential immediately (3, 4). (ii) Coincidence detection operating on the same train of excitatory PSPs, with the integration time constant reduced by a factor of five and the size of the PSPs increased by a factor of two, leads to a qualitatively different behavior. Synchronously arriving PSPs trigger an action potential nearly instantaneously (5). Furthermore, most PSPs have no effect on the output (68%), even if they contributed to an action potential in the temporal integration scheme (6, 7). To improve clarity of the simulation shown in panels (i) and (ii), the number of PSPs has been kept small and their size large. **(B)** Models of sparseness (taken from (Barth and Poulet, 2012)). (i) Variability across trials (from cell-intrinsic or network properties) creates the appearance of sparseness that is reduced with longer time-intervals for analysis. (ii) A small but constant subset of cells fires more reliably across many trials than the rest of the population. (iii) The fraction of firing neurons can be changed by brain state, for example, from anesthetized to waking. (iv) Highly stimulus-specific neurons will create the appearance of sparseness. As stimulus space expands, more neurons will fire.

starting point through the learned intrinsic dynamics to a stable end state ("attractor") in which its activity matches one of the originally learned inputs (recall phase). This attractor state can act as a form of memory formation and recall, perceptual switching and decision making (Freedman, 2001; Wang, 2008; Wills et al., 2005). For example, it is theorized that during the learning phase of visual recognition a stereotypic activity pattern is repeatedly elicited. This pattern can be triggered again later in time leading to recognition. Although this is an appealing theoretical model, it has been difficult to prove or disprove it. In the past, neuronal readouts in the intact brain were restricted to single cell recording (or few neurons) or to population measures, such as multiunit activity or local field potentials (LFP). With the rise of multi-electrode arrays with hundreds of contacts, measurements of population activity in cortex became possible, however with limited spatial resolution. With optical imaging methods and the help of calcium indicators it is now possible to monitor the activity of neuronal populations of up to 500 neurons in a region of 300 µm in diameter at a depth of up to 500 µm measured from the pia (see below). This permits studying local population dynamics in vivo.

*Sparse coding*

There is growing evidence from experiments that some modalities (across different organisms) could employ a sparse coding strategy, where information is encoded by a small number of active neurons at any given point in time (Figure 2B; (Barth and Poulet, 2012; Crochet et al., 2011; Hahnloser et al., 2002; Houweling and Brecht, 2007; Hromádka et al., 2008; Huber et al., 2008; Olshausen and Field, 2004)). The idea of sparse coding was put forward by theoretical neuroscience since it has several advantages (Olshausen and Field, 2004): 1) the storage capacity in associative memory is increased (Hebb's ensemble, see above), 2) the structure in natural stimuli are becoming explicit or discrete (Bathellier et al., 2012), 3) complex stimuli are represented so that it is simpler to read out at subsequent levels of processing (Niessing and Friedrich, 2010) and 4) energy is saved (Attwell and Laughlin, 2001; Lennie, 2003).

There is increasing agreement that layer 2/3 pyramidal neurons have significantly lower firing rates than excitatory neurons in layer 4 and layer 5 for both spontaneous and stimulus evoked activity (Barth and Poulet, 2012; Petersen and Crochet, 2013). Furthermore, it has been shown that a small subset of neurons exists that reliably respond with multiple spikes (Kerr et al., 2007; Margolis et al., 2012; O'Connor et al.,

2010a; Yassin et al., 2010). In studies that distinguish between excitatory and inhibitory neurons, many of the neurons with high firing rates were in fact inhibitory interneurons (Crochet et al., 2011; Gentet et al., 2010; O'Connor et al., 2010a). Hence, strong recurrent inhibition could be a mechanism for reducing the overall firing output from pyramidal cells and for increasing sparseness of response probabilities. The output of interneurons can be tuned by subcortico-cortical neuromodulatory projections, which in turn would tune the activity of pyramidal neurons. This temporary modulation of sparseness would allow for map plasticity and stimulus association (Froemke et al., 2007; Letzkus et al., 2011). The sparse coding strategy may be a good candidate for stimulus representation in the cortex.

*Perceptual decision making*

A perceptual decision can be understood as a simple sensory-motor task, where a stimulus triggers a rewarded motor output. From an experimental point of view, the advantage of these simplified decision making tasks is the ability to precisely control sensory input, to quantify motor output, and to record from relevant brain regions. Perceptual discrimination tasks are widely used experimental approaches as their implementation is relatively straight-forward (Wang, 2008). We can repeat the decision making process many times under very controlled conditions and study the regions and functions involved in the process. This allows correlation of neuronal activity in the brain to different behavioral categories. One of the key questions is how the sensory percept is encoded in the nervous system and how this leads to decision making process and response behavior. Most of the decisions we make happen within a very short time (in 100 ms range), without too much effort and are often a tradeoff between speed and accuracy (performance improves with slower response times (Wickelgren, 1977)). How does the brain arrive at the best option in such a short time? How is the goal-directed and reward associated behavior established? Current research attempts to address these issues.

*Why use rodents to study perceptual decision making?*

Experiments with awake-behaving head fixed primates are currently the gold standard for behavioral neurophysiology and decision making studies (Romo and de Lafuente, 2013; Wang, 2008). Head fixation is critical in these experiments, providing excellent behavioral control and repeatability across trials. Several recent studies emphasize the new opportunities for understanding decision making offered by the rodent model, and

utilize the whisker somatosensory cortex (barrel cortex) through vibrotactile stimulation, surface discrimination (roughness) and object (pole) detection. For example, rats were trained to discriminate between different vibrotactile whisker stimulation (Gerdjikov et al., 2010; Stüttgen and Schwarz, 2010). At the cellular level, the firing rate in layer 4 of the barrel cortex was correlated with decision making regarding surface roughness (von Heimendahl et al., 2007). In mice trained on pole detection, the most discriminative neurons were in layer 4 and 5 of the barrel cortex, but also a sparse population of layer 2/3 neurons were highly discriminative (O'Connor et al., 2010a, 2010b). For the same task processes such as learning, the sensorimotor interaction and manipulation of layer 4 via photo-stimulation was studied (Huber et al., 2012; O'Connor et al., 2013; Petreanu et al., 2012). Evidence also suggests behavior-dependent recruitment of long-range projections occurred in mice trained for surface discrimination and object detection (Chen et al., 2013a). Furthermore, the reward prediction error encoded by dopaminergic neurons was studied in rats performing an odor discrimination task (Roesch et al., 2007).

The emergence of novel behavioral tasks for rodents (see review of (Stüttgen et al., 2011) for overview), the development of new tools to record from many identified neurons over long time (Lütcke et al., 2013) and specific manipulation of defined subsets of neurons (Fenno et al., 2011; Yizhar et al., 2011) makes the rodent a powerful model to study perceptual decision making on a mechanistic level. More than 150 years after G.T. Fechner we can start to translate psychophysics to a neuronal basis (Fechner, 1860).

## 3.3 Whisker system in mouse and rat

*An "expert" sensory system*

The rodent whisker system is an "expert" sensory system which is crucial for the animal's survival and navigation in their environment (Diamond and Arabzadeh, 2012; Yang and Zador, 2012). Rodents use the array of moveable whiskers to actively and passively explore their environment. In recent decades, different whisker-related tasks have been developed highlighting the capabilities of this sensory system: texture discrimination, gap crossing, aperture width discrimination, pole detection and discrimination, pulse detection and frequency discrimination task are only a subset of

many (Adibi et al., 2012; Carvell and Simons, 1990; Jenkinson and Glickstein, 2000; Knutsen, 2006; Krupa et al., 2001; Mayrhofer et al., 2013; O'Connor et al., 2010b).

*Whisker pathway – from the vibrissa to the cortex*

On the animal's snout the vibrissae are organized in a two-dimensional grid. Rows are labeled with letters from A (dorsal) to E (ventral), and columns with numbers from 1 (caudal) – 12 (rostral). In addition, there are four macro-vibrissae (alpha, beta, gamma, delta; sometimes also termed straddlers) at the caudal side of the whisker pad between rows (Woolsey and Van der Loos, 1970). Each individual whisker's follicle is innervated by around 200 ganglion cells (Diamond et al., 2008). The cell bodies of the ganglion cells are located in the trigeminal ganglion and form a central and peripheral branch (Figure 3). The peripheral branch of the ganglion cells with their Merkel, lanceolate, Pacinian or free nerve endings transduce the mechanical energy applied on the vibrissa to the neural code of action potentials (Ebara et al., 2002; Gerdjikov et al., 2010; Rice et al., 1986). The signal is sent via the central branch of the ganglion cells to the trigeminal nuclei (TN) in the brain stem. These nuclei are the starting point of multiple afferent pathways that may form sensorimotor loops below the cortical level (Kleinfeld et al., 2006). Four afferent pathways eventually reach at the cortical level (Figure 3; (Diamond et al., 2008; Feldmeyer, 2012; Feldmeyer et al., 2012)).

**Lemniscal pathway 1 and 2:** The cell bodies of second-order neurons in the principal TN are clustered into "barrelettes". The axons of these neurons cross the midline and ascend via the lemniscal pathway to the "barreloids" in the dorsomedial section of the ventral posterior medial nucleus (VPMdm) of the thalamus. Both barrelettes and barreloids are topographic projections of the whisker array: neurons in a given topographic projection region respond primarily to the somatotopically connected whisker. The axons of VPMdm neurons project to the primary somatosensory cortex (S1), where they terminate on discrete clusters of small neurons in layer 4, which form the basis of the ''barrel'' map (Woolsey and Van der Loos, 1970). The layer 4 barrel map is again a somatotopic representation of the whiskers on the snout of the rodent and can be easily visualized (Figure 3C; (Petersen, 2007)). The second lemniscal pathway also originates from principal TN and carries multi-whisker signals via barreloid "heads" (VPMh) to the septa between the barrels (and dysgranular zone) of S1.

**Extralemniscal pathway:** In the caudal part of the interpolar TN, neurons also form whisker-related barrelette clusters. Their target is the ventrolateral domain of the VPM

(VPMvl), where the targeted neurons are clustered into the "tails" of the VPMdm barreloids. In turn, VPMvl neurons carrying multiple-whisker information send their axons to the septa between the barrels of S1 and to the secondary somatosensory cortex (S2).

**Paralemniscal pathway:** Neurons in the rostral part of the interpolar TN have no whisker-related topographic organization and carry multiple-whisker information to the medial sector of the posterior nucleus (POm). The axons of POm neurons project to targets immediately ventral to the barrels, in layer 5a of S1, S2 and to the primary motor cortex (M1).

*The primary somatosensory cortex barrel field– layering and microcircuitry*

The whisker somatosensory cortex is divided into barrel columns reaching from layer 1 down to layer 6 (radial dimension is defined by the thalamocortical innervation of a single whisker from the lemniscal pathway, see above). There are two main excitatory cell classes in the barrel cortex, the spiny stellate neurons and the pyramidal neurons. Spiny stellate neurons are exclusively located at the borders of the barrel columns. Pyramidal neurons are located in layer 2 to 6, where the lowest cell density is in layer 4. Furthermore, five main types of inhibitory interneurons neurons exist: (i) chandelier cells (targeting exclusively axon initial segments), (ii) basket cells (targeting largely somata and proximal dendrites), (iii) Martinotti cells (targeting distal dendrites, often in layer 1), (iv) neurogliaform cells (largely thought to signal using volume transmission) and (v) bipolar/bitufted cells (often targeting dendritic shafts and spines) (Feldmeyer et al., 2012). For the excitatory circuit, most of the input from the periphery is received in layer 4 and less in layer 5 (lemniscal pathways).

Layer 4 projects most of its axons to layer 2/3. Layer 2/3 projects down to layer 5 and has long-rang axonal projections to distal cortical areas (Lefort et al., 2009; Petersen and Crochet, 2013). The septa regions of the barrel column receive multi-whisker input from the paralemniscal pathway and are less prominent in mice compared to rats. Another excitatory microcircuit is the thalamo-cortico-thalamic feedback circuit between layer 4 spiny neurons, layer 5b (projecting to POm) and layer 6 pyramidal cells (projecting to VPM) and the thalamic nuclei. Because of its predominant layer 4 input, its stereotypical neuronal wiring diagram within a discrete column and its thalamo-cortico-thalamic feedback circuit the barrel column is thought to be a prototype of a cortical column or canonical circuit (Figure 1D; (Douglas and Martin, 2004; Yang and Zador, 2012)).

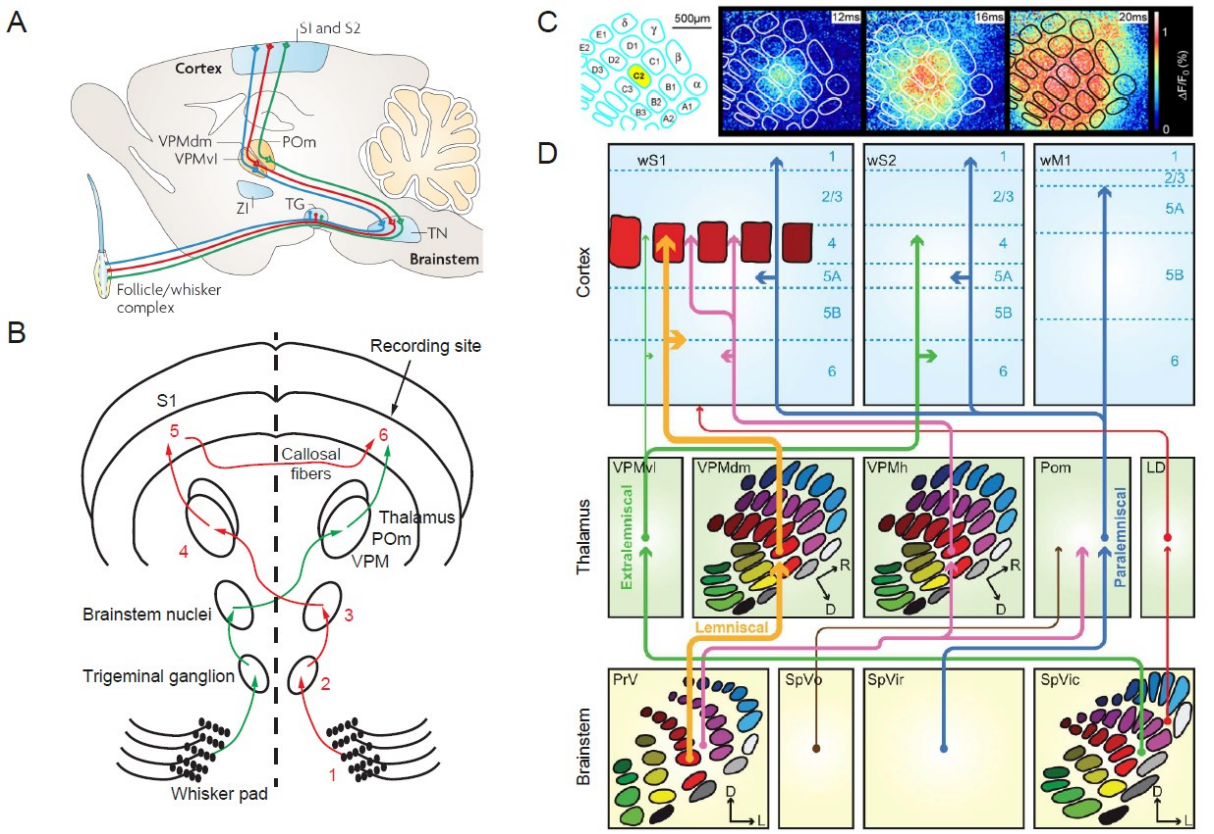


**Figure 3. Whisker pathway – from the vibrissa to cortex.**
**(A)** Neurons of the trigeminal ganglion (TG) send a peripheral branch to the skin and a central branch into the trigeminal nuclei (TN) of the brainstem. Multiple afferent pathways originate from these nuclei, some of them forming sensorimotor loops below the cortical level. Three main afferent pathways eventually reach cortical level (adapted from (Diamond et al., 2008)). **(B)** Ipsilateral and contralateral whisker-related pathways to the SI. Ipsilateral pathway is marked 1–6 (red arrows); contralateral pathway is denoted by green arrows. Callosal connections arising throughout the SI (except layer IV barrels) sprout collaterals in layer 5, as well as in layer 1, of the contralateral SI (6). **(C)** The spatiotemporal dynamics of supragranular membrane potential changes imaged with millisecond temporal resolution and subcolumnar spatial resolution using voltage-sensitive dye imaging. A brief deflection of the C2 whisker induces an early localized depolarization limited to the C2 cortical barrel column (12 ms), over the next milliseconds, the depolarization spreads across the barrel field. Hence, a single whisker deflection can inform a large area of the cortex (adapted from (Petersen, 2007)) **(D)** Schematic representation of the trigemino- thalamo- cortical pathways (Bosman et al., 2011). The arrow heads indicate the termination areas of the axons and line thickness indicates the relative importance of the pathways. The barreloids in VPM and the barrelettes of the trigeminal nuclei are shown. Laterodorsal nucleus of the thalamus (LD), medial posterior nucleus of the thalamus (Pom), primary trigeminal nucleus (PrV), rostral and caudal part of spinal trigeminal nucleus pars interpolaris (SpVic and SpVic), spinal trigeminal nucleus pars oralis (SpVo), dorsomedial part of the VPM (VPMdm), “head” area of VPM (VPMh), ventrolateral part of VPM (VPMvl); wM1, whisker motor cortex; wS1, whisker part of primary sensorimotor cortex; wS2, whisker part of secondary sensorimotor cortex.

Inhibitory connections can also be classified by their axonal projection pattern (Feldmeyer et al., 2012): (i) local (i.e. intracolumnar) inhibitors (including chandelier neurons), (ii) lateral (i.e. transcolumnar) inhibitors, (iii) translaminar layer 2/3-to-layer 4/5 inhibitors, and (iv) translaminar layer 2/3-to-layer 1 inhibitors. These different types of inhibitory neurons have been associated with feedback as well as feed-forward inhibition.

*Interhemispheric interaction*

On a cortical level the bilateral interaction of the rodent's left and the right whisker pad is most likely taking place in the septa region of the barrels (Figure 3B; (Alloway, 2007)). Contralateral stimulation of a single whisker triggers reliable neuronal responses in the corresponding barrel, whereas ipsilateral stimulation leads to a weaker response and modulation in the rat (Shuler et al., 2001). Another locus of bilateral interaction is the somatosensory cortex 2 (S2) (Debowska et al., 2011). S2 forms reciprocal connections with ipsilateral S1 and also receives direct thalamic input from the paralemniscal and the extralemniscal pathway (Bosman et al., 2011). In turn, S2 sends callosal connections to the contralateral S1 and S2 (Carvell and Simons, 1987).

*Supragranular layers in S1 – baseline activity and stimulus induced activity*

Layer 1 only contains GABAergic neuron somata and is about 125 µm thick (mouse). The axons of excitatory neurons from layer 2/3 locally innervate layer 2/3 and layer 5 (see above) and send their axons to distal cortical areas (Alloway, 2007; Fox, 2008; Petersen, 2007), likely forming the basis of multi-whisker integration (Andermann and Moore, 2006; Fox, 2008). In the primate visual cortex, it has been shown that the level of complexity encoded by single neurons increases from layer 4 to layer 2/3 (Hubel and Wiesel, 1968). A similar situation is thought to occur in the barrel cortex (Andermann and Moore, 2006). Layers 2/3 neurons are sparse in response, which can partly be explained by their hyperpolarized resting membrane potential (which is 10 mV more than layer 5 pyramidal neurons) and by their strong and fast inhibition by local GABAergic neurons (Petersen and Crochet, 2013). It is thought that converging input of many layer 4 neurons is needed to activate layer 2/3 neurons (Feldmeyer et al., 2002; Lefort et al., 2009). In the upper layers, burst activity shows a high dependency on the state of the animal (anesthetized or awake) (Petersen and Crochet, 2013). Bursting is thought to be important in network characteristics and for driving behavior (Douglas and Martin, 2004; Kerr et al., 2007; de Kock and Sakmann, 2008). On a network basis it

is known that the cortical regions are not isolated but rather have corticocortical connections and neuromodulary projections (Aronoff et al., 2010; Douglas and Martin, 2004). These complex networks are likely to be involved in processes of attention, expectation and perception (Gilbert and Sigman, 2007; Harris and Thiele, 2011; Hubel et al., 1959; Letzkus et al., 2011).

## 3.4 Two-alternative forced choice task

Perceptual decision making is usually studied under laboratory conditions, where the subject is presented with different sets of stimuli (e.g. horizontal versus vertical bars; high auditory versus low auditory frequencies; different amplitudes of a tone). Presenting the subject with different stimuli leads ultimately to the psychometric curve (for certain stimulus features). From the psychometric curve two important properties, the threshold and the slope can be extracted. The threshold indicates how well a certain stimulus feature (e.g. orientation of a bar; frequency of a tone; amplitude of a tone) can be differentiated or detected by a sensory system. The slope describes how well the system is tuned (sensitive) in differentiating or detecting a feature of stimulus. A general approach for understanding perceptual decision making is to compare the psychometric curve to so called neurometric curves. The neurometric curves describe how well different stimuli can be differentiated by an objective observer when looking at neuronal stimulus responses in a decision related area (see review (Parker and Newsome, 1998; Stüttgen et al., 2011); (Stüttgen et al., 2011) for pitfalls of this approach).

*The 2AFC paradigm*

The forced choice paradigm forces the subject to make a decision between a rewarded (S+; e.g. apple juice as reward) and non-rewarded stimulus (S-; e.g. cider vinegar as punishment) in each trial. The stimuli S+ and S- are presented either simultaneously or with a inter stimulus interval. The subject has to report where the S+ was presented. It can also be implemented as a location task. If a correct response is given, the subject is rewarded, and for incorrect responses the subject does not receive a reward or is punished. The 2AFC task has distinct behavioral response categories of correct (hit), incorrect (error) and no response (miss). For comparison, in a Go-NoGo paradigm the subject is either presented with the S+ (Go stimulus) or the S- (NoGo stimulus) in a single trial. In a Go trial the subject has to report the occurrence of the S+ (hit) whereas in the

NoGo trial the subject has to withhold the response (reject). The behavioral responses can be classified into hits, correct rejections, false alarms or misses.

*2AFC versus Go/No-Go task*

When implementing such tasks for animals a water restriction schedule is typically used for motivation. Deprived animals, however, are prone to impulsive behavior as the measured responses are tightly linked to the pressure of retrieving a reward. In a 2AFC task, impulsive behavior is less of problem because it forces the animal to make a decision and it can obtain a reward in each trial. In a Go-NoGo paradigm it is difficult to ensure that the animal receives a reward in the Go and in the NoGo condition. Another obstacle present in the Go-NoGo paradigm is that animals can contaminate the measured threshold by developing a strong response bias toward Go or NoGo stimuli (Stüttgen et al., 2011). Stereotypical response behavior can also exist in a 2AFC task (e.g. positional bias: left or right side preference, left/right switching behavior). However, this kind of behavior can easily be inhibited by implementing a bias correction algorithm or by introducing a-symmetrical cost function (e.g. shifting the reward location on one side a little further away). In the Go-NoGo task it is difficult to distinguish a lack of motivation or lapses of attention from false rejections or correct rejections. Apart from all these more technical differences the task design influences the cortical and subcortical structures which are involved in the decision making process (Stüttgen et al., 2011). It may well be that in Go-NoGo designs the involvement of the neocortex is less critical than in 2AFC tasks (Diamond and Arabzadeh, 2012).

## 3.5 Chronic two-photon calcium imaging

*Calcium signals in neurons*

Calcium acts as an important intracellular messenger in mammalian neurons. Cells at rest have a calcium concentration of about 50 - 100 nM, but when electrically activated this level rises about 10 – 100 fold (Grienberger and Konnerth, 2012). Calcium influx triggers exocytosis of neurotransmitter-containing synaptic vesicles in presynaptic terminals. Postsynaptic elevation of calcium levels in dendritic spines is critical for the generation of activity-dependent synaptic plasticity (Zucker, 1999). Furthermore, somatic calcium signals are involved in the regulation of gene transcription. The free intracellular calcium is determined by the balance of influx and efflux between cytosol and extracellular space, by calcium exchange from internal storages and calcium

buffering by calcium-binding proteins (parvalbumin, calbindin-D28k and calretinin). The influx from the extracellular space is mediated by voltage-gated calcium channels, ionotropic glutamate receptors, nicotinic acetylcholine receptors, and transient receptor potential type C channels, whereas efflux is established by the plasma membrane calcium ATPase and the sodium-calcium exchanger (Grienberger and Konnerth, 2012). Fast changes in somatic calcium concentrations are mainly produced by voltage depended calcium channels and can therefore be used as a surrogate measure for neuronal spiking activity (Grewe et al., 2010; Kerr et al., 2007).

*Genetically encoded calcium indicators*

In the last decade, the viral vectors have found increasing application in neuroscience. Different types of viruses were used to transfect neuronal tissue and to express functional fluorescent proteins. The expression can be restricted to neurons (e.g. synapsin) or even subtypes of neurons (e.g. using Cre-transgenic mouse line) by using appropriate promoters. Recent genetically encoded calcium indicators (GECIs) have been improved to have similar signal to noise ratios as synthetic dyes. There are two major types of indicators for measuring calcium in neurons: FRET (Förster resonance energy transfer between donor and acceptor fluorophores) and single fluorophore based indicators (Figure 4A). The FRET based indicators change the emission spectra depending on the relative position of the donor and acceptor fluorophores. Binding of a calcium ion to the active zone of the indicator (e.g. calmodulin in the case of Yellow Cameleon 3.60) leads to a conformational change of the protein and thereby to FRET (ratiometric signal: (acceptor signal) / (donor signal)). Single fluorophore based indicators also contain a calcium binding site. Again calcium binding leads to a structural change of the protein complex which in turn leads to a change of the spectral properties e.g. the indicator becomes brighter if the calcium is bound. The FRET based indicators are advantageous because ratiometric signals are less susceptible to motion artifacts induced by brain pulsation or motor activity of awake animals (Lütcke, 2010).

*Chronic window preparation*

GECIs provide the opportunity to functionally follow neuronal activity over extended time. In recent years, many research groups have established chronic window preparation to exploit this advantage (Holtmaat et al., 2009). It is now possible to image the same neuronal population (~100 neurons) over months, which opens the possibility

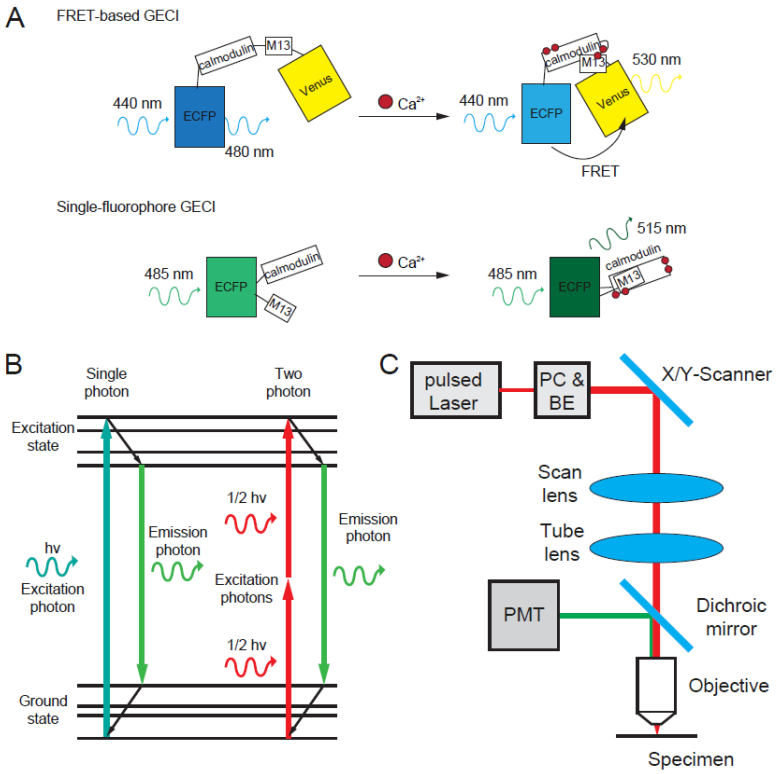


**Figure 4. Two-photon $Ca^{2+}$ imaging.**
**(A)** Genetically encoded calcium indicator (GECI). FRET based GECI: Binding of calcium ions to yellow cameleon 3.60 (YC3.60) leads to an approach of two fluorescent proteins, ECFP (donor) and Venus (acceptor), which enables Förster resonance energy transfer (FRET; the blue fluorescence of 480 nm decreases, whereas the fluorescence of 530 nm increases). Single-fluorophore based GECI: Binding of calcium to GCaMP triggers conformational intramolecular changes which lead to an increase in the emitted fluorescence of 515 nm (adapted from (Grienberger and Konnerth, 2012)). **(B)** Simplified Jablonski diagram of the single photon and two-photon excitation process **(C)** Schematic of a two-photon microscope: pulsed infrared laser, Pockels cell (PC) and beam expander (BE), galvo X/Y-scanners, scan lens, tube lens, dichroic mirror, objective, photo multipler tubes (PMT)

to study cortical stability and plasticity in the same cells(Huber et al., 2012; Margolis et al., 2012). Previously, plasticity studies required animals to be sacrificed at different time points to extract information about map changes. Chronic window implantation permits plasticity map changes to be followed in one animal and changes in individual neurons can be visualized (Lütcke et al., 2013). Apart from the scientific advantage, there is an ethical benefit since animal numbers can be drastically reduced in such studies.

*Two-photon imaging method*

Two-photon imaging was established more than 20 years ago (Denk et al., 1990). In combination with calcium indicators it has become one of the standard tools in monitoring neuronal activity (Helmchen and Denk, 2005; Svoboda and Yasuda, 2006). Fluorophores are excited by femtosecond pulsed infrared lasers, which provide deeper penetration into highly scattering brain tissue due to the non-scattering nature of infrared light (Boulnois, 1986). Pulsed lasers are needed to take advantage of non-linear optical effects through high photon density. Only in the focal spot of the laser beam is the probability high enough that a dye molecule will absorb two long wavelength photons simultaneously (time span of about $10^{-15}$ s (Boitier et al., 2009)). Hence, the combination of the energy from two photons induces an excited state of the dye (Figure 4B). Using this point-like excitation, a picture can be generated by moving the focal point over the tissue through a pair of mirrors (scanning). At any mirror position, the light collected over a certain time span (e.g. 6 µs) using a photo multiplier tube (PMT) can be assigned to certain pixels in the picture. The main advantages compared to confocal microscopy are (1) that all the emitted light can be used (no pinhole like in confocal microscopy is needed for reducing the scatter light) and (2) that the excitation light is spectrally well separated from the emission light. The depth penetration of two-photon imaging is about 500 µm if no additional compensation is used. Figure 4C shows generic parts of a two photon microscope.

# 4 Aims and questions

The characterization of cortical map plasticity in the context of experience and learning has been a research focus for many years. However, the stability of neuronal stimulus representation under constant conditions remains understudied and unclear. The aim of my thesis is to study how the internal representation of a stimulus evolves over long time periods. Is there a behavioral correlate manifested in perceptual stability or variability? Ultimately, can we predict decisions based on the neuronal signature of these stimuli in the brain? I focus on the representation of vibrotactile stimuli in neuronal ensembles of the primary whisker cortex. Since motor activity can influence the neuronal activity in the primary sensory areas (Petreanu et al., 2012) but also vice versa (Chen et al., 2013a), stimuli are presented passively to the rodents. Furthermore, the study is restricted to the supragranular layers of the barrel cortex primarily because of methodological reasons. The overarching question of the thesis is: What is the perceptual and neuronal stability of whisker stimulation? I would like to divide this aim into four more specific questions:

- How constant is the somatosensory perception of animals performing a decision making task? (projects 1 and 2)
- How constant is the stimulus representation in individual cortical neurons? (project 2)
- How stable is the stimulus representation on the cortical network level (preservation)? (project 2)
- Can we detect modulations of these stimulus representations depending on the behavior response of the animal? (project 3)

# 5 Project 1: “Novel two-alternative forced choice paradigm for bilateral vibrotactile whisker frequency discrimination in head-fixed mice and rats”

Johannes M. Mayrhofer*, Vida Skreb*, Wolfger von der Behrens, Simon Musall, Bruno Weber and Florent Haiss

Institute of Pharmacology and Toxicology, University of Zürich, Zürich, Switzerland

* These authors contributed equally to this work.

Published: Mayrhofer JM, Skreb V, von der Behrens W, Musall S, Weber B, Haiss F.
J Neurophysiol. 2013 Jan; 109(1):273-84. doi: 10.1152/jn.00488.2012. Epub 2012 Oct 10.

*Author Contributions*

J.M., V.S. and F.H. conception and design of research; J.M., V.S., W.B. and S.M. performed experiments; J.M. and W.B. wrote analysis scripts; J.M. and S.M. analyzed data; J.M. and F.H. interpreted results of experiments; J.M and S.M. prepared figures; J.M. and F.H. drafted manuscript; J.M., B.W. and F.H. edited and revised manuscript; J.M., V.S., W.B., S.M., B.W. and F.H. approved final version of manuscript.

## 5.1 Abstract

Rats and mice receive a constant bilateral stream of tactile information using their large mystacial vibrissae when navigating in their environment. Using a two-alternative forced choice paradigm (2-AFC), head-fixed rats and mice learned to discriminate vibrotactile frequencies applied simultaneously to individual whiskers on the left and the right side of the snout. Mice and rats discriminated 90 Hz pulsatile stimuli from pulsatile stimuli with lower repetition frequencies (10 – 80 Hz) but with identical kinematic properties in each pulse. Psychometric curves displayed an average perceptual threshold of 50.6 Hz and 53.0 Hz frequency difference corresponding to Weber fractions of 0.56 and 0.58 in mice and rats, respectively. Both species performed more than 400 trials a day (>200 trials per session; two sessions per day), with a peak performance of more than 90% correct responses. In general, rats and mice trained in the identical task showed comparable psychometric curves. Behavioral readouts, such as reaction times, learning rates, trial omissions and impulsivity, were also very similar in both species. Furthermore, whisking of the animals before stimulus presentation reduced the task performance. This behavioral paradigm combined with whisker position tracking, allows precise stimulus control in the 2-AFC task for head-fixed rodents. It is compatible with state-of-the-art neurophysiological recording techniques, such as electrophysiology and two-photon imaging, and therefore represents a valuable framework for neurophysiological investigations of perceptual decision-making.

Keywords: head fixation, psychophysics, operant conditioning, whisker, rat, mouse, inter-hemispheric, somatosensory cortex

## 5.2 Introduction

Rats and mice are nocturnal animals that use their array of movable whiskers to explore and navigate the environment. These tactile sensors enable rodents to acquire sensory information of the surrounding world. Several studies, mostly performed in rats, have reported that rodents are able to discriminate different textures (Carvell and Simons, 1990; Morita et al., 2011), the size of apertures (Krupa et al., 2001), gap size (Jenkinson and Glickstein, 2000) and the position of objects (Mehta et al., 2007). More recent work has shown that psychophysical measurements can be acquired during active palpation (Carvell and Simons, 1995; Knutsen, 2006; Morita et al., 2011; Prigg et al., 2002) or during the passive deflections of individual stationary whiskers (Gerdjikov et al., 2010; Stüttgen and Schwarz, 2008, 2010). Most of these studies employed paradigms in which the animals are able to move freely in the experimental arena. However, head-fixed paradigms are becoming increasingly popular as they allow precise stimulus presentation and monitoring of whisker motion (Hentschke et al., 2006). Furthermore, fixing the animal’s head is a requirement for several neuroscientific methods.

To investigate the neuronal code underlying perception and cognitive functions, it is necessary to combine behavioral measurements with recordings from the individual neuronal elements involved in these processes. Simultaneous acquisition of psychophysical and neural data is indeed one of the gold standards in cognitive neuroscience (Parker and Newsome, 1998; Stüttgen, 2010). The current knowledge in this field has been obtained mainly from the head-fixed non-human primate preparation (Wurtz, 1968). Although recent developments in head-fixed rodent Go-NoGo paradigms allow single neurons to be recorded concomitantly with psychophysics, these complex head-fixed paradigms are still rare for rats and in particular for mice. On the other hand, the mouse is the major mammalian genetic model that allows targeting of specific cell types with genetically encoded proteins. These proteins can be used to manipulate and visualize neural activity in subsets of neurons. Combining such specific manipulations and measurements with behavioral paradigms will allow to pinpoint the contribution of individual cell types to perception and decision-making processes (O’Connor et al., 2009). We therefore developed a two-alternative forced choice (2-AFC) task for mice and rats allowing us to report psychophysical metrics for both species. We have chosen a 2-AFC paradigm as it has clear advantages over Go-NoGo paradigms since it allows a

cleaner classification of behavior into correct rejections and omitted trials on a single trial basis. Go-NoGo paradigms are more susceptible to biases due to fluctuations of motivation compared to 2-AFC tasks (for review, see (Stüttgen et al., 2011)).

We found that mice and rats learned to discriminate frequencies that were simultaneously applied to single whiskers on the left and the right side of the muzzle in the head-fixed situation. Furthermore, mice and rats showed similar psychometric curves. Other behavioral readouts, such as reaction times, learning rates, trial omissions and impulsivity, were also very similar in both species. Reaction times did not depend on the level of difficulty but were in general higher for error trials. Prior whisking of the animal before stimulus onset decreased the task performance significantly. To our knowledge, this is the first description of a 2-AFC task in head-fixed mice and rats. This paradigm allows precise behavioral control and readouts, which can be combined with techniques that take advantage of genetic tools available in the mouse and which are starting to become available in rats

## 5.3 Methods

*Animals*

All experimental and surgical procedures were approved by the local veterinary authorities, conforming to the guidelines of the Swiss Animal Protection Law, Veterinary Office, Canton Zürich (Act of Animal Protection 16 December 2005 and Animal Protection Ordinance 23 April 2008). In total, six female adult Sprague Dawley rats (r1, r2, r3, r4, r5, r6; 250–350 g), one male and two female adult C57BL6J mice (m1, m2, m3; 20–26 g) were trained in a 2-AFC task. The animals had to discriminate between two simultaneously presented vibrotactile stimuli in a head-fixed situation. The age of the animals on the day of headpost implantation was 10–15 weeks. The rats were housed in groups of two with food *ad libitum*, whereas the mice were housed individually with food *ad libitum*. The animals were subjected to water deprivation for five days a week during the behavioral training. Body weight was monitored prior to each of the two daily training sessions during which water acted exclusively as reward. When body weight dropped below 90% of the initial weight, additional water was given after the training session. The animals were housed under an inverted 12-hour light/dark regime such that they were trained during their dark cycle when they are active.

*Surgical procedure*

The animals were anesthetized with isoflurane (1–3%; Abbott, North Chicago, USA). The depth of the anesthesia was monitored by both hind paw withdrawal and corneal reflexes. The animal’s temperature was monitored with a rectal temperature probe and maintained at 37°C by a feedback controlled heating pad (Harvard Apparatus, Holliston, MA, USA). The head was fixed in a stereotaxic apparatus and a local anesthetic (Bucain; 5mg/ml; Actavis, Steinhausen, Switzerland) was given subcutaneously preceding the scalp incision. Eyes were protected with ointment (vitamin A eye cream; Bausch & Lomb, Zug, Switzerland). For rats nine titanium cortical screws (Modus 1.5, 3 mm length; Medartis, Basel, Switzerland) were inserted into the cleared skull, acting as anchors for the headcap. The exact positions of these screws have previously been described (Schwarz et al., 2010). Cortical screws were not used in mice. A bonding agent (Gluma Comfort Bond; Heraeus Kulzer, Hanau, Germany) was applied to the cleaned skull and was polymerized using a hand-held blue light source (600 mW/cm$^2$; Demetron LC, Bioggio, Switzerland). The headcap was formed by layers of transparent light-curing

dental cement (Tetric EvoFlow; Ivoclar Vivadent AG, Schaan, Principality of Liechtenstein) applied on top of the bonding layer. A screw (M5x15) turned head-down was cemented into the head-cap at the midline (2 mm caudal to lambda) and subsequently acted as the post for rat head-fixation. In mice a custom-made aluminium headpost was placed at the same position and connected with dental cement to the underlying bonding layer. After rinsing the wound with saline, an antibiotic ointment was applied (Cicatrex; Janssen-Cilag AG, Baar, Switzerland). The open skin was sutured and attached to the implant with acrylic glue (Histoacryl, Braun, Tuttlingen, Germany). After surgery the animals were kept warm and provided with analgesics (Novaminsulfon; 50%; Sintetica, Mendrisio, Switzerland). In the first week of recovery an antibiotic was added to the drinking water (Baytril (enrofloxacin); 200 mg/l drinking water; Bayer, Leverkusen, Germany).

*Behavioral apparatus*

In the 2-AFC task used in this study, head-fixed animals had to discriminate between pairs of simultaneously presented vibrotactile single whisker stimuli (Figure 5A). A custom-made headfixation box was built for this purpose (Figure 5B). The animal was fixed to a head-rotation mechanics (Figure 5A), which allowed movement in a defined way (maximum ±30° from its initial central head position) when a mechanical brake was released (see inset Figure 5B). The head rotation mechanics consist of a brake (Figure 5B, blue part), which is moved by a DC motor with a motion controller (rat box: 3564K024B CS, Faulhaber, Schönaich, Germany; mouse box: DC motor 1628T024B and the motion controller MCBL-3006-S, Faulhaber, Schönaich, Germany) with the help of a knee lever (Figure 5B, green part). The head post holder (Figure 5B, red part) is pivoted by a ball bearing. For the prompting procedure the head post holder was directly connected with the motor through an additional lever (lever not shown; Note: Knee lever was detached in this case). This allowed direct setting of the head rotation angle. The tactile stimulus consisted of single whisker deflections generated by a piezo bending actuator (T223-H4CL-303X; Piezo Systems, Woburn, USA). A single whisker was plugged into a glass capillary, which was mounted on the piezo actuator (Figure 5A). The control voltage driving the piezo actuator was generated by a custom-written LabVIEW program (National Instruments, Austin, USA) using a multifunctional data acquisition card (PCI-6259; National Instruments) and was amplified by a piezo controller (MDT693A; Thorlabs, Newton, USA). The stimulator system was attached to an articulated arm

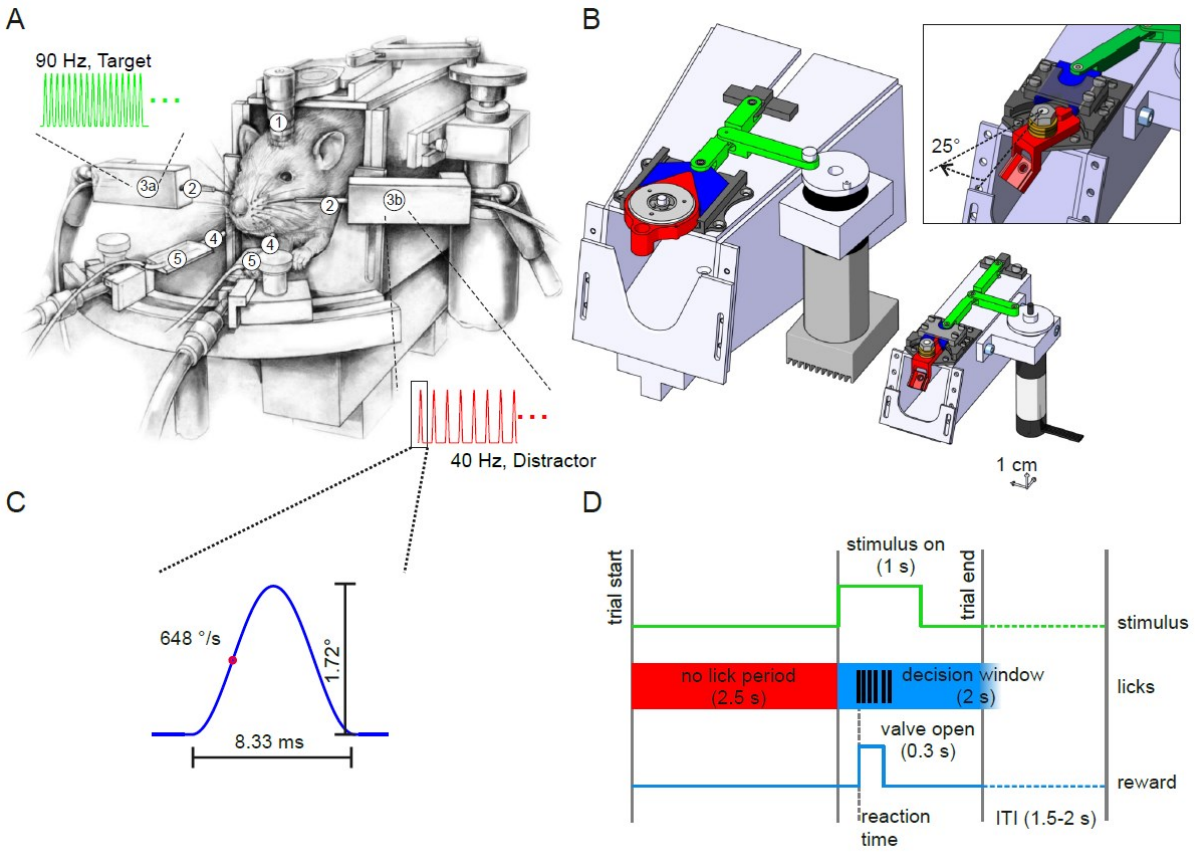


**Figure 5. Set-up, paradigm, head rotation mechanics and stimulus.**
**(A**) schematic representation of a rat in the behavioral apparatus that is connected to the rotation mechanics via an implanted head post (1). A single whisker is inserted into a glass tube (2) that is glued to a piezo actuator (3 a, b) used to deliver simultaneously the vibration stimuli e.g. 90 Hz (3a) as target and 40 Hz (3b) as distractor. The water reward is delivered with two waterspouts (4), which are mounted on a semi-circular rail in front of the animal and equipped with piezo lick sensors (5). (**B**) CAD renderings of the rat (left) and the mouse (right) behavioral apparatus. The inset shows the mouse apparatus with an opened head rotation brake. The head rotation mechanics consist of a brake (blue part), which is moved by a DC motor with the help of knee lever (green part). The head post holder (red part) is pivoted by a ball bearing. For the prompting procedure the head post holder was directly connected with the motor through an additional lever (lever not shown; Note: Knee lever was detached in this case). This allowed direct setting of the rotation angle. (**C)** schematic representation of a single stimulus pulse and **(D)** the time sequence of an individual trial.

(Baitella, Zürich, Switzerland) to allow precise and rapid positioning of the stimulator. Movement of the stimulator was calibrated using a laser displacement sensor (0.1 µm resolution at 2.5 kHz sampling rate, ILD1700-2; Micro-Epsilon, Ortenburg, Germany) and strain gauge sensors mounted directly on the piezo element. The vibrotactile stimulus consisted of a series of deflections to a single whisker on the animal’s left and right whisker pads. The C1 whisker was stimulated in all animals except for m2 where the gamma whisker was stimulated. The peak velocity of a prototype pulse (taken from a single period 120 Hz cosine wave) was kept constant and the repetition rate of pulses was varied randomly from 10 to 80 Hz in steps of 10 Hz for the distractor stimulus (non-rewarded side) and kept constant at 90 Hz for the target stimulus (rewarded side) (Figure 5C). The stimulus duration was 1 s. The peak velocity was 648°/s for both rats and mice. The stimulator was placed 10 mm away from the whisker pad for the rats and 4 mm away for the mice. In the beginning training sessions were done without whisker trimming. Subsequently, only the stimulated whisker on each side was kept untrimmed. At least once every two weeks the animals were lightly anesthetized (isoflurane) to re-trim the whiskers that were not stimulated to a length of 15 mm for the rats and 5 mm for the mice. Additionally, in four animals (r1, r2, r3 and r4) the left C2 whisker was elongated with a light polyimide tube (diameter: 250 µm; length: 2–2.5 cm; weight: ~0.7 mg) such that it covered the hair 3–5 mm from its origin to its free end. The C2 whisker position was quantitatively recorded using a laser curtain and a linear CCD array (RX 03, Metralight, San Mateo, USA) with a resolution of 3.5 µm in space and 2.5 kHz sampling rate (Hentschke et al., 2006). The behavioral apparatus was placed in a light- and soundproof box.

Auditory masking noise (80 dB white noise) was presented with a loudspeaker located 10 cm above the animal´s head to prevent auditory cues. CMOS cameras with infrared illumination were used to monitor the animal´s whiskers to ensure that they stayed in the glass capillary of the stimulator for the entire session. Two drinking spouts (Figure 5A) were placed on the left and the right sides of the animal´s heads in a way that they could only be reached while the head rotation brake was released. After 5–10 weeks of initial training the angle of the two spouts was gradually reduced such that the animals could reach them from a fixed center position. Licking was detected with piezo sensors (Figure 5A) mounted on the waterspouts (LDT0-028K; Measurement Specialties, Hampton, USA). Two solenoid valves (Bürkert, Ingelfingen, Germany) were used to

control the water delivery to the drinking spouts. All the components of the behavioral apparatus were controlled and monitored with millisecond temporal precision by a custom-written LabVIEW programs (National Instruments) running on personal computers using multifunctional data acquisition cards (PCI-6259; National Instruments).

*Behavioral paradigm*

Handling of the animals started after two weeks of recovery from the headcap implantation (Figure 6). The animals were water-deprived 24 hours before the head fixation training started. Animals were slowly familiarized with the experimenter in 2-3 daily sessions lasting roughly 10 min for 1 - 2 weeks. In the following 2 - 3 weeks the animals were trained to tolerate head fixation. Water was given manually from a syringe in the head fixation training. As soon as the animal tolerated the head fixed situation for up 10 min without any signs of stress, the animal was placed into the behavior setup. A drinking spout was placed in front of the animal’s snout. In the first 1-3 sessions water was given every 5-6 s. Later, the animal had to first lick once and then a couple of water drops were delivered through the drinking spout (referred to as the “reward on lick” mode). In the next step the procedural training started (Schwarz et al., 2010). The rodents were subjected to a prompting procedure (6–15 sessions) in order to establish an association of the vibrotactile stimulus location with the reward location. The 90 Hz target stimulus was presented without a distractor stimulus and the animal’s head was gently turned by the motorized system to the stimulus side where water was delivered via the spout. After about two sessions the ‘reward on lick’ mode was turned on as soon as the animal started licking without waiting to sense water coming from the correct spout. Next, actual behavior measurements started and the animal’s performance was recorded. The animal had to turn its head to reach the reward location. First, rats and mice had to detect the side of the 90 Hz target stimulus. When they reached a stable performance (rats: ~18 sessions, mice: ~11 sessions), gradually more difficult distractor stimuli (10 to 80 Hz pulse trains in steps of 10 Hz) were introduced and they had to discriminate the higher frequency (90 Hz pulse train target stimulus) from the lower one. The distractor and the rewarded target stimuli were presented simultaneously on both sides (Figure 5D). To preserve the animal’s motivation, more difficult distractor stimuli (40 to 80 Hz) were always intermingled with less difficult ones (10 to 30 Hz). In the initial training phase, the head rotation brake was released 0–0.2 s after stimulus

onset. After an additional waiting time of 0–0.2 s, the animal was given a 2 s long window of opportunity (Figure 5D) to respond with a lick at one of the two waterspouts. The animal was able to turn its head to the left and the right side, reaching the drinking spout with its tongue to report the perceived target stimulus side. Correct choices led to water delivery (rats: 20–50 µl/trial, mice: 5–20 µl/trial). During the aforementioned window of opportunity, a lick emitted to the incorrect waterspout (distractor side; not rewarded) or no lick response for 2 s after stimulus onset led to a closure of the head-rotation mechanics, bringing the rodent back to the center position. Initiation of the next trial was preceded by a randomly varied inter-trial interval (ITI, 1.5±0.3 s; Figure 5D). Lick events in a 2.5 s long pre-stimulus time window (no lick period; Figure 5D) were punished with a temporal delay (1–2.5 s) of the stimulus presentation. A temporal jitter of maximal ±30% was added to the no lick period in order to avoid prediction of the stimulus onset. In the learning phase, a bias correction algorithm was used to avoid stereotypical response biases (Knutsen et al., 2006b), thus preventing the animals from developing a preference to one side and acting against stereotypic licking such as left-right alternation. When the animals reached a stable performance and non-impulsive behavior, both the head rotation angle and the angle of the waterspouts were gradually narrowed until the brake remained closed (time span over 1–2 weeks). The rats performed up to 400 trials per session and the mice up to 380 trials per session. Two sessions per day were conducted, one in the morning and one in the evening.

*Data analysis*

The dataset consisted of behavioral recordings from six rats (r1, r2, r3, r4, r5, r6) and three mice (m1, m2, m3). There was no significant difference in performance between the morning and the evening sessions (data not shown). A trial was counted as a correct response when the animal licked at the rewarded spout first. An error was counted when the animal licked at the non-rewarded spout first. A no lick response within the 2 s time window after the start of the decision period was classified as a missed trial. To compute the performance, only trials with a behavioral response were taken into account (correct response and error): correct responses / (correct responses + errors). To analyze whisker position traces, whisker velocity was computed by taking the first derivative of the low-pass filtered (Butterworth $4^{th}$ order, cut-off frequency 200 Hz) whisker movement recording. For each trial, the root mean square (RMS) velocity was computed in the pre-stimulus period from -200ms to stimulus onset. If pre-stimulus

RMS velocity exceeded a threshold of 0.02 m/s the trial was classified as movement trial, otherwise it was classified as a non-movement trial (as in Hentschke et al., 2006). To test whether behavioral performance was different in movement versus non-movement trials, a fourfold Chi-square test was done. All data analysis was performed with Matlab (Mathworks, Natick, USA).

*Psychophysics*

A psychometric curve was obtained by computing the performance for each stimulus pair and plotting it against the difference between distractor and rewarded frequency. The confidence intervals were computed on the basis of a binomial distribution with a confidence level of 95%. Psychometric functions were fitted using the software package psignifit (version 2.5.6, see http://bootstrap-software.org/psignifit/), that implements the maximum-likelihood method described by Wichmann and Hill (Wichmann and Hill, 2001). A logistic function

$$\psi(x;\alpha,\beta,\gamma,\lambda) = \gamma + (1-\gamma-\lambda)F(x;\alpha,\beta),$$

where $F(x;\alpha,\beta) = 1 / (1 + \exp[(\alpha - x) / \beta])$

was fitted (fit parameters: $\alpha$, $\beta$, $\gamma$, $\lambda$; $\gamma$ fixed to 0.5 and $\lambda$ constrained between [0 0.2]) to the data points and used to obtain the discrimination threshold and slopes. The discrimination threshold (DTh) was defined as the frequency difference between distractor and target frequency at which the logistic fit reached 50% of its cumulative value. This value was used to compute an additional measure of sensitivity; the Weber fraction: DTh / 90Hz. For the psychometric curves, only the last 270–300 trials (20–40 sessions) in each category were taken into account. For r5, r6, r1, r3, m1 and m2 the frequency range from 10-80 Hz in steps of 10Hz was sampled. A reduced set of distractor frequencies was presented to r2, r4 and m3 (r2 and r4: 0Hz, 10Hz, 40Hz, 60Hz and 80Hz; m3: 0Hz, 10Hz, 20Hz, 40Hz and 60Hz). Peak performance of each animal was determined at 10 Hz distractor frequency and with no distractor present. The learning curves were generated and quantified by analyzing the performance over sessions in trials with no distractor frequency. A cumulative Weibull function was fitted to the mean performance over sessions (first 60 sessions, r1, r2, r3, r4, m1, m2), except for m3 as this mouse reached stable performance within the first session after the prompting procedure. The dynamic phase of learning was defined as the range between the first and ninth decile ordinate values of the fitted cumulative Weibull function. The performance stability was computed by taking the standard deviation of the session

performance during detection (0 Hz distractor frequency) over the last 60 sessions. Reaction times were defined as the time span between stimulus onset and first lick response and were estimated by the median of the first lick latencies of the trials (same dataset as for the psychophysics). Latencies were measured in 10 ms bins and used to construct cumulative plots on a probit scale with a reciprocal time axis (Carpenter and Williams, 1995) – the median first lick latency was the interception of the 50% ordinate value with the cumulative lick count distribution. The relative reaction time difference between error trial ($time_{error}$) and correct trial ($time_{correct}$) was computed per session (i=1, 2, 3, …N) and averaged over sessions:

Reaction time = $2/N \sum_i (time_{error}(i) - time_{correct}(i)) / (time_{error}(i) + time_{correct}(i))$ .

This relative value was computed in order to compensate for session-to-session variability over weeks. In addition, only trials with first lick emission 200 ms after stimulus onset were considered. The influence of session number on the reaction time was tested with the Kruskal-Wallis test. The significance of a behavioral response was tested by the Wilcoxon signed-rank test. The average number of trials where an early lick was detected served as a measure for impulsivity and represented the average number of trials where a lick was emitted within the *no lick* period. This value was taken as zero when there were no early licks before the stimulus onset. A value of 10% denoted that the animal did on average an early lick every tenth trial. For each frequency the percentage of missed trials was computed and statistically tested with the Kruskal-Wallis test. To facilitate the comparison between different animals, the curves were normalized to mean value over all stimulus categories. A control session for each of the animals was performed to rule out the use of auditory cues in the discrimination task. In the first half of the session, the animal had to discriminate between 90 Hz and no distractor frequency or 80 Hz frequency difference of the distractor to the target frequency. In the second half of the session the whiskers on both sides were unplugged from the whisker stimulator and the animal had to continue without mechanical stimulation. It was ensured that the stimulators were as close to the head as in the normal stimulus situation but without touching any whisker. The influence of the bias correction was measured by comparing the % correct of the left and right side with each other: |% correct left side - % correct right side| / (% correct left side + % correct right side) for each session and testing the first 15 sessions against the last 15 sessions with bias correction switched on.

*Statistics*

Statistical errors are standard errors of the mean unless noted otherwise. For binary values a binomial distribution was used to compute the 95% confidence intervals. The Kruskal-Wallis test Wilcoxon signed-rank test and the Chi-square test (Matlab implementations) were used for statistical analyses.

## 5.4 Results

*Training procedure*

All animals entering procedural training reached the frequency discrimination training after 7–10 weeks of training with two daily sessions (Figure 6). Slow adaptation to the head fixation and regular daily trainings (five days per week) were important for a good performance (data not shown, see Schwarz et al., 2010). The criterion to enter discriminative training was that the animals accepted drinking water from a syringe in the head-fixed condition. The animals that required more handling sessions to reach this criterion did not perform worse than the animals which adapted more rapidly (e.g. m1 9.7 weeks: 96% and 222 trials/session compared to m2 7.5 weeks: 93% and 228 trials/session). The mice adapted to the head-fixation and behavioral apparatus in a similar time frame as the rats (rats (r1, r2, r3, r4): 3 weeks, mice (m1, m2, m3): 2.5 weeks).

*Discriminative training*

The discriminative training started with a prompting procedure in which the animal’s head was gently turned to the side where the stimulus was presented (passive training; Figure 6). The motorized head rotation mechanics allowed well-controlled direction of the animal’s head to the rewarded waterspout during presentation of the vibrotactile stimulus. This helps the animal to establish an association between stimulus and reward location but may not be necessary for the animal to learn the task. The rewarded frequency (90 Hz pulse train 1 s duration; Figure 5C) without a distractor was presented (detection paradigm). The rats only needed six sessions (about 500 trials) to establish an association between stimulus and reward location. A lick response to the side of the target stimulus presentation was taken as a criterion for the association. The mice needed 11 sessions for this step (about 1600 trials). Following the passive training, the animals had to indicate their decision by turning the head to the reward location in order to collect the water. In the first sessions, water was given automatically without an initial lick to the spout. During the early phase of training, the animals performed a detection task without any distractor stimulus. After reaching a stable performance in the detection paradigm (rats: ~18 sessions, mice: ~11 sessions of active training), task complexity was increased by introducing distractor frequencies in the paradigm. The animals were trained to discriminate between the rewarded 90 Hz stimulus and the

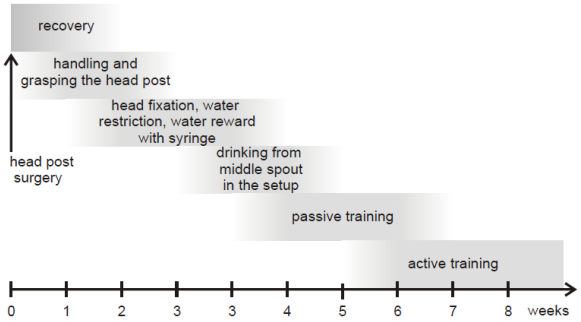


**Figure 6. Training procedure.**
The different training phases are shown, starting with the head post surgery through to the acquisition of the psychometric curves. Grey shadings indicate that the duration of the individual phases was adapted for each animal.

simultaneously presented non-rewarded distractors ranging from 10 to 80 Hz (in 10 Hz steps) frequency difference. The animals performed several hundred trials per session, twice a day. The average median number of trials per session was 202±18 (rats) and 231±6 (mice).

*Psychophysics*

Figure 7 shows the psychometric curves computed from 20–40 sessions for each of the nine animals. For each stimulus category, only the last 270–300 presented trials were taken into account, thus excluding the initial learning phase (Figure 7A-E). For each animal a logistic function was fitted to the stimulus pair performance values to obtain the thresholds and slopes in the transition region of the psychometric curve (see Methods). The best performing rat (r6, not shown separately) had a discriminative threshold of 42.0 Hz frequency difference (95% confidence interval (CI95):38.8–45.1 Hz) and a slope of 2.32±0.50% $Hz^{-1}$. The highest threshold for the rats (r4) was 71.9 Hz frequency difference (CI95: 69.5-76.7 Hz). The population mean of the thresholds of all six rats was 53.0±4.4 Hz frequency difference. Peak performance in one animal (rat r3; Figure 7B) for the least difficult discriminative category (80 Hz distractor to target frequency difference) went up to 93.0% (CI95: 90.3–96.0%) (group mean: 84.1±2.5%) and for the detection up to 97.3% (CI95: 95.3–99.0%) (group mean: 93.0±1.2%). In the three mice the psychometric curves showed similar characteristics. Peak performance for discriminating a distractor to target frequency difference of 80 Hz reached 93.0% (CI95: 90.0–95.7%) for the first mouse (m1; Figure 7C) and 85.0% (CI95: 81.0–89.0%) for the second mouse (m2; Figure 7D). The mean for three mice was 85.0±5.6%. In the detection task, a performance of 96.0% (CI95: 98.0–93.7%) for the first mouse (m1) and 87.7% (CI95: 84.0–91.4%) for the second mouse (m2) was reached (group mean: 89.7±3.2%). The discriminative threshold was 49.4 Hz frequency difference (CI95: 48.1–51.9 Hz) for m1 and 48.5 Hz (CI95: 42.5–56.2 Hz) for m2 (group mean: 50.6±1.7 Hz frequency difference). In summary, rats and mice displayed very similar psychometric measures. The discrimination threshold averaged over three mice was 50.6±1.7 Hz frequency difference compared to a mean of 53.0±4.4 Hz frequency difference for all six rats. These values correspond to Weber fractions of 0.56±0.02 and 0.58±0.04, respectively. The peak performance for the detection task was 93.0±1.2% for the rats and 89.7±3.2% for the mice. The slope of the psychometric curve in the transition regime, which captures the sensitivity fluctuation of the sensory process, was

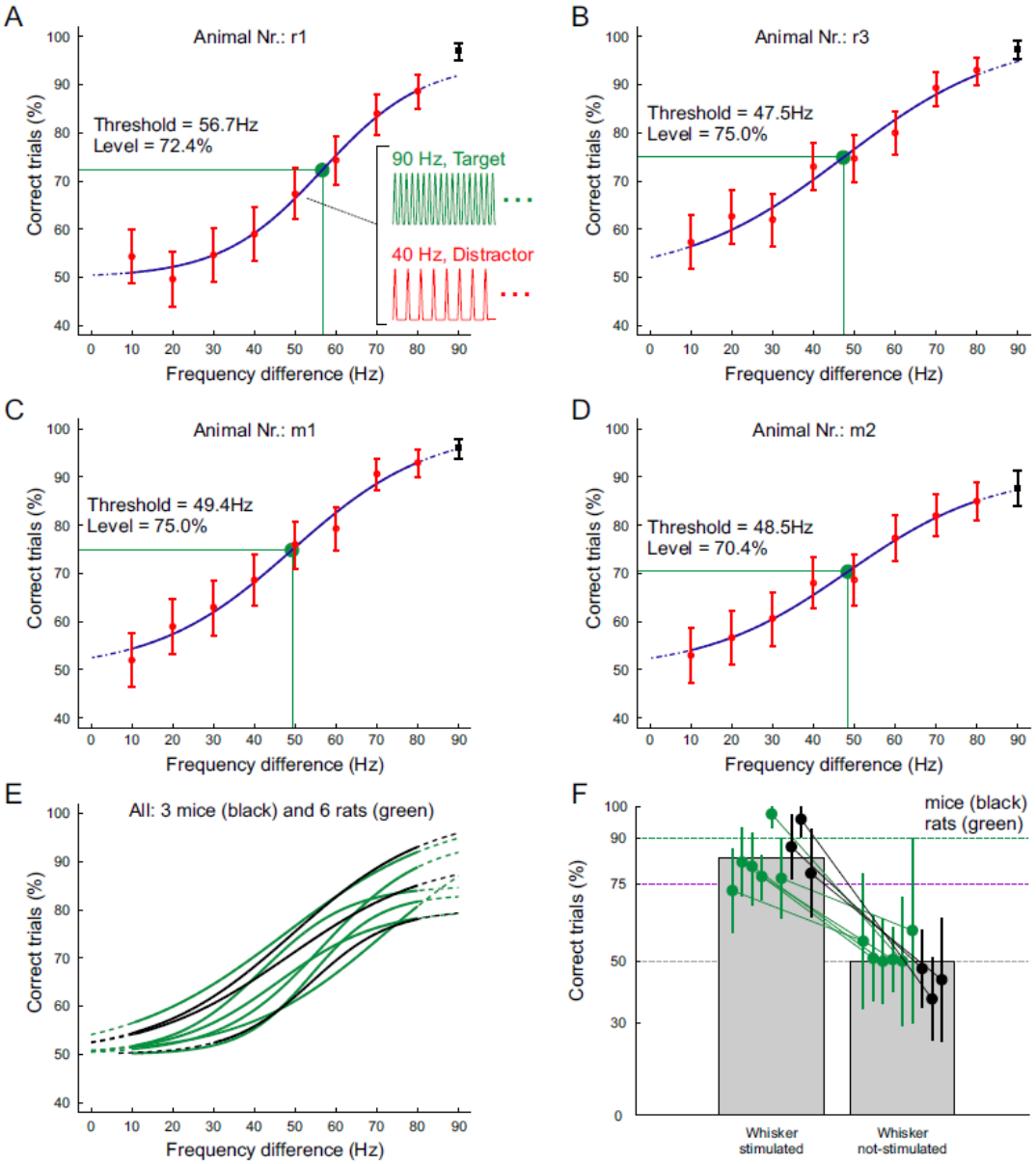


**Figure 7. Psychophysical performance – performance over difference between distractor and target frequency (90 Hz).**

**(A) – (D)** psychometric curves of four of the animals (rats: r1, r3; mice: m1, m2) with logistic fits (blue) and thresholds (green). The detection performance is shown as a black square symbol at 90 Hz difference and was not used for the fitting procedure. Inset in subplot (**A)** shows the stimulus pair close to the threshold regime for the 50 Hz frequency difference data point (90 Hz target and 40 Hz distractor). **(E)** psychometric curve fits from all the animals. The black lines correspond to the mouse data and the green lines to the rat data. **(F)** control session for all nine animals (rats in green, mice in black). The first half of the training session was performed with normal stimulation (whisker attached to the piezo stimulator) where all animals performed above chance ($p<0.05$). In the second half of the training session, the stimulators were retracted from the whiskers (no mechanical contact). The performance of correct trials dropped to the chance level for all the animals when the stimulators were retracted ($p<0.05$). Error bars are plotted as 95% confidence intervals.

2.00±0.25% $Hz^{-1}$ and 1.82±0.36% $Hz^{-1}$ for rats and mice, respectively. Note that an ideal sensory process would have a step function as a psychometric curve and therefore a high slope value at the threshold e.g. 5% $Hz^{-1}$ and above. For each animal at least one control session was recorded to ensure that the animal was exclusively using the vibrotactile whisker stimulus for making the decision (Figure 7F). In the first half of the control session, the animal was in the normal situation with a single whisker stimulated on each side. In the second half of the session, the whiskers were unplugged from the stimulator. The stimulator was placed as close as possible to the animal’s head without touching the whiskers. All of the animals performed above chance level in the first half of the control session (binomial test of performance against chance level, p-value <0.01 for all rats (n=6) and mice (n=3). As soon as the stimulators were detached from the whiskers, the performance dropped to chance level (binomial test of performance against chance level, p-value >0.05 for all animals).

*Learning and behavioural performance stability*

To characterize the learning phase, a cumulative Weibull function was fitted to the mean performance of the detection paradigm over sessions (Figure 8). The dynamic range where most of the performance change was observed was characterized as the range between the first and the ninth decile of a fitted cumulative Weibull function (Figure 8 insets). The first session after the dynamic learning phase was chosen as a criterion for reaching stable performance. Rat r1, r2 r3 and r4 were able to perform the detection task (90 Hz target frequency and no distractor frequency) within 18.2±9.0 sessions (2,256±1373 trials, 1.8 weeks; Figure 8A, B), while the mice needed 16.5±10.8 sessions (1,312±835 trials, 1.7 weeks; Figure 8C, D) to reach the aforementioned criterion. The dynamic learning phase varied across the animals and was 30.9 sessions (mouse m1), 1.2 sessions (mouse m2), 12.2 sessions (rat r1) and 11.0 sessions (rat r3) long. The animals showed session-to-session variability but never dropped to chance level after the dynamic learning phase. To quantify the performance stability over days, the standard deviation was computed over the last 60 sessions of the shown dataset. The mean variability for the rats was 5.6±0.25% (r1, r2, r3, r4) and 3.9±0.26% (m1, m2, m3), demonstrating that rats and mice had comparable levels of performance variability in the 2-AFC discrimination task.

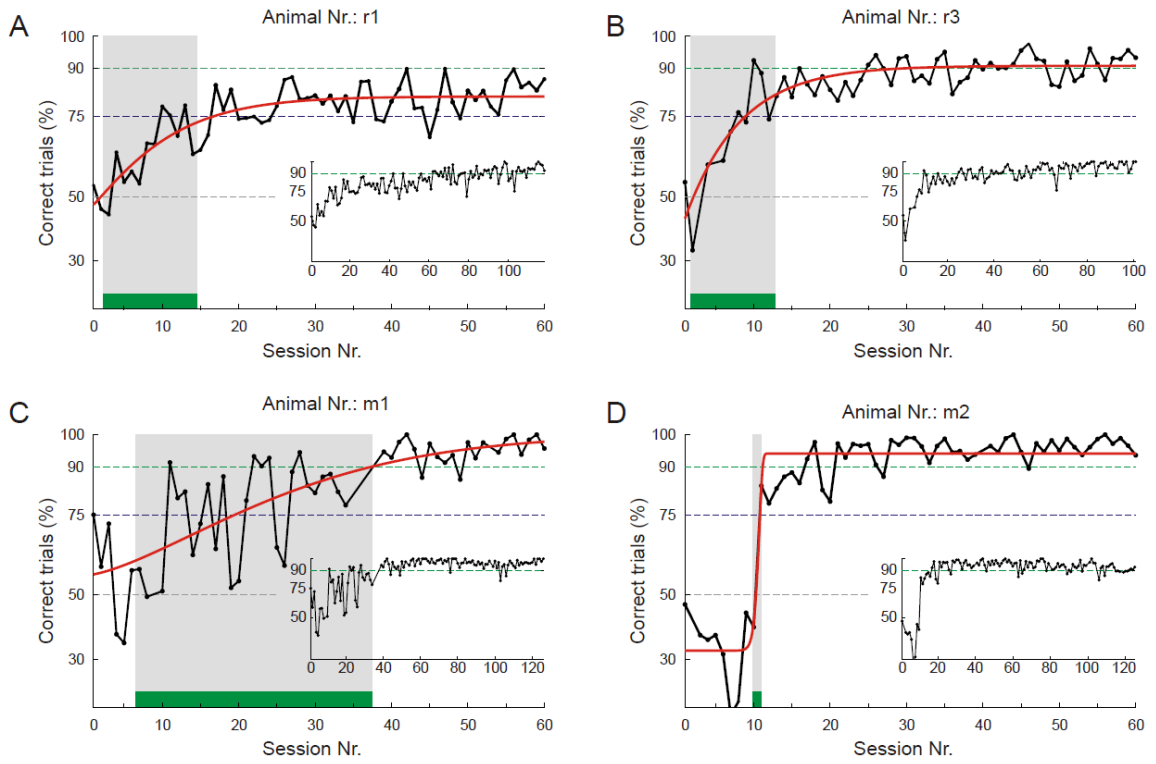


**Figure 8. Learning and stability – performance in detection paradigm over initial learning phase and period of stable behavioral performance.**
**(A) - (D)** performance over time for the detection stimuli for four of the animals (rats: r1, r3; mice: m1, m2). The insets show the initial learning phase which was fitted with a Weibull function. The grey-shaded areas show the dynamic learning phase.

*Reaction times*

In Figure 9 the distribution and analysis of the first lick latencies for behavioral (error and correct) and different stimulus categories (easy and difficult) are shown. The time span between the stimulus onset and the first lick detected was used to compute the reaction time of the animals. These measurements were performed when the animals were not allowed to rotate their heads. The head rotation mechanism brake was kept closed during the whole session and the rodents solely indicated their decision by licking one of the two waterspouts that were in reachable distance. To depict the stochastic distribution of the reaction times (first lick event), the cumulative probability is plotted on a probit scale as a function of reciprocal latency (reciprobit lick histogram in Figure 9A) (Carpenter and Williams, 1995). The median first lick latency is the interception of the 50% ordinate value with the cumulative lick count distribution. The shortest median reaction time was 232±3 ms for the rats and 337±3 ms for the mice. The average of all the rats was 334±49 ms and for the mice 486±120 ms. A straight line in this type of diagram denotes that the underlying distribution has a Gaussian-like shape. All the curves are composed of two almost linear components, one with a shallow inclination and the other with a steep inclination. The reaction time curves shown in Figure 9A have a similar form as saccadic eye latency distributions where subjects had to do a saccade from a central fixation point to a left or right appearing target (Carpenter and Williams, 1995). Note the inset, where similar number of counts in the correct and error condition occurred in the early phase and the form of correct and error distributions in the late phase look similar, suggesting two underlying processes for the observed distribution. Nevertheless, all the animals except one showed a significantly longer reaction time for error trials compared to correct trials (Wilcoxon signed-rank test p-values $<0.05$ for six rats and two mice; Figure 9B). The reaction time difference between the error and correct trials was computed for each session and averaged over sessions (Figure 9B). This step was necessary in order to compensate for session-to-session variability over weeks (Kruskal-Wallis test, $p<0.001$, indicating session dependency). The inset Figure 9B shows example raw reaction times for the error and correct condition and the resulting relative reaction time over sessions. With the exception of one animal, we did not observe a significant difference in reaction times depending on the level of difficulty (i.e. distractor frequency).

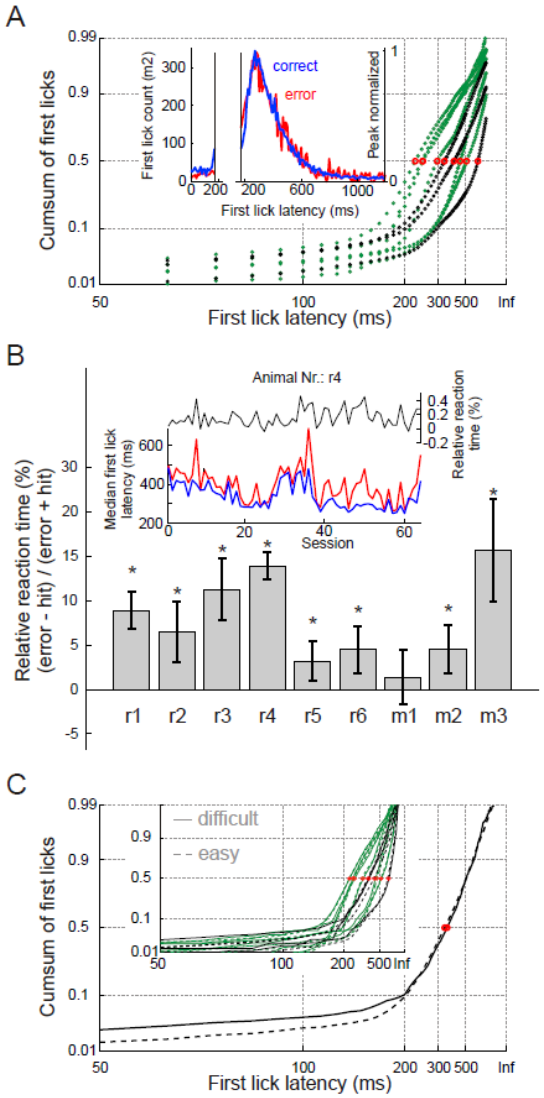


**Figure 9. Reaction times – distribution and analysis of the first lick latencies for behavioral (error and correct) and different stimulus categories (easy and difficult) for all the animals.**

**(A)** cumulative first lick latency count for the different animals (rats: r5, r6, r1, r2, r3, r4 in green; mice: m1, m2, m3 in black) with a probit scale as a function of reciprocal latency. The red dots depict the median first lick latency, corresponding to the interceptions of the 50% ordinate value with the cumulative lick count distributions. The inset shows the first lick histogram for m2 for correct and error trials. The second part (>180ms) was normalized to the peak of the histograms to highlight the similar form of the distributions. (**B**) percentage of the median reaction time of error trials relative to correct trials. Significance level $p<0.05$ is indicated by an asterisk (n=9). The inset shows raw median reaction times for error and correct trials and the resulting relative reaction times over sessions. (**C**) same plot as in (**A)** but split into easy (0–40 Hz distractor) and more difficult stimulus pairs (50–80 Hz distractor) for mouse m2. The inset shows an overview for all the animals (in black mice and in green rats). Solid lines correspond to the difficult category and dashed lines to the easy category.

The comparison of difficult (50 to 80 Hz distractor frequency) to less difficult stimulus pairs (0 to 40 Hz distractor frequency) in the first part of the reciprobit lick histogram (20–100 ms; Figure 9C) for correct trials revealed no significant differences in the distribution in all but one animal (Kolmogorov-Smirnov test, $p<0.01$ for one rat). This finding suggests that the underlying process for the lick responses in the 20–100 ms time window is independent of the level of difficulty and may reflect impulsive behavior. Analyzing only those trials where the animal responded in the 20–100 ms time window after stimulus onset showed that, except for two animals, the performance of correct trials never exceeded chance level (Binomial test, $p<0.05$ for one rat and one mouse).

*Impulsive behaviour and motivation*

To address the questions how much impulsive behavior and motivation vary over different animals or species, the percentage of early licks and misses were plotted in Figure 10. One of the major advantages of a 2-AFC paradigm is that correct rejections can be distinguished from omitted trials (e.g. lack of motivation) on a single trial basis in contrast to a Go-NoGo paradigm. However, it is essential that the animals do not develop a response bias in the 2-AFC task (e.g. positional bias). This can be avoided by training the animals with a bias correction algorithm in the learning phase (see Methods). Comparing the early phase with the late phase of the training with bias correction switched on 4 out 9 animals had significant less response bias to one side (see Method, Kruskal-Wallis test, $p<0.05$). The response bias was quantized as the absolute value of % correct on left side minus % correct on right side divided by the sum of both (Figure S 1; r1 from 0.144±0.044 to 0.052±0.008, r2 from 0.138±0.028 to 0.052±0.014, r3 from 0.226±0.069 to 0.076±0.011, r4 from 0.087±0.017 to 0.083±0.015, r5 from 0.035±0.006 to 0.048±0.011, r6 from 0.048±0.010 to 0.036±0.007, m1 from 0.131±0.023 to 0.065±0.0151, m2 from 0.214±0.052 to 0.050±0.01, m3 from 0.053±0.011 to 0.049±0.009). To characterize the impulsive behavior, the licks before stimulus presentations were measured and classified as early licks in the situation where the animals were not allowed to rotate their heads and solely indicated their decision by licking one of the two waterspouts. This impulsive licking behavior can be completely abolished if the head rotation brake is released and the animal can only reach the waterspouts by rotating their heads. Nevertheless, impulsive behavior could be quite different across species. Thus, licking behavior in the condition in which the head rotation brake was closed was measured. The early lick count represents the average

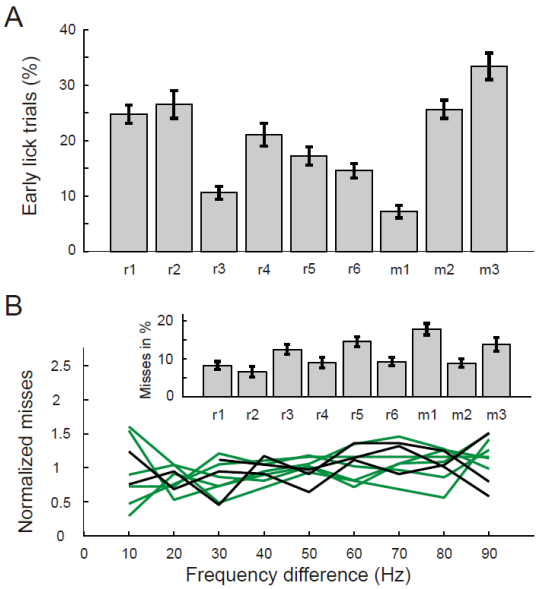


**Figure 10. Impulsivity and missed trials – percentage of early lick trials and missed trials are similar for rats and mice.**

**(A)** average number of early lick trials expressed in percentage for all the animals (n=9). (**B)** percentage of missed trials over frequencies normalized to the mean over all frequencies (rats in green, mice in black). The inset shows the mean value for the corresponding animal (n=9).

number of trials where a lick occurred before the actual stimulus presentation (Figure 10A). Note that in the case of an early lick, the stimulus presentation was shifted backwards so that each stimulus was preceded by a ‘lick free’ period (Figure 5D). The average value number of trials with early licks over the last sessions (same dataset as for the psychophysics) was 19.3±2.5% for rats and 22.1±7.7% for mice. These almost identical early lick counts for rats and mice indicate that both species are highly comparable in terms of impulsivity. It is worth mentioning that the task design allowed chance performance only if the animal licked irrespective of the stimulus side. As shown in the reciprobit plots in Figure 9A, only a small fraction of licks occurred at very short latencies (<100 ms) and these lick time points appear to originate from a different behavioral process reflected in a separate distribution compared to the majority of the responses (linear fits in Figure 9C).

Does the level of difficulty influence the number of trials without a response? The average numbers of omitted trials over all distractor frequencies are shown in Figure 10B. In order to compare between animals, the values were normalized to the mean over all frequencies. Of each session, only the first 30 omitted trials were taken, thus avoiding a dominance of omitted trials usually occurring at the end of a session when the animal is not engaged in the task anymore. The mean values for each animal are shown in the inset of Figure 10B. There was no significant effect of the distractor frequency on the number of omitted trials in eight animals (Kruskal-Wallis test p-values: m1: 0.080, m2: 0.223, m3: 0.429, r5: 0.358, r6: 0.063, r1: 0.287, r2: 0.455, r3: 0.114, r4: 0.016).

*Whisker movements and behavioral performance*

In order to clarify if whisker motion has an impact on the psychometrics measured during the bilateral frequency discrimination paradigm the position of one whisker (C2) was tracked with a linear CCD sensor (Figure 11A) in four rats. The measured RMS velocity of this whisker was used for classifying trials in non-movement and movement trials (Figure 11B). About 9% of all trials (r1: 15.44% of 3095 trials; r2: 6.76% of 6095 trials; r3: 10.68% of 7807 trials; r4: 5.15% of 6022 trials) were classified as movement trials. Comparing these two categories showed that trials with motion had a significantly reduced discrimination performance (Chi-square test, $p<0.01$). The mean performance for all four animals was 70.01% (CI95: 67.88-72.09%) in movement trials and 73.93% (CI95: 73.28-74.59%) in non-movement trials. When only detection trials are considered

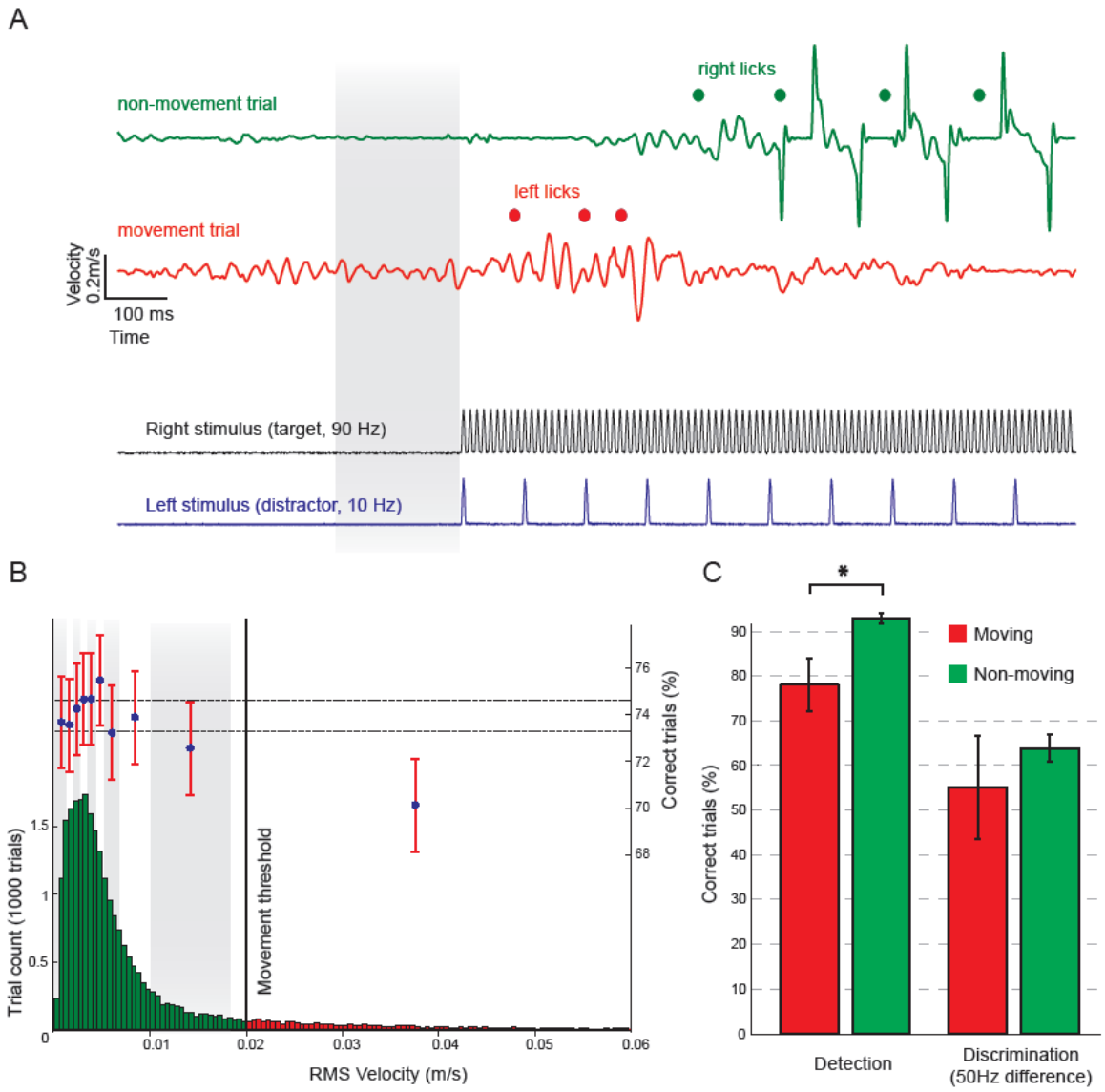


**Figure 11. Whisker motion and behavioral performance – whisking prior stimulus presentation decreased task performance.**

**(A)** example trials demonstrating the presence or absence of whisker movements in the pre-stimulus phase of sensory stimulation (-200 ms, grey shading). Top traces show whisker velocity for a non-movement (green) and a movement (red) trial. Red and green dots indicate left and right licks respectively. The two traces below show sensory stimuli as measured by a strain gauge sensor on each stimulator. Sensory stimulation was the same for both trials with the target being presented on the right side. (**B)** the histogram shows the distribution of pre-stimulus RMS velocity over all trials. The vertical black line indicates the RMS velocity threshold for the classification of movement trials. This was the case for ~9% of all trials (2268 out of 25287 trials). To visualize the distribution of behavioral performance for different RMS velocities, trials were binned into 0.1-quantiles (grey shading) and behavioral performance was computed for each bin. Error bars represent 95% confidence intervals and horizontal lines the 95% confidence interval for all trials. (**C)** behavioral performance in trials without whisker movements is better than trials with whisker movements. Analyzing only detection trial led to a stronger and a significant drop (Chi-square test, $p<0.01$) compared to trials in the discrimination case (at the threshold, 50 Hz difference).

a larger effect was observed (movement: 71.79%, CI95: 61.53-82.05%; non-movement: 89.62%, CI95: 87.15-92.09%), which is in line with the study of Ollerenshaw et al., 2012. At the discrimination threshold (50 Hz frequency difference) a similar trend was present, but no significance was reached (movement: 48.00%, CI95: 28.00-68.00%; non-movement: 59.29%, CI95: 52.65-65.93%; Figure 11C).

## 5.5 Discussion

In the present study, we describe a frequency discrimination paradigm for head-fixed rats and mice. Two vibrotactile frequencies were presented simultaneously to individual whiskers on the left and the right side of the animal’s snout. The task was to report the presentation side of the target frequency by licking from one of two possible waterspouts. To our knowledge, this is the first bilateral frequency discrimination paradigm and the first description of a 2-AFC task concerning head-fixed rats and mice. We found that both, the perceptual thresholds and the psychometric curves were very similar for rats and mice. Hence, our results show that mice can achieve complex discriminative behavior in a paradigm initially designed for rats in our laboratory. The average perceptual threshold was 50.6 Hz (Weber fraction of 0.56) and 53.0 Hz frequency difference (Weber fraction of 0.58) in mice and rats, respectively. The slopes of the psychometric curves of mice and rats were 1.82 and 2.00, respectively. Mice and rats performed on average more than 400 trials a day (>200 trials per session; two sessions per day), with a peak performance of more than 90% for the detection task in both species. The average reaction time for rats was 334 ms and for mice 486 ms and was longer for error trials as compared to correct trials. Reaction time distributions found in this study were similar to previously reported tasks (Carpenter and Williams, 1995). Motivation and impulsivity varied over animals but were similar for both species. Finally, we could demonstrate that trained animals rarely moved their whisker prior to stimulus presentation (9% of trials). In trials where whisker motion occurred, we observed a significant drop of discrimination performance. Response biases could successfully be reduced by using a previously published bias correction (Knutsen, 2006). Although, the head rotation mechanics was closed for most of the data presented in this study and it is not essential for the entire training procedure, it is a valuable tool for prompting the animals and avoiding early lick events. Furthermore, it allows a simple implementation of a working memory tasks. Animals can be forced to wait after stimulus offset by keeping the brake system closed for variable delay period before a response is allowed by opening the brake. The fact that the animal can turn its head to retrieve a reward from two different locations would also to study neuronal correlates head orientation movements (Erlich et al., 2011; Taube et al., 1990) while keeping the advantages of the head-fixed preparation.

*Frequency discrimination in different species*

Frequency discrimination paradigms have previously been performed in rats, monkeys and humans (Gerdjikov et al., 2010; LaMotte and Mountcastle, 1975; Mountcastle et al., 1990). The perceptual threshold for frequency differences, however, depends on the location and the timing of the stimuli. The majority of tasks published to date involved a working memory component. In these paradigms, frequencies were presented consecutively to the sensory organ and thus the subject had to compare them in sequence (2-interval forced choice; see e.g. (Hernández et al., 1997). Our paradigm is different in that the simultaneously applied single whisker stimuli had to be compared between the left and the right whisker pads while the stimuli were presented. The inter-hemispheric communication and the concomitant perception of two stimuli required to solve this task may involve neuronal processes that are distinct from those involved in a working memory task. Frequency thresholds and the resulting Weber fractions were higher as reported in working memory tasks in rats (Gerdjikov et al., 2010), monkeys and humans (LaMotte and Mountcastle, 1975; Mountcastle et al., 1990). Additionally, it has been shown in human subjects that discrimination performance was more accurate when frequencies were applied sequentially to the same finger. Discrimination performance dropped when the frequencies were presented to corresponding fingers on both hands (Harris et al., 2001). However, vibrotactile input arriving simultaneously from both sides might be behaviorally relevant when rodents navigate in darkness in narrow environments. Whisker vibrations may be generated by the texture of walls and ground on both sides of the animal and lead to simultaneous inputs that can be used for orienting in these situations. Passive whisker vibrations (i.e. when the animal is not actively whisking) may be a common setting that rodents encounter in their natural environment. Previous work showed that freely moving rats were able to accurately discriminate small variations of aperture sizes without the need of active whisker movements (Krupa et al., 2001). Furthermore, we observed lower discrimination performance when the animals moved their whiskers just before stimulus presentation. Active whisker movements are often observed when animals have to lean over a gap to discriminate different textures (Carvell and Simons, 1990; Cybulska-Klosowicz and Kossut, 2000; von Heimendahl et al., 2007; Morita et al., 2011) and therefore hamper the use of body movements to contact textures. However, whisker-tracking data from

freely moving animals discriminating wall properties in very close proximity are still lacking.

*Mice and psychophysics*

The question as to why there is a need to transfer a psychophysical task that has been developed for rats to mice requires addressing. The mechanical difficulties of downsizing the behavioral apparatus components and the potential problems of tracking the whisker motion of an animal about a tenth of the weight of a rat argue against such an endeavor. There are, however, several benefits, especially with respect to the combination with state-of-the-art imaging and electrophysiology techniques that demand well-controlled behavioral paradigms for head-fixed mice. The mouse is currently the best developed mammalian genetic model organism, allowing cell type-specific readouts and manipulation of neuronal activity (Luo et al., 2008). The parallel acquisition of psychometric and neurometric curves is one of the gold standards in cognitive and systems neuroscience for understanding the role of individual neurons in behavior (Parker and Newsome, 1998). The psychophysics described here will therefore allow the expansion of these types of investigations to a cell type-specific level and shed light on the contribution of individual neuronal elements to perceptual decision-making processes. Here we demonstrate that mice are able to perform tasks that have long been a standard in head-fixed monkey behavior and neurophysiology (Wurtz, 1968). The animals were highly motivated at all levels of difficulty and performed several hundreds of trials per day with high maximum performance levels. In conclusion, we can report that the two rodent species (rats and mice) have very similar capacities for frequency discriminations in the 2-AFC paradigm described here.

*2-AFC paradigm versus Go-NoGo paradigm*

Several laboratories are currently using Go-NoGo paradigms to measure psychophysics in head-fixed rodents (Andermann, 2010; Gerdjikov et al., 2010; O’Connor et al., 2010b). These paradigms are well suited to obtain psychometric curves from head-fixed rodents performing sensory discrimination and detection tasks. In all of these tasks animals are subjected to water deprivation for motivation. Deprived animals, however, are prone to impulsive behavior as the measured responses are tightly linked to the pressure of retrieving a reward. In a Go-NoGo paradigm it is difficult to implement that the animal receives a reward in the Go and in the NoGo condition. This is more straightforward in 2AFC tasks as the animal can retrieve a reward in each trial. Another obstacle present in

the Go-NoGo paradigm is that animals can contaminate the measured threshold by developing a strong response bias toward Go or NoGo stimuli (for review of different task strategies see (Stüttgen et al., 2011). Although, animals did not show strong stereotypical response behaviour (positional bias: left or right side preference, left/right switching behavior, etc.) this can be a problem in a 2AFC task. Nevertheless, this kind of behavior can easily be inhibited by implementing a bias correction algorithm. In the Go-NoGo task it is difficult to distinguish a lack of motivation or lapses of attention from false rejections or correct rejections. The 2-AFC paradigm is therefore ideal for investigations of behavioral state-dependent neuronal processing. The uncoupling of reward retrieval *per se* (i.e. licks) from the stimulus report action (i.e. the choice of one of two reward locations) allows a clear distinction of correct, incorrect and missed trials. Furthermore, the task can easily be modified to accommodate a yes-no paradigm by providing only a single stimulus per trial.

*Outlook*

The presented apparatus and behavioral paradigm have been designed to combine two-photon imaging and electrophysiology with simultaneous psychophysical measurements. The dura mater of mice is transparent and therefore facilitates the use of high-resolution functional imaging such as two-photon imaging. The quality of two-photon images of neocortical neurons obtained in mice appears to be superior to those obtained in rats (own observations and personal communication with Helmchen F. and Kampa BM.). Vessel density and size may play a role in the amount of scattered photons that can be collected. Although it is possible to reduce these effects by blood exchange techniques in anesthetized animals (Haiss et al., 2009), the long-term use of this technique in behaving animal seems not to be feasible in the near future. The mouse is therefore an excellent model organism that combines genetic tools and the feasibility to image large populations of neurons in behaving animals (Dombeck et al., 2010). In addition, the use of transgenic animals such as Cre driver lines permits the expression of functional indicators or markers in specific subsets of neurons (O’Connor et al., 2009; Zariwala et al., 2011). The presented head-fixed 2-AFC paradigm therefore promises to be a valuable framework to conduct two-photon imaging in the mouse while measuring its psychophysics.

## 5.6 Acknowledgements

We thank Stefan Weber, Markus Küpfer and Vasiliki Panagiotopoulou for technical assistance. We also thank Peter Roth for the illustration in Figure 5A, and Renaud Jolivet, Björn Kampa, David Margolis and Maik Stüttgen for comments on an earlier version of the manuscript. We also thank Medartis for providing the cortical screws. This work was supported by the EU-FP7 program (BRAIN-I-NETS project 243914 to F.H. and V.S. and BrainScales project 269921 to F.H. and S.M.), the Swiss National Science Foundation (grant PP00B-110751/1 to F.H. and B.W.) and SystemsX.ch (project 2008/2011-Neurochoice to J.M.M., W.B. and B.W.).

# 6 Project 2: “Sparse, reliable and persistent frequency processing in the mouse barrel cortex”

Johannes M Mayrhofer (1, 3), Florent Haiss (1, 4, 5, 6), Fritjof Helmchen (2, 3) & Bruno Weber (1, 3)

(1) Institute of Pharmacology and Toxicology, University of Zurich, Zurich, Switzerland
(2) Brain Research Institute, University of Zurich, Zurich, Switzerland
(3) Neuroscience Center Zurich, Zurich, Switzerland
(4) IZKF Aachen, Medical Faculty of the RWTH Aachen University, Aachen, Germany
(5) Institute for Neuropathology, RWTH Aachen University, Germany
(6) Department of Ophthalmology, RWTH Aachen University, Germany

In preparation for publication

*Author Contributions*

J.M.M., F.Ha., and B.W. conception and design of research; F.Ha. and J.M.M. performed surgeries; J.M.M. performed experiments, wrote analysis scripts, analyzed data, interpreted results of experiments, and prepared figures; J.M.M. and B.W. drafted manuscript; J.M.M., B.W., F.He., and F.Ha. edited and revised manuscript;

## 6.1 Abstract

The rodent whisker system is a favored model for studying cortical plasticity. Conversely, little work has been done characterizing the stability of neuronal activity in the barrel cortex. What is the neuronal correlate of a stable percept in the somatosensory cortex? We studied the stability of the whisker frequencies processing in populations of neurons over long time periods (up to months) and in rodents performing a frequencies discrimination task. Tuning towards higher frequencies was seen for most of the active neurons (89%) and was preserved over days. Repeated stimulation activated the imaged population of neurons in a stereotypic way within and over different days. A small population of highly responsive neurons (~2%) is sufficient to decode the stimulus identity. Finally, the stability of the frequency processing in population of neurons correlates with the perceptual stability of the animals trained to discriminate frequencies.

Keywords: head fixation, psychophysics, whisker, mouse, somatosensory cortex, in vivo two-photon microscopy, Yellow Cameleon 3.60

## 6.2 Introduction

Rodents are nocturnal animals, which have a highly-sensitive whisker system. This tactile sense is essential for navigation and object recognition. Rodents are able to actively and passively use their whiskers to solve different kinds of tasks, such as roughness discrimination, gap crossing, pole detection, and frequency discrimination tasks (Adibi et al., 2012; Carvell and Simons, 1990; Gerdjikov et al., 2010; Jenkinson and Glickstein, 2000; Mayrhofer et al., 2013; Morita et al., 2011; O’Connor et al., 2010b). A hallmark of the whisker system is its overrepresentation in the somatosensory cortex (S1) compared to rest of the body and its organization in specific cortical units the so-called barrel columns (Woolsey and Van der Loos, 1970). At this cortical level input from the contra- and ipsilateral whisker pad converge for the first time in the ascending somatosensory pathway (Shuler et al., 2001; Wiest, 2005). One way to reliable activate the whisker pathway is ensured by rapid changes of the whisker’s position (stick-slip events) which corresponds to high velocity deflections (Jadhav et al., 2009; Lottem and Azouz, 2009; Wolfe et al., 2008). The frequency of successive stick-slip events created either by active whisking against a rough surface or passive deflection when the animal runs along a wall characterizes the texture of a surface. When rodents navigate in dark tunnels different textures of walls or objects could be used for orientation decisions (Hutson and Masterton, 1986; Mayrhofer et al., 2013). Key questions are how different event frequencies are processed in the barrel cortex and whether simultaneous bilateral activation alters these processes. Whiskers could act as resonators with each whisker having a distinct characteristic frequency (100 – 700 Hz). The spatial organization of the whiskers on rodents snout would directly translate to frequency representation similar to the auditory system (Andermann et al., 2004; Moore, 2004). On the other hand barrel cortex neurons show a stimulus locking up to frequencies as high as 1000 Hz (Ewert et al., 2008). Theoretically the temporal code could be used for differentiating different textures. A third hypothesis is that integrated spike counts could be used for animal’s judgment of texture (von Heimendahl et al., 2007).

Most of the knowledge about vibrotactile stimulus processing is based on electrophysiological recordings (Gerdjikov et al., 2010; Shuler et al., 2001; Simons, 1978) being a reliable measure of neuronal activity with a high temporal precision. However, they remain biased towards active neurons in the granular and sub-granular layers and

only allow relatively short recording periods (Petersen and Crochet, 2013). With the advent of the functional two-photon imaging on the single neuron level it is now possible to obtain a more unbiased view on the population of neurons encoding a certain stimulus (Grewe and Helmchen, 2009; Lütcke et al., 2013; Petersen and Crochet, 2013; Svoboda and Yasuda, 2006). Furthermore, genetically encoded $Ca^{2+}$ indicators (GECIs) allow for the first time to monitor a (genetically marked) population of neurons over extended periods up to months. This opens the possibility to study changes and stability of activity patterns in a population of neurons (Huber et al., 2012; Margolis et al., 2012).

The somatotopic representation of individual whiskers to specific areas of the somatosensory cortex is one of the reasons why the whisker system is widely used to study cortical plasticity. For example whiskers were cut or removed to study map reorganization (Diamond et al., 1994; Feldman, 2005; Margolis et al., 2012). On the other hand little work has been done on characterizing the persistency of the cortical stimulus representations on a single cell level so far (Lütcke et al., 2013) (however, see (Masino and Frostig, 1996; Minderer et al., 2011) for studies measuring the bulk signal). The need for a balance of these two processes is clear. On the one hand, plasticity enables us to learn new experiences and adapt to new stimulus conditions. On the other and, stability of stimulus representation enables us to recognize familiar stimuli even under noisy conditions (Lütcke et al., 2013). In the whisker system the temporal event structure (few or many event per time; from now on termed frequency) can be differentiated and is most likely essential for navigation of rodents in the dark. What is the perceptual stability on a neuronal level and a behavioral level of repeated whisker deflections? The present study investigates three main questions: 1) How are different stimulation frequencies processed by populations of neurons in the barrel cortex. 2) How stable is this stimulus processing over time and 3) how are these neuronal responses related to behavior of rodents in frequency discrimination?

Contralateral whisker stimulation elicited reliable $Ca^{2+}$ transients. Tuning towards higher frequencies was seen for almost all neurons (89%) and stayed stable over the entire imaging period (~5 weeks). Repeated stimulation activated the imaged population of neurons in a stereotypic way on the same imaging day and over different imaging days. From a decoding perspective a small population of highly responsive neurons (~8/460 neurons) is already sufficient to discriminate different stimulus frequencies. Animals

trained to discriminate these frequencies exhibit a stable performance over extended periods. This perceptual stability is mirrored by the stability in neuronal representation of naïve animals.

## 6.3 Results

*Chronic two-photon $Ca^{2+}$ imaging and stimulation paradigm*

To follow the activity of the same population of neurons over long period chronic two-photon $Ca^{2+}$ imaging with a genetically encoded $Ca^{2+}$ indicator was performed (n = 7 mice; see Methods). Pulsatile stimulus trains with different repetition rates of 10, 40, 90 and 110 Hz and 1 s duration were used to stimulate a single contra vibrissa (Figure 12A). Intrinsic optical imaging was performed to visualize the barrel representation (Figure 12B, left panel) which was used for identification of virus injection site and the respective imaging field of view during two-photon imaging. The area under the $Ca^{2+}$ transient measured the stimulus evoked activity of a single neuron ($Ca^{2+}$ response) for the different stimulation frequencies (Figure 12C, see Methods). The combination of the chronic window preparation and GECI (Yellow Cameleon 3.60) allowed functional monitoring populations of neurons over periods as long as 3 months (Figure S 2). As an example an imaging spot is shown at different experimental days with responses to a 90 Hz stimulus (Figure 12D). In addition the “population activity matrix” for the chosen neurons is illustrated: Here each element corresponds to a single trial $Ca^{2+}$ response of one neuron and a column vector corresponds to a single trial response of the considered population of neuron. All trial vectors together give rise to the population activity matrix of a single imaging day (Figure 12D: trials and neurons are in the same order as single trial examples (left) and sorted (right); see also Methods). On average neurons were followed over a time span of 35 ± 19 days (mean ± standard deviation of the mean (SD), n = 1549 neurons in 7 mice), where an entire imaging location was functionally monitored for 39 ± 27 days (mean ± SD, n = 20 spots in 7 mice). The average number of neurons per spot and day was 71 ± 58 (mean ± SD, n = 20 spots in 7 mice) (Figure S 2).

*Most barrel cortex neurons are tuned towards higher whisker frequencies*

We first characterized the spontaneous (0Hz) and stimulus (10, 40, 90 and 110Hz) evoked activity of single neurons. Since barrel cortex neurons display adaptation to periodic whisker deflections (Khatri, 2004; Melzer et al., 2006) the $Ca^{2+}$ response was plotted over a logarithmically scaled x-axis. Figure 13A shows the $Ca^{2+}$ response to the different stimulus frequencies of all neurons and animals. Furthermore, neurons were divided into three categories (high, medium and low responding neurons, see inset of Figure 13A). Pooling over animals was done after normalizing the responses of each

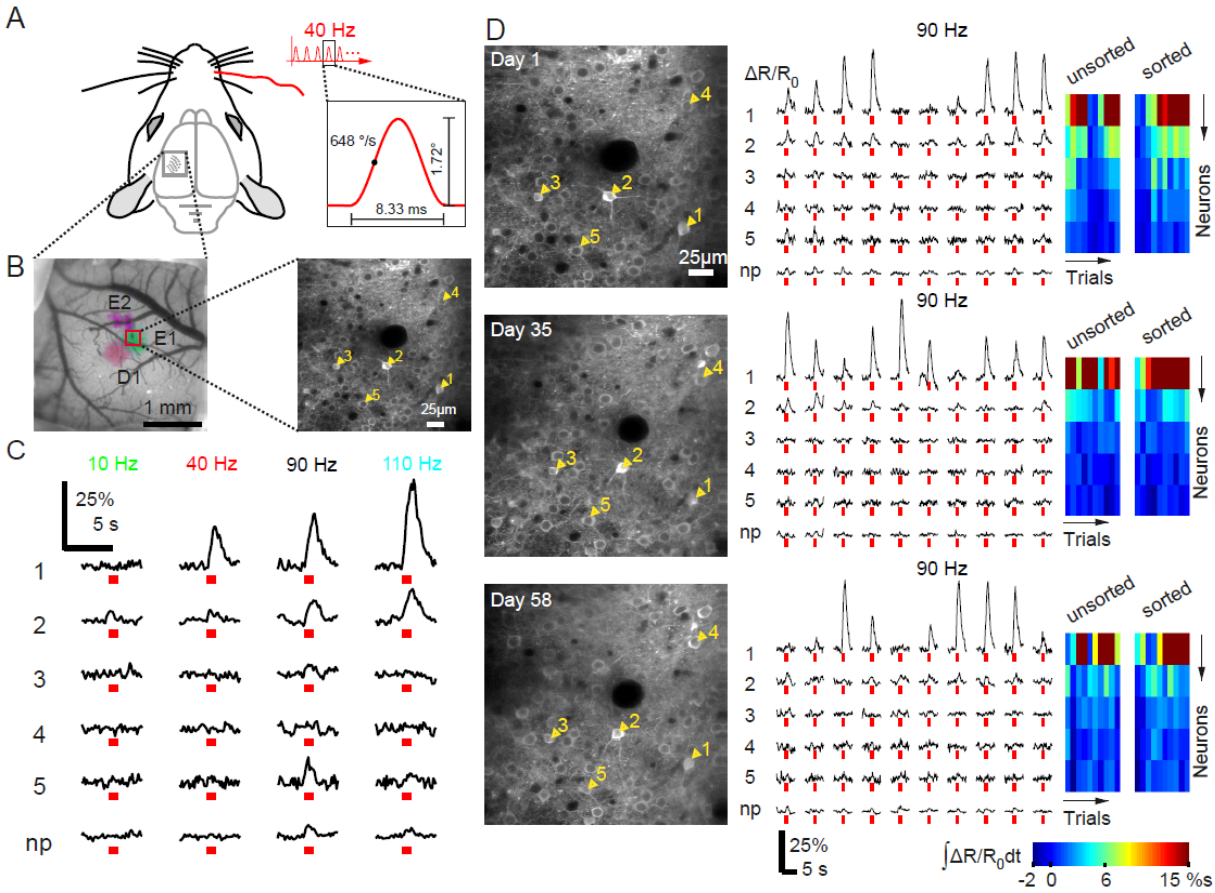


**Figure 12. Stimulation paradigm and chronic two-photon $Ca^{2+}$ imaging.**
**(A)** Stimulation paradigm: contralateral stimulation relative to the imaging location with pulsatile stimulus derived from a 120 Hz cosine wave (see inset). **(B)** Chronic window with intrinsic optical imaging map of whisker E1, E2 and D1 thresholded and colored overlaid at day 19 after window implantation (right). Yellow Cameleon 3.60 expression of the red square marked on the left (right) **(C)** Examples of $Ca^{2+}$ transients in response to 10, 40, 90 and 110 Hz 1 s long contralateral pulsatile stimulus (neurons marked in (B) left panel and neuropil (np)). Stimulus duration is indicated as red bar below the traces. **(D)** The same imaging location at different experimental days with 10 $Ca^{2+}$ transient examples from the 5 marked neurons and the neuropil evoked by a 1 s long 90 Hz stimulus. Stimulus duration is indicated as red bar below the traces. Next to the raw traces the neuronal response measured as the area under curve from 100 ms until 1200 ms after stimulus onset ($\int \mathbf{\Delta} R/R_0 dt$) is shown color-coded for individual trials and ROIs (left same order as $Ca^{2+}$ transients; right sorted accordingly to increasing mean activity of all 5 neurons).

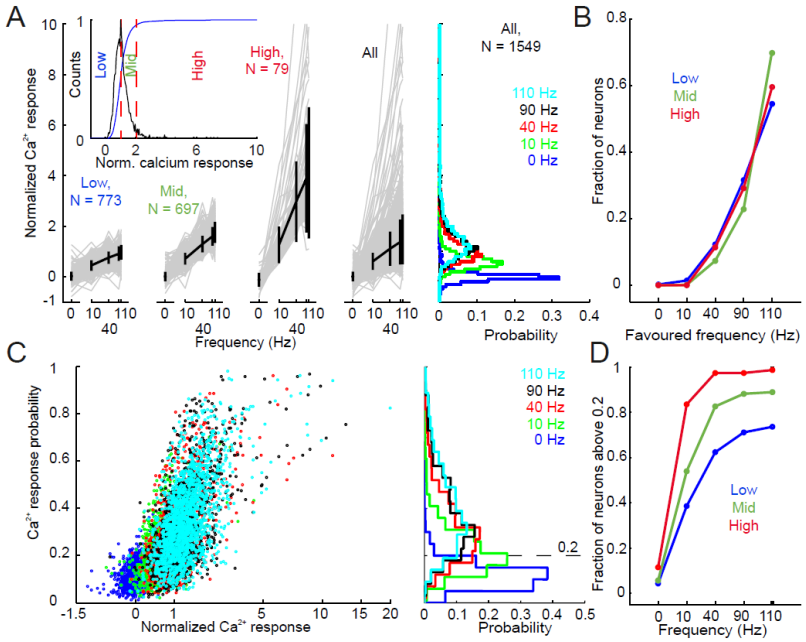


**Figure 13. Frequency processing: individual neuronal $Ca^{2+}$ responses.**
**(A)** Average neuronal $Ca^{2+}$ responses of all recorded neurons (category “All”, n = 1549 neurons in 7 mice) and for different response categories (“Low”, “Mid” and “High”). The inset shows the histogram of the response amplitude to mean of all contralaterally presented stimuli of the individual neurons. This distribution was used to classify the neurons: “Low” (0-50%), “Mid” (50-95%) and “High” (95-100%) responders. Grey traces show averaged tuning curves of individual neurons. The average and SD is shown in black. On the right the histogram of the response amplitude for the different stimulation categories is presented. **(B)** shows how many neurons had at 0, 10, 40, 90 or 110 Hz their peak response (favored frequency) for the response categories shown in **(A)**. **(C)** The average $Ca^{2+}$ response probability is plotted over the average response amplitude for different stimulus categories for all neurons (n = 1549 neurons in 7 mice). Each dot corresponds to an individual neuron. On the right the histogram of the $Ca^{2+}$ response probability for the different stimulus categories is shown. **(D)** shows how many neurons were on average at least in each fifth trial activated over the different stimulus frequencies for the response categories shown in **(A)**.

animal to its median $Ca^{2+}$ response over all frequencies and recorded neurons. The average neuronal activity of individual neurons as well as the entire population activity increased with increasing stimulation frequency. 762 out of 1549 neurons had monotonic tuning, 1380 out of 1549 neurons had either at 90 Hz or 110 Hz as their favored frequency (89%, Figure 13B). No difference of the distribution of favored frequency over different response categories was seen (Figure 13B). This indicates that the different response categories are not representing a weaker or stronger adapting population of neurons. To find out if the neurons which show on average a high stimulus evoked response are also the ones which responded most reliable over trials the $Ca^{2+}$ response probability was computed. The $Ca^{2+}$ response probability quantifies how often a neuron is activated above a baseline derived threshold in response to the stimulus (see Methods). Neurons with high average response were more often activated (n = 1549 neurons in 7 mice, correlation for 0 Hz: $\rho$ =0.386, 10 Hz: $\rho$ =0.389, 40 Hz: $\rho$ =0.513, 90 Hz: $\rho$ =0.529 and 110 Hz: $\rho$ =0.516; Figure 13C). Additionally, higher stimulus frequencies more often evoked a detectable $Ca^{2+}$ transient as compared to low frequencies (Figure 13C). At frequency above 40 Hz the number of repeatedly activated neurons (neurons with a $Ca^{2+}$ response probability above 0.2) stayed almost unchanged (Figure 13D). The spatial distribution of activity within imaging spots (imaging location were centered on the barrel) was similar in form for the different frequencies, with an increased $Ca^{2+}$ response for high stimulation frequencies (Figure S 3).

*Different frequencies elicit similar ensemble activity patterns*

How are different frequencies processed by the population of neurons in the somatosensory cortex? To characterize whether different frequencies activate different activity patterns in the barrel cortex the correlation coefficient of the activity vectors between different stimulus frequencies was calculated (for each trial, but only within one day) (Niessing and Friedrich, 2010). A high correlation between different stimuli indicates that the stimulus induced activity pattern is similar. Low correlation can be caused by either little stimulus-driven activity or by different activation patterns evoked by different stimuli. The latter case would cause a high correlation for one particular stimulus (high reliability) but a low correlation between different stimuli (low similarity). Figure 14A shows an example population activity matrix for different stimuli from one spot and Figure 14B provides the corresponding similarity matrix. The upper/right triangular part shows the single trial-to-trial correlation coefficients for different stimuli

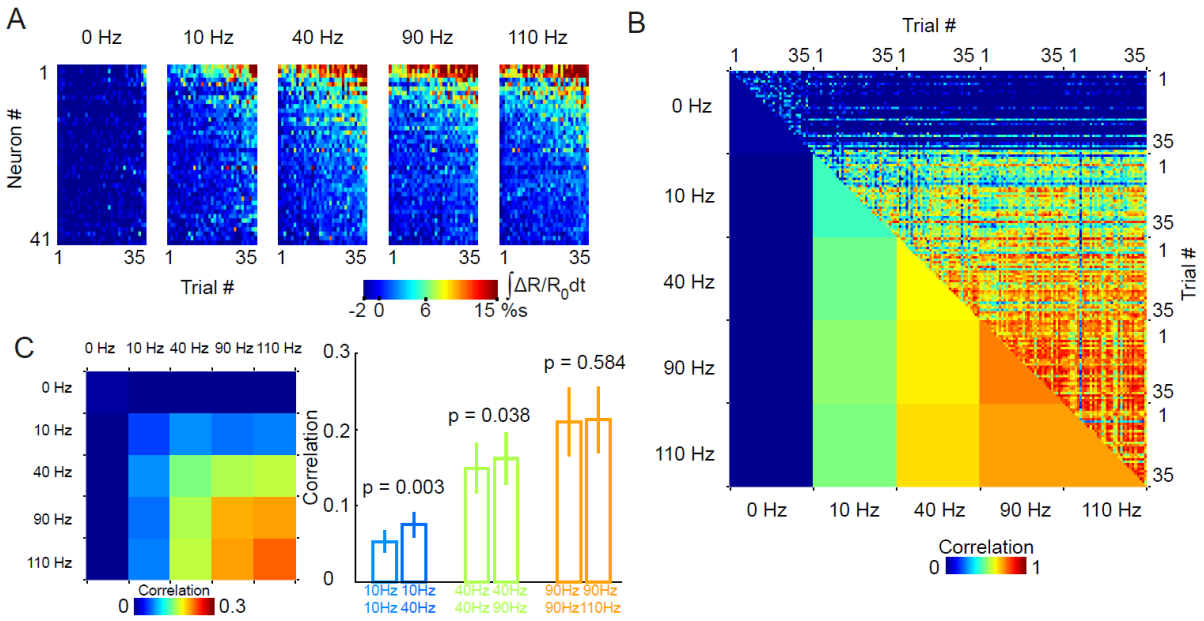


**Figure 14. Frequency processing: population responses of S1 ensembles.**
**(A)** Example population activity matrix for 0 (spontaneous activity), 10, 40, 90 and 110 Hz: rows correspond to neuron ID and columns to trial ID. 35 trials per stimulus category are presented. **(B)** Similarity matrix of the same neuronal population as shown in **(A)**: The upper triangular part of the matrix shows the individual trial-to-trial correlation of the population activity for one stimulus and for two different stimuli in a single day (self-correlation omitted). The lower part shows the average of the trial-to-trial correlations for one stimulus and for two different stimuli in a single day: The diagonal elements correspond to the average reliability of a stimulus (see Figure 15). **(C)** Similarity matrix for all spots (n = 20 spots in 7 mice). Right panel: comparison of several matrix elements with each other e.g. “10 Hz 10 Hz” (reliability for 10 Hz) vs. “10Hz 40Hz” (similarity between 10 Hz and 40 Hz). Statistical analysis: Student’s t test. Plots are mean ± SEM.

(self-correlation omitted). The lower/left triangular part displays the mean correlation for the different stimulus comparisons. Pooled over spots (20 spots in 7 mice) the similarity matrix arrives at the form shown in Figure 14C. For the 10 Hz stimulus a weak correlation with the other stimulation frequencies is seen. This is due to the fact that the 10 Hz stimulation evoked only weak pattern activation (small reliability value; Figure 13). For higher stimulation frequencies the correlation increases between stimuli and for the individual stimulus (higher reliability). The right subpanel of Figure 14C compares neighboring pairs of matrix elements. The similarity of the pairs shows that different frequencies elicit similar activity patterns, indicating that different frequencies did not activate distinct populations of neurons- most strongly seen for 90 and 110 Hz stimulation frequency. This agrees with the observation that not more neurons get measurable activated but the evoked $Ca^{2+}$ response is increased with frequency (Figure 13D).

*High frequencies drive reliable and stable stimulus processing in the neuronal population*

How stable is a certain whisker frequency (e.g. 90 Hz) processed in the barrel cortex over different timescales (seconds to days)? The reliability-stability matrix was derived by correlating the population activity vectors from different trials either from the same imaging day (reliability) or from different days (stability) with each other (Bathellier et al., 2012). Figure 15B shows the matrix for the population activity matrix example in Figure 15A. The upper/right triangular part of the matrix shows the single trial-to-trial correlations (self-correlation was removed). In the lower/left part the mean single trial-to-trial correlation within imaging day is shown. Another way of presenting the averaged matrix elements is to plot them over their inter-session interval (time span between the imaging days, which are compared; Figure 15C). For this example there was no correlation of the reliability-stability matrix elements with the inter-session interval indicating that the trial-to-trial variability within a day was in the same range as over different days ($n = 15$ matrix elements, $\rho = -0.09$, $p = 0.75$). In Figure 15D diagonal elements (mean intra-day correlation: reliability) and the off-diagonal elements (mean inter-day correlation: stability; gray shaded) are shown as mean values. To show that there is a certain stereotypical activity pattern in the population the matrix elements were compared to the case where the activity vectors were shuffled along the neuron ID axis within a trial. The reliability and the stability dropped to near-zero values. Shuffling the activity matrices along the trial ID axis for each neuron individually did not change

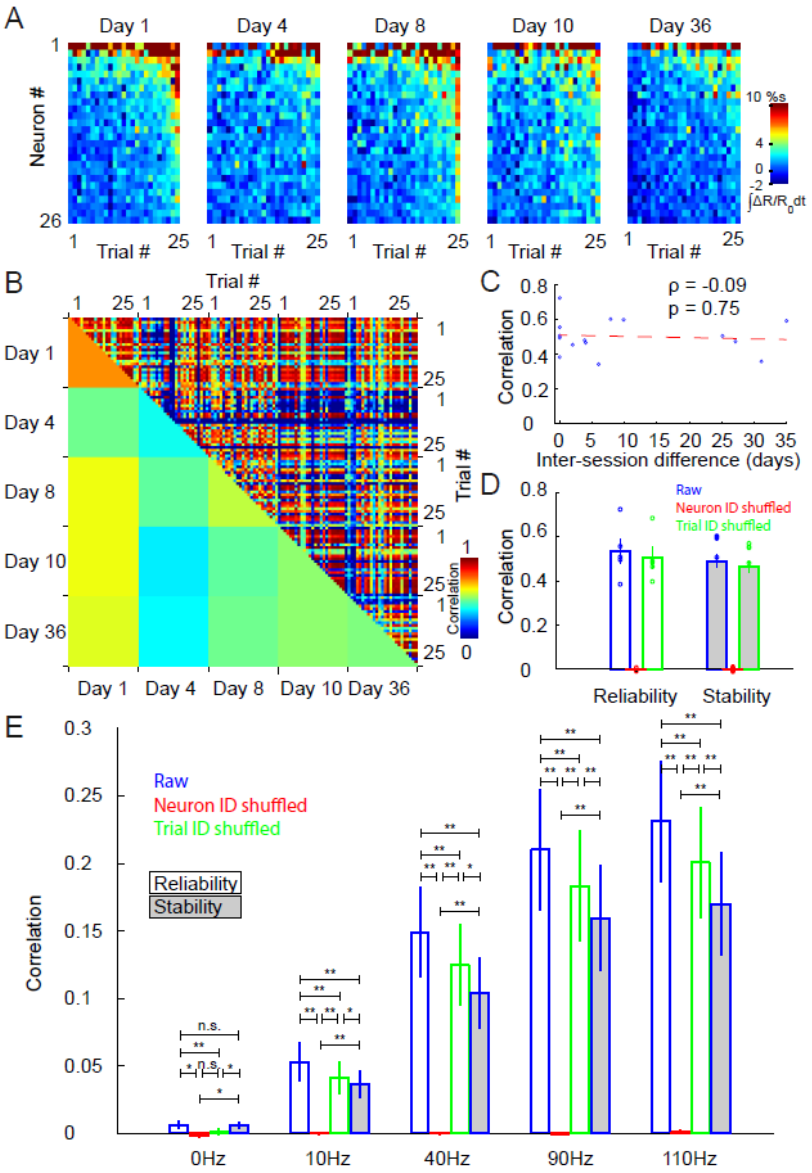


**Figure 15. Reliability and stability of whisker frequency processing in S1.**
**(A)** Example population activity matrix for 90 Hz contralateral stimulation from the same population of neurons over different experimental days: rows correspond to neuron ID and columns to trial ID. 25 trials per day (session) are presented. **(B)** Reliability-stability matrix of the same neuronal population as shown in **(A)**: The upper/right triangular part of the matrix shows the individual trial-to-trial correlation of the population activity within a session (day) or over different days. The lower/left part shows the averages of the trial-to-trial correlations within a day or over two different days: The diagonal corresponds to the reliability of a stimulus representation, whereas the off-diagonal elements represent the stability of the stimulus representation. **(C)** Average correlation of the reliability-stability matrix over the inter-day difference. **(D)** Comparison of the stimulus representation reliability with the stability over days (blue). The reliability and the stability are also shown for the same data set where either the neuron ID or the trial ID was shuffled. **(E)** The reliability and the stability values of the stimulus representation for different stimulus frequencies (0Hz: spontaneous activity) is shown for all spots (n = 20 spots in 7 mice). In addition, the reliability where either the neuron or trial ID was shuffled is depicted. Statistical analysis: Pearson’s correlation and Student’s t test. Plots are mean ± SEM. $p < 0.05$ (*), $p < 0.01$ (**) and not significant (n.s.).

the correlation significantly. This demonstrates that there is a stereotypical activity pattern, which remains constant over trials and days. Figure 15E displays the matrix elements of pooled spots plotted over the different stimulus frequencies: bar plots for reliability (intra-day correlation, n = 20 spots in 7 mice), stability (inter-day correlation, gray shaded, n = 17 spots in 6 mice), and shuffled along neuron ID and trial ID axis cases for the reliability case. The highest correlation values were reached for high frequencies. On average the reliability (mean trial-to-trial correlation within a day) was higher than the stability (mean trial-to-trial correlation over days) and stayed for both well above the control condition in which the neuron ID was shuffled (Figure 15E, red bars vs. blue bars). Shuffling along the trial ID axis reduced the reliability but not to the level of the stability matrix elements (Figure 15E, green bars). Hence, there is a stereotypic activation of the imaged neuronal ensemble, which is preserved over days. Furthermore, increased stimulus strength in terms of higher frequency established a more reliable and stable network activation (n = 20 spots in 7 mice, correlation between reliability and stimulus frequency: $\rho = 0.51$, $p < 0.01$; n = 17 spots in 6 mice, correlation between stability and stimulus strength: $\rho = 0.50$, $p < 0.01$; see also Figure 15C). The neuron-to-neuron correlation was also increased with increased stimulus strength and neurons closer to each other showed an increased stimulus induced correlation (Figure S 4) (Kerr et al., 2007). A non-significant correlation of the reliability-stability matrix elements with the inter-session interval was seen, indicating that the trial-to-trial variability within a day was in the same range as over different days (n = 352 matrix elements in 7 mice: 0 Hz: $\rho = 0.088$, $p = 0.098$; 10 Hz: $\rho = 0.056$, $p = 0.296$; 40 Hz: $\rho = -0.016$, $p = 0.784$; 90 Hz: $\rho = -0.036$, $p = 0.504$; 110 Hz: $\rho = -0.035$, $p = 0.510$; see Figure 15D as example).

*Perceptual stability correlates with neuronal stability*

We have previously investigated the ability of rodents to discriminate different frequencies of whisker deflections (Mayrhofer et al., 2013). However, it remained unknown how such stimuli are processed in the population activity of cortical neurons over extended period of time. To this end we applied a machine learning approach in order to identify how well the system can maximally discriminate different whisker frequencies based on the neuronal activity we saw in S1. Ultimately, we wanted to know if the neuronal stability or variability is reflected by the animal performing a frequency discrimination task. To address these questions a classifier (linear support vector

machine) was trained to differentiate between the different whisker frequencies (see Methods). Here the individual neurons were taken as features for the classification. In Figure 16B a single spot example is shown for the activity matrix shown in Figure 16A (left subpanel). Along the y-axis the ID of the training day is shown, whereas the x-axis corresponds to the sample ID. Hence, the first row indicates that the classifier was trained on the first data set (or subset in the case of intra-day classification, see Methods) and tested (cross-validated) on all other days in the data set. The matrix is summarized in the right subpanel of Figure 16B. Here the diagonal elements correspond to the intra-day accuracy (cross-validation within a day) and the off-diagonal elements to the inter-day accuracy (cross-validation over different days) of the classification algorithm. For both cases a performance above chance (20% for five different stimuli) was reached ($n = 16$ matrix elements, $p < 0.001$). The classifier was able to differentiate the stimuli within a day and over days (Figure 16D, right panel). Pooled over animals and spots the classification accuracy was well above chance meaning that the stimuli can be discriminated within a day ($n = 20$ spots in 7 mice, $p < 0.01$) and over days ($n = 17$ spots in 6 mice, $p < 0.01$) with a pre-set decision criteria derived from the same or a different day (Figure 16E, red bars: “Population”). Neurons can be used as features for the classifier to discriminate stimuli within a day and over days. This demonstrates a considerable stability of the population activity pattern over days. This result is also supported by a general preservation of individual neuronal frequency response over days (Figure S 5). To approach the question whether the information about the identity of the individual neurons (neurons as classification feature: “Population”) improves discrimination performance the mean activity of all neurons of the spots were taken as a classification feature for comparison (Figure 16E, green bars: “Mean”). On average the two classification methods did not perform differently for intra-day discrimination of the stimulus categories ($n = 20$ spots in 7 mice; All, $p = 0.13$; 50%, $p = 0.76$ and 30%, $p = 0.67$), whereas a difference was seen for the classification performance over days. Here, the “Mean” criterion performed better than the “Population” criterion ($n = 17$ spots in 6 mice, All, $p < 0.01$; 50%, $p < 0.01$ and 30%, $p < 0.05$). The mean activity is better suited to differentiate stimulus frequencies because it is less prone for slight changes in the population activity distribution within the population. When only the 50% or 30% most active trials of a given data set were considered the results generally were very similar, but the classification accuracy was superior (Figure 16C; “50%”and “30%”). Therefore,

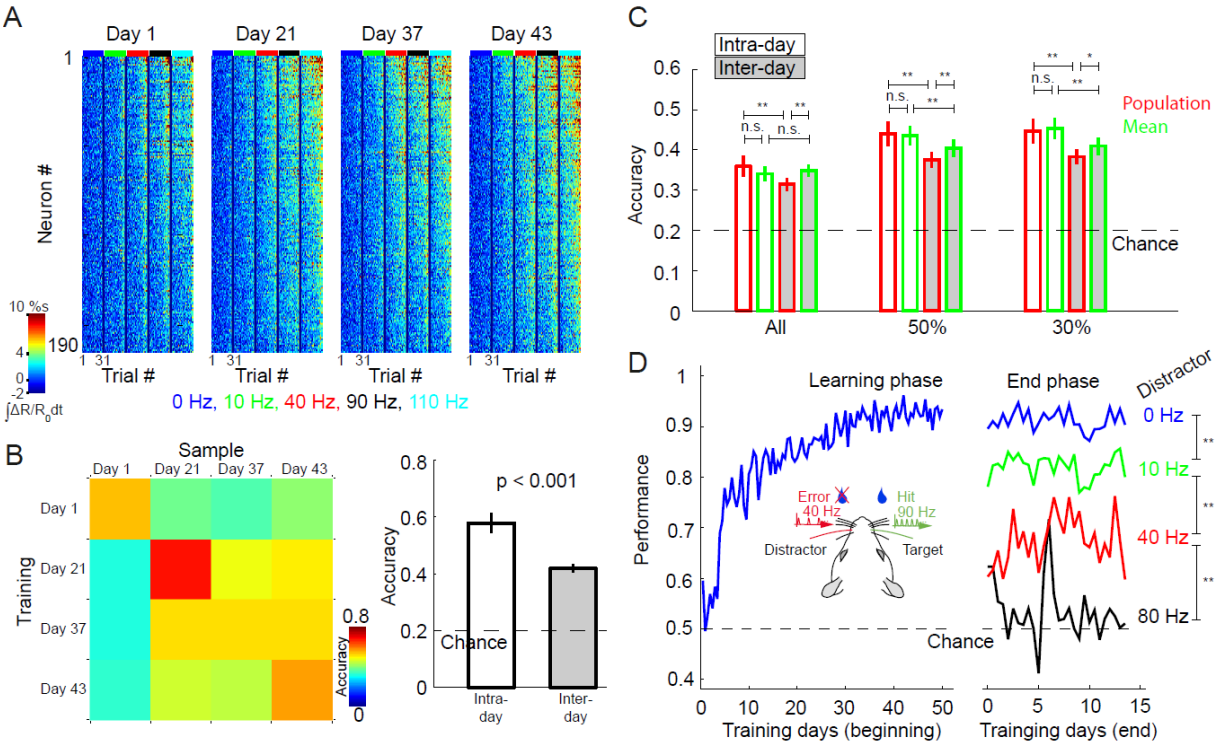


**Figure 16. Discriminability of different stimulus frequencies.**

**(A)** Example population activity matrix for 0 (spontaneous activity), 10, 40, 90 and 110 Hz stimulation from the same imaging location over different experimental days: rows correspond to neuron ID and columns to trial ID. 31 trials per stimulus frequency are presented. Trials were sorted for each stimulus frequency according to the mean response amplitude of the population. Neurons were sorted with respect to their mean response amplitude over all trials, experiments and stimulus frequency. **(B)** Left panel, discriminability matrix: Classification accuracy (cross-validation) over days for the same data set shown in **(A)**. The y-axis indicates which day was used for training the classifier and the x-axis labels shows the sample day for cross-validation. Right panel shows the mean of the intra-day accuracy (diagonal elements of the left discriminability matrix) and the inter-day accuracy (off-diagonal elements of the left discriminability matrix). **(C)** Classification accuracy within days (n = 20 spots in 7 mice) and over days (n = 17 spots in 6 mice) for different classification criteria for all spots: Left (“All”) shows the accuracy for all trials of the data sets. Middle block (“50%”) accuracy for the 50% highest activity of trials. Right (“30%”) shows accuracy the 30% highest activity trials. “Population” (red bars) corresponds to the case where the neurons were used as classification features. Whereas, in the case of “Mean” (green bars) the mean activity of the entire neuronal ensemble of a spot was used as a classification feature. **(D)** Learning phase and stable end phase of training. Inset on the left shows behavioral paradigm. Left panel shows correct behavioral responses over days averaged over animals for 90 Hz target and no distractor (n = 6 animals). Right panel shows detection and discrimination performance (10, 40 and 80 Hz difference) of the last 27 sessions averaged over animals (n = 9). Statistical analysis: Student’s t test. Plots are mean ± SEM. $p < 0.05$ (*), $p < 0.01$ (**) and not significant (n.s.).

trials which low stimulus evoked activity, most likely recorded during down states of the animal, diluted the information about the frequency identity. Is this neuronal “discrimin-st-ability” also displayed in the animal’s behavior in discriminating frequencies? To test this, mice and rats were trained to discriminate simultaneously presented pairs of frequencies (Figure 16D, left panel inset). As soon as the rodents have learned the task (Figure 16D, left panel) they showed stable perceptual interpretation of the presented frequencies by successfully discriminating the different stimuli over extended time periods (Figure 16D, right panel, $p < 0.01$). Discrimination performance over days was fluctuating unsystematically showing random variation of the perceptual stability rather than a systematic change over days (correlation of performance over days, 0 Hz: $\rho = -0.106$ $p = 0.591$; 10 Hz: $\rho = -0.081$, $p = 0.681$; 40 Hz: $\rho = 0.235$, $p = 0.229$ and 80 Hz: $\rho = -0.277$, $p = 0.154$). Taken together, we saw a stable discrimination performance of animals which is mirrored by a stable neuronal population activity for the different frequencies over extended time periods.

*Most active neurons encode the stimuli best*

Barrel cortex shows sparse responses to whisker stimulation manifested in the long-tailed response distribution ((Barth and Poulet, 2012; Petersen and Crochet, 2013); Figure 13A). Is there critical population size of neurons overlapping with high responsive neurons to reliable represent and decode the stimulus identity? A neuronal population from all recorded data was generated by pooling neurons from different animals (Figure 17A, in total 460 neurons and 100 trials per stimulus from 6 mice, see Methods). How important are the most active neurons for the reliability and the similarity of the stimuli? The population from Figure 17A was taken and varied in three different ways. One way was to include first the most active neurons leading to a fast increase of the reliability of a stimulus and decreases again with increased population size (Figure 17B, red line). This can be seen as adding noise to the system. When the least active neurons were taken first again an increase was observed but the reliability stays rather low when compared to the random sampling and the “most active first” scenario. Only, when the most active neurons are added, it reaches the final value (Figure 17B, blue line). In the third scenario, where neuronal populations were generated by randomly selecting neurons from the data set (for each population size this selection procedure was repeated multiple times, see Methods) the reliability increases with population size (Figure 17B, green line). Concerning the similarity between stimuli a comparable result

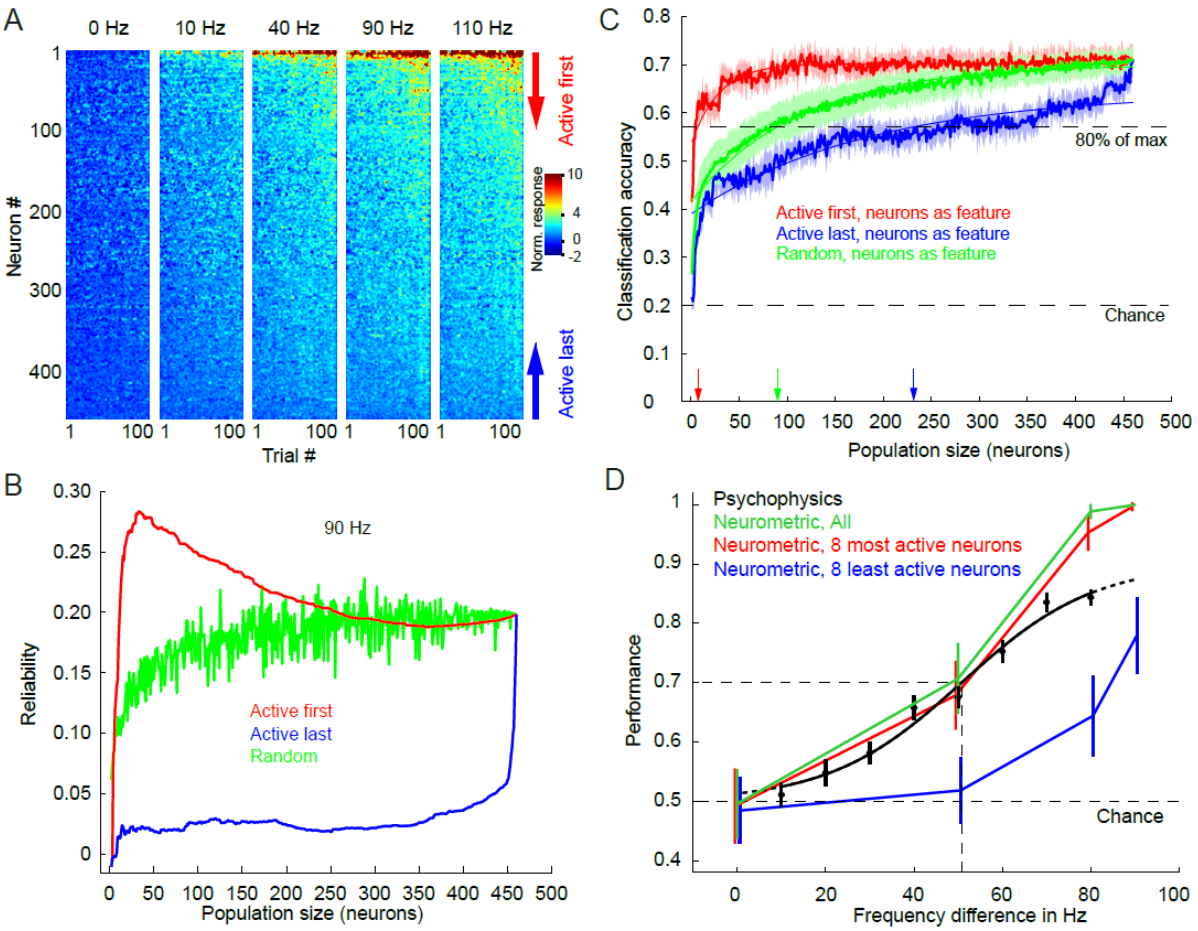


**Figure 17. Critical population size.**

**(A)** Population activity matrix for 0 (spontaneous activity), 10, 40, 90 and 110 Hz stimulation derived from all recordings: rows correspond to neuron ID and columns to trial ID. 100 trials per stimulus category are presented and matrix was smoothed (Gaussian low-pass filter) for illustration. **(B)** Reliability of 90 Hz stimulus over different population size varied in three different ways: active neurons were added first, least active neurons were added first and random selection of neurons (see also arrows in **(A)**) **(C)** Classification accuracy over different population size was tested in three different ways as in **(B)**. Thin lines correspond to fits of the form: y(x) = A + B*exp(-x/C). **(D)** Psychophysical performance (n = 9 mice and rats; Behavioral classification performance for 90 Hz target and different distractors (10 – 80 Hz in steps of 10Hz)) in comparison with the neuronal classification accuracy (n = 460 neurons, **(A)**). Black curve corresponds to performance plotted over frequency difference and compared to the neurometric data derived from all neurons (green curve), the 8 most active neurons (red curve) and the 8 least active neurons (blue curve). Plots are mean ± SD, except for psychophysics (mean ± CI95).

can be seen. Adding first the most active neurons markedly increases the correlation between stimuli (data not shown). Hence, the activity pattern elicited by the different stimuli is governed by a small number of neurons which are the most active ones in the population and the low active neurons add variance to the stimulus processing.

Do these high responsive neurons also decode the stimulus identity best? Different population sizes were generated by randomly selecting neurons from the data set. For each population size this selection procedure was repeated multiple times (see Methods). For each population size half of the data set was used to train the classifier and then to test it on the rest of the data set. The classification accuracy increased monotonically with increased population size and reached already 80% of its top performance for the population size of 90 neurons (Figure 17B). A fit of from $y(x) = A – B*\exp(-x/C)$ was performed to extract this value (fit parameters: A = 0.7006, B = 0.2845, C = 114.3616; $R^2$ of fit 0.96). If the population was ordered in a systematic way by including high responding neurons first and least active neurons last only the 8 most active neurons were required to reach 80% of the classification top performance (A = 0.7024, B = 0.1686, C = 28.7370; $R^2$ of fit 0.80). Conversely, where the population was generated by including first the least responding neurons and last the highly active neurons, an increase of the classification performance similar to the random chosen sample was seen for small population sizes but needed a much larger number of neurons to reach the 80% level (232 neurons were needed to reach 80% of the final accuracy; A = 0.6418, B = 0.2519, C = 182.8839; $R^2$ of fit 0.86, Figure 17B).

Are these high responsive neurons the ones which also reflect best the animal behavior in discriminating frequencies? To characterize the sensibility of the animals in discriminating frequencies psychophysical curves were measured. How does the neurometric curve compare with the animals’ behavior? To answer this question the activity evoked by a 0 (spontaneous activity), 10, 40 and 90 Hz stimulus (Figure 17A) was considered. A trial consisted of the average activity vector taken from the 90 Hz target stimuli and the average activity vector taken from the 0 (spontaneous activity), 10, 40 and 90 Hz population activity (see Methods).The ipsilaterally induced modulation was neglected because it is comparable weak (Figure S 6). Our idea of using anaesthetized data to extract the neurometric curve was supported by the similar $Ca^{2+}$ responses in the awake and anaesthetized state of the animals in a subset of spots (Figure S 7; Supplemental Experimental Procedures). Figure 17D shows the psychophysical

performance (n = 9 mice and rats) overlaid with the neuronal classification accuracy. In addition, the average psychometric threshold is marked at 50.9 Hz. The neurometric curve for all neurons (green curve) displays a similar shape when compared to the psychometric curve (black curve). Moreover, at the psychophysical threshold also the neurometric curve is at half of its top value. Taking only the 8 least active neurons into account the neurometric performance is significantly reduced. However, the 8 most active neurons reached as high neurometric performance as taking all neurons together. Hence, only small fraction of very active neurons is sufficient to mirror the animal’s psychophysics.

## 6.4 Discussion

Using chronic two-photon $Ca^{2+}$ imaging in mice we found a stable and stereotypic frequency processing in supragranular layers of somatosensory cortex, which is preserved over months. Stimulus evoked activity was tuned towards higher frequencies in almost all neurons (89%). In addition, the network activity patterns elicited by the different whisker deflection frequencies were relatively stable over time, with similar inter- and intra-day variability. Different stimulation frequencies did not activate orthogonal population activity patterns (Srivastava et al., 2008; Wick et al., 2009) in somatosensory cortex, indicative of similar processing of the different frequencies on the network level . A small population of highly responsive neurons (~2%) was sufficient to decode the different frequencies. The observed stability of neuronal activity derived from naïve anesthetized animals reflects the long-term perceptual stability of animals trained to perform frequency discriminations. Neurometric curves derived from these naïve animals are reflected by the psychophysics of trained animals, indicating that the stimulus induced activity in SI could limit discriminative performance.

*“Continuous representation” of frequencies in somatosensory cortex*

Since the amplitude of the $Ca^{2+}$ transient is linear proportional to the neuronal firing (Lütcke, 2010), an increased $Ca^{2+}$ response can be related to an increased integrated firing. Therefore, the response of individual neurons seems to be rather simple in the way that higher frequencies increase the firing rate of single neurons (Figure 13) (Arabzadeh et al., 2003; Melzer et al., 2006). In addition, periodic whisker deflection leads to adaptation of single neuron responses during stimulus presentation (Khatri, 2004; Melzer et al., 2006). This was revealed in our data by the fact of logarithmical increase of the $Ca^{2+}$ response with increased frequency of the population of neurons (Figure 13).

On the population level we saw that different frequencies did not activate different population of neurons. Different stimulation frequencies elicit a similar response pattern in the population of neurons imaged (Figure 13D, Figure 14). The modulation of the activity can be seen as a fixed subpopulation of neurons, which is modulated according to the stimulus strength. In contrast, varying a stimulus by mixing two different stimuli can lead to abrupt switch between two distinct neuronal ensemble activity (olfactory system zebra fish (Niessing and Friedrich, 2010)). In the auditory

cortex it was found that discrete neocortical dynamics predicted the behavioral categorization of sounds (Bathellier et al., 2012). But, passively perceived whisker frequencies in this frequency range seem not to be represented in discrete states as shown for other sensory systems.

*Stable stereotypic activity distribution over days*

We found a stereotypic activation pattern in the imaged population of neurons within a day and over weeks (Figure 15). As soon the neuron ID was shuffled the correlation between trials within a day and over different days was lost. This indicates a strong preservation of neuronal activity distribution within local ensembles of neurons and stands in strong agreement with the observation of Margolis et al. 2012 that sparse activity is stable over weeks. The sparse activity manifested in the long-tailed activity distribution (Figure 13A) has been observed repeatedly in the last years for the somatosensory cortex (Barth and Poulet, 2012). Here, we could find that not only the sparse activity is stable over weeks but also its spatial distribution is preserved. The functional role of this spare firing in layer 2/3 neurons could be a high stimulus selectivity (Petersen and Crochet, 2013) in our case of repeated single whisker deflection in one direction. How this sparseness is functionally implemented in the cortex is still not clear. A strong recurrent inhibition could be the mechanism in the reduction of overall firing output from pyramidal neurons and increased sparseness of responses probabilities (Crochet et al., 2011; Gentet et al., 2010; O’Connor et al., 2010a). Whereas, a change in the interneuron output by neuromodulation leading to a disinhibition of pyramidal neurons could be used to temporary modulate sparseness and in turn allows map plasticity and stimulus association (Froemke et al., 2007; Letzkus et al., 2011). Therefore, the spare coding strategy may be good candidate for stimulus representation in the cortex.

*Total population activity encodes the stimulus frequency best over days*

The stimulus evoked activity of individual neurons can be used as a feature (the spatial activity pattern is taken into account) to discriminate frequencies inter- and intra-day-wise. An improved decoding performance of the different stimuli over days was observed if the mean activity of the population is taken as classification feature instead of using the individual neurons as features (Figure 16C). The use of the mean activity to discriminate different frequencies over day is most likely superior because it is less sensitive to slight changes in the population activity distribution compared to the case

where neurons are used as features. Therefore, it would be advantageous for the animal to use the mean activity for stimulus comparison over days. The stable discriminability of the whisker frequencies based on the neuronal responses is reflected by the animals performing a frequency discrimination task with the same pulsatile stimuli. When rodents are trained to discriminate pairs of different frequencies they show a rather large variability in their learning phase duration (Mayrhofer et al., 2013). As soon as the animals have learned the task they showed stable perceptual interpretation of the presented frequencies by successfully discriminating the different stimuli over weeks (Figure 16D).

*Sparse but reliable stimulus processing matches stable percept of animals in discriminating frequencies*

A small group of neurons (~2%) which shows large and reliable stimulus evoked activity is already sufficient to discriminate the different stimuli to a large extent. These high responders – which are likely to be excitatory cells (Barth and Poulet, 2012; Lefort et al., 2009; Margolis et al., 2012; O’Connor et al., 2010a; Yassin et al., 2010) – could be the result of rare large-amplitude synaptic connections which drives these neurons in a reliable way (Lefort et al., 2009). The reliability for this small subpopulation is highest (Figure 17B). On the other hand a large fraction of the neurons shows a weak response to stimulation and a large variability over trials. However, a large population of these low responsive neurons again leads to high prediction strength of the stimulus (Figure 17). Two distinct and complementary coding strategies could be the basis of these observations: 1) A sparse coding strategy of a relatively small subpopulation of neurons, which is activated in a stereotypic way over trials. This sparseness is preserved over long periods (weeks) and could be the neuronal basis for a constant percept. 2) A weak activation and higher response variability of individual neurons, which results in high prediction of the stimulus by reading out the activity of a large neuronal population. The results of the present study indicate that most information about stimulus frequency is carried by a small number of neurons (~2% in supragranular layers, see Figure 17B) and that this information is sufficient to account for most of the neuronal stimulus classification success (80 %). This result clearly favors the first option and supports a sparse coding hypothesis (Olshausen and Field, 2004). Recently, it has been shown that texture encoding was heterogeneous and sparse in the rat barrel cortex (Safaai et al., 2013), supporting our current finding. There is additional experimental evidence that

rats use the integrated spike count (which is proportional to $Ca^{2+}$ response measured here (Lütcke, 2010)) to discriminate frequencies (Gerdjikov et al., 2010; Stüttgen and Schwarz, 2010) or spike rates to differentiate between textures (von Heimendahl et al., 2007). In mice trained on pole detection the most discriminative neurons were in layer 4 and 5 of the barrel cortex but also a sparse population of layer 2/3 neurons highly discriminative (O’Connor et al., 2010a, 2010b). Similarly, psychophysical thresholds for frequency discrimination in primates were best reflected by the neuronal firing rate (Hernández et al., 2000; Luna et al., 2005; Salinas et al., 2000). This fit our finding for rodents where the neurometric derived from the mean population activity matches the psychophysics of animals trained in discriminating vibrotactile stimuli. Mice trained on surface discrimination and on object detection showed behavior-dependent recruitment of long-range projection (Chen et al., 2013a). Here it would be of interest if these projecting neurons also overlap with the sparse population of highly active neurons and act as “hub” cells.

*Competition between plasticity and stability*

As soon as sensory input is withdrawn there is functional reorganization in the corresponding somatosensory cortex (Diamond et al., 1994; Feldman, 2005; Margolis et al., 2012). After whisker trimming, responses evoked by stimulation of the trimmed whisker are reduced. Neurons in the supragranular and infragranular layers respond rapidly to changes in sensory experience (Diamond et al., 1994; Margolis et al., 2012). On the one hand, plasticity enables us to learn new experiences and adapt to new stimulus conditions. On the other and, stability of stimulus representation enables us to recognize familiar stimuli even under noisy conditions (Decharms and Zador, 2000; Lütcke et al., 2013). Our main finding is a remarkable stability of cortical whisker frequency processing on the single cell and population level over many weeks governed by a small population of highly active neurons. The present work probes the stability of cortical stimulus representation on a population level over weeks - made possible by chronic functional neuronal ensemble imaging. The observed map conservation in neuronal ensembles led by a small set of high responsive neurons could be building block for reliable and stable representation of sensory percepts sawn in trained animals.

## 6.5 Methods

*Animals*

In total seven female adult mice (strain: C57BL6J; weight: 20–26 g, Harlan Laboratories, Netherlands) were imaged over time periods of up to 3 months. The age of the animals on the day of headpost implantation was >14 weeks. Mice were housed individually with food *ad libitum* under an inverted 12-hour light/dark regime. All surgical and experimental procedures were approved by the local veterinary authorities, conforming to the guidelines of the Swiss Animal Protection Law, Veterinary Office, Canton Zurich (Act of Animal Protection 16 December 2005 and Animal Protection Ordinance 23 April 2008).

*Headpost implantation, virus injection and cranial window implantation*

The preparation of the animals was split into two separate surgeries (1-3 weeks apart). In a first surgery the area of the barrel cortex was identified and marked by means of intrinsic optical imaging (IOI, Figure 12B) through intact skull and a headpost was implanted for precise and rapid positioning of the animal in the setup. In a second surgery the virus injection was targeted at the single barrel in S1 and cranial window implantation was performed (Supplemental Experimental Procedures).

*Setup and stimulus*

The vibrotactile stimulus consisted of single whisker deflections generated by a piezo bending actuator (T223-H4CL-303X; Piezo Systems, USA). A single whisker was plugged into a glass capillary (GB 120-8P, Science Products GmbH, Germany; tip was melted to reduce dead space), which was mounted on the piezo actuator. The control voltage driving the piezo actuator was generated by a custom-written LabVIEW program (National Instruments, USA) using a multifunctional data acquisition card (PCI-6229; National Instruments, USA) and was amplified by a piezo controller (MDT693A; Thorlabs, USA). Amplitude of the stimulator was calibrated using a laser displacement sensor (ILD1700-2; Micro-Epsilon, Germany). The stimulus consisted of a series of deflections to a single whisker on the animal’s left and/or right whisker pads. Depending on the IOI map and the virus expression area different principal whiskers were used in different animals. The peak velocity of a prototype pulse (taken from a single period 120 Hz cosine wave) was kept constant and the repetition rate of pulses was varied (10, 40, 90 and 110 Hz) on the contralateral side with respect to imaging side. For ipsilateral

stimulation only 90 Hz repetition rate was used. The stimulus duration was 1 second. The stimulator was placed 4 mm away from the whisker pad and led to maximum velocity of 648 °/s. The stimulus sets (pure contra- and ipsilateral stimulation and combinations) were presented in a randomized order within an imaging day to minimize the influence of changes in anesthesia (inter stimulus intervals: 10 -14 s). Each stimulus was presented at least 30 times per imaging day.

*Chronic two-photon imaging*

Chronic imaging started earliest three weeks after virus injection using a custom-built two-photon laser-scanning microscope (Supplemental Experimental Procedures). Functional signals (128 × 128 pixels) were acquired at a frequency of 8 Hz and 256x128 at 11.84 Hz bidirectional scan. Anatomical imaging was performed with a resolution of 256×256 or 512x512 pixels. The scan software and the stimulation generation were controlled with millisecond temporal precision by custom-written LabVIEW programs (National Instruments, USA) running on personal computers using multifunctional data acquisition cards (PCI-6259; National Instruments, USA). Recordings were performed under isoflurane anesthesia (0.7 - 1.1%; Abbott, USA). The respiratory rate was monitored with a piezo element (7BB-35-3, Murata Manufacturing Co., Ltd., Japan) attached to an oscilloscope and was kept at around 150 bpm by adjusting the anesthesia level. For each animal 1 - 4 imaging locations (mean ± SD: 2.9 ± 1.1, n = 7 mice) were followed over a time course of up three month (Figure 12D). The average field of view was 318 ± 86 µm (mean ± SD, n = 20 spots in 7 mice). The medial - lateral and anterior - caudal position of the imaging locations were chosen on the basis of the IOI mapping and the $Ca^{2+}$ responses. Imaging locations were in the supragranular layer (measured from cortex surface, mean ± SD: 146 ± 62, 20 spots in 7 mice).

*Behavior*

Mice and rats (n = 9) were trained to discriminate different pairs of simultaneously presented frequencies on a single whisker in the head fixed situation. The same type of stimuli was used as in the imaging: A 90 Hz pulse train target stimulus (rewarded stimulus) had to be discriminated from distractor pulse train with lower frequencies (0 – 80 Hz in steps of 10 Hz). For a detailed description of the behavioral paradigm consult Mayrhofer et al. 2013. The behavioral data shown here were reanalyzed from the dataset of Mayrhofer et al. 2013.

*Data analysis*

Data analysis was performed using Matlab (MathWorks, USA) and ImageJ (ImageJ, U. S. National Institutes of Health, USA, http://imagej.nih.gov/ij/, 1997-2012). For each channel a background subtraction was performed. First the minimum pixel value in each imaging movie was found and then subtracted from all pixels of the movie. Regions of interest (ROIs), covering either single neuronal cell bodies or neuropil areas, were drawn manually in ImageJ. Pixel values within each ROI were summed for the yellow fluorescent protein (YFP) and cyan fluorescent protein (CFP) photomultiplier channel separately. Dividing the YFP by CFP photomultiplier channel values for each ROI led to the ratio time series (R). The mean R value in the 1100 ms pre-stimulus time interval was used as baseline activity ($R_0$). Individual ROI ratio changes were obtained by applying the following formula: $\mathbf{\Delta}R/R_0 = (R-R_0)/R_0$. High pass filtering was performed to reduce slow shifts (cut off frequency: 0.025 Hz, Butterworth filter, implemented in Matlab). ROIs were drawn manually for each imaging day and were matched manually over different experiments in ImageJ. Movies were aligned over trials by maximizing correlations through xy-rigid shifts of the frames. To compare the activity over different stimulus conditions and recordings for each neuron the $\mathbf{\Delta}R/R_0$ from 100 ms to 1200 ms relative to stimulus onset was integrated for each trial ($\int \mathbf{\Delta}R/R_0 dt$: area under $Ca^{2+}$ transient in %s). 100 ms after stimulus onset was used because of assumed weak baseline activity and therefore fast decay of $Ca^{2+}$ transients from baseline activity. Additional 200 ms were used because of $Ca^{2+}$ transient raise time. The $Ca^{2+}$ response is linear proportional to the action potential fired in a certain time span (Lütcke, 2010). Spontaneous activity was measured either by using a void stimulus (0 Hz) or by shifting the analysis windows back by 1200 ms. From these values a population activity vector for each trial was built where each element corresponds to the stimulus-evoked activity of a single neuron. All population activity vectors of a single imaging day lead to the two-dimensional population activity matrix (with neuron identity and trial identity as dimensions). The $Ca^{2+}$ response probability of a neuron was obtained by using a Schmitt trigger approach: The $Ca^{2+}$ transient had to cross an upper threshold of 1.75 SD relative to baseline and had to stay above a lower threshold of 0.5 SD for at least another 300 ms to be counted as a detected response. The $Ca^{2+}$ response probability was then computed by comparing number of the detected responses to the number of total of presented trials. Individual tuning curves were generated by averaging all trials from all recordings of a neuron. Pooling over animals was done by normalizing the responses to

the median neuronal activity elicited by contralateral stimulation of each animal (median $Ca^{2+}$ responses: 0.938 %s; 1.284 %s; 1.223 %s; 1.422 %s; 0.544 %s; 0.570 %s; 0.505 %s). Correlations between trials of the same or a different stimulus were computed by using the corresponding population activity vector (Pearson's correlation coefficient, corrcoef, Matlab). Reliability-stability matrix: correlation coefficients of the same stimulus and recording day were used to build the reliability values, where correlation coefficients of the same stimulus category but different recording day led to the stability values. The similarity matrix was derived by taking the correlation coefficients between different stimuli within the same recording day. Activity pattern stability was tested by shuffling the population activity matrix either along the neuron identity axis or along the trial identity axis.

*Classification algorithm*

For the quantification of the discriminability of the different stimuli within an imaging day or over days a linear support vector machine (Chang and Lin, 2011) was used on the basis of the population activity matrix. The discriminability of the stimuli was expressed as the cross-validation accuracy (accuracy) by either training the classifier on one half of the data set and testing it on the other half (2-fold cross validation, was repeated 10 times, random splitting) or by training the classifier on data set from one day and testing it with a data set from a different imaging day. To investigate the influence of the population size on the representation of the stimuli a neuronal population was generated from all recordings (spots, days and animals): From each day only 50% of the trials with highest activity were considered. From this remaining data set only the neurons entered the data set where at least 100 trials were left. For neurons for which more than 100 trials were available, 100 trials were chosen randomly. Population size was varied either by picking randomly neurons from the data set, choosing neurons starting with highest activity or neurons starting with lowest activity. In the case of random selection of neurons the selection was repeated 6 times (total number of neurons in data set) / (current number of neurons considered) for the computation of the similarity and the discriminability. The accuracy for each chosen population was derived by the 2-fold cross validation of 10 times. The neurometric curve was defined by the spontaneous population activity and the population activity in response to 10, 40 and 90 Hz stimulation. A trial consisted of the mean of one activity vector drawn from the 90 Hz frequency and the mean of one activity vector drawn from the 0

(spontaneous), 10, 40 or 90 Hz of the population activity without placing back. In half of the cases it was first drawn from the 90 Hz and then from the other categories and in the other half it was done in the reversed way. The classifier was then trained on half of the derived trials and tested on the other half. This procedure was repeated 100 times.

*Statistics*

Statistical errors are standard errors of the mean (SEM) unless otherwise specified. The Wilcoxon signed rank test or paired t-test (Matlab implementation) was used to statistically test differences between two dependent groups. Correlations were computed using Pearson's correlation coefficient (Matlab implementation).

## 6.6 Acknowledgements

We thank Wolfger von der Behrens, Simon Musall and Renaud Jolivet for comments on an earlier version of the manuscript. We also thank Stefan Weber for technical assistance. This work was supported by the EU-FP7 program (BRAIN-I-NETS project 243914 to F.H. and BrainScales project 269921 to F.H.), the Swiss National Science Foundation (grant PP00B-110751/1 to F.H. and B.W.) and SystemsX.ch (project 2008/2011-Neurochoice to J.M.M., and B.W.).

# 7 Project 3: “Two-photon calcium imaging of neuronal population activity during complex discriminative behavior in the head-fixed rat”

Florent Haiss (1, 8, 9, 10)*, Johannes M Mayrhofer(1, 3)*, Milan Scheidegger (1, 4)*, Nadja Olini (1, 3, 5), David J Margolis (2, 3), Dominik Langer (2, 3), Sebastian Kügler (6), Mazahir T Hasan (7), Fritjof Helmchen (2, 3) & Bruno Weber (1, 3)

(1) Institute of Pharmacology and Toxicology, University of Zurich, Zurich, Switzerland
(2) Brain Research Institute, University of Zurich, Zurich, Switzerland
(3) Neuroscience Center Zurich, Zurich, Switzerland
(4) Institute for Biomedical Engineering, University and ETH Zurich, Zurich, Switzerland
(5) Clinical Research Priority Program Sleep and Health, University of Zurich, Zurich, Switzerland
(6) Department of Neurology, Univ. Göttingen, Göttingen, Germany
(7) Max Planck Institute for Medical Research, Heidelberg, Germany
(8) IZKF Aachen, Medical Faculty of the RWTH Aachen University, Aachen, Germany
(9) Institute for Neuropathology, RWTH Aachen University, Germany
(10) Department of Ophthalmology, RWTH Aachen University, Germany

*these authors contributed equally to this work

In preparation for publication

*Author Contributions*

F.Ha., B.W. and J.M.M. conception and design of research; M.S. and N.O. performed pilot behavioral experiments; F.Ha. performed surgeries; D.L. and F.He provided scanning software; S.K. and M.T.H provided virus construct; J.M.M. performed experiments, wrote analysis scripts and analyzed data, J.M.M. and F.Ha. interpreted results of experiments and prepared figures; F.Ha. drafted manuscript; F.He., J.M.M., B.W, D.J.M. and F.Ha. edited and revised manuscript.

## 7.1 Abstract

Discrimination of sensory inputs relies on neural representations in the neocortex. Although two-photon imaging has enabled direct visualization of cortical population activity, its application to awake animals performing complex tasks has been limited to date. Here we present a combined system that allows cellular imaging of the rat neocortex in parallel with psychophysical measurements. Head-fixed rats were trained to discriminate vibrotactile whisker stimuli in a two-alternative forced choice paradigm. Using a newly developed task, rats had to collect a reward from two possible locations to report which stimulus it perceived. Rats were able to discriminate frequency differences of 50 Hz, performing hundreds of trials per day with a performance of up to 90% correct responses. We combined this paradigm with chronic two-photon imaging of somatosensory cortex neurons transfected with the genetically encoded fluorescent calcium indicator Yellow Cameleon 3.60 (YC3.60), enabling long-term imaging of neuronal activity in multiple neurons during the behavioral task for several months. Continuous imaging of identical neuronal populations across trials and days was possible due to a chronic cranial window and the stable expression and function of YC3.60. The combination of the presented behavioral paradigm and genetic sensors thus enables cellular studies of cortical activity during perceptual decision making and learning.

Keywords: head fixation, psychophysics, operant conditioning, whisker, rat, inter-hemispheric, somatosensory cortex, in vivo two-photon microscopy, Yellow Cameleon 3.60

## 7.2 Introduction

One of the prerequisites for experiments designed to investigate neuronal function related to behavior is a tight control of the input that is given to the brain. Ideally, the resulting change of activity upon stimulation should then be measured with a method that is able to simultaneously capture the activity of large populations of neurons. A common method to reduce variability in stimulus delivery is the use of head fixation in non-human primates and rodents. Neurophysiology experiments in head-fixed awake monkeys have a long tradition and have been used to study single and multiple neuron responses to visual stimuli (Wurtz, 1968). The combination of a fixed head position with recording of the eye position allowed the precise control of the retinal input in the awake animal. Similar preparations have been proven to be very useful for many other sensory modalities such as the auditory (Beaton and Miller, 1975), somatosensory (Mountcastle et al., 1990) and vestibular (Angelaki et al., 1999) systems.

The mechanical stability attained by head restriction also facilitates usage of the entire palette of neurophysiological techniques currently available. An enormous amount of behavior-related neuronal data has been acquired in recent decades with single and multi-electrode recordings from single and multiple neurons as well as with imaging techniques such as intrinsic optical and voltage-sensitive dye imaging (Ferezou et al., 2007; Orbach et al., 1985). Furthermore, recent developments in two-photon microscopy enabled *in vivo* structural and functional high-resolution imaging of large populations of neurons (Garaschuk et al., 2006; Grewe and Helmchen, 2009; Svoboda and Yasuda, 2006) with the possibility to determine the subtype and location of these neurons. Initial examples demonstrate that two-photon microscopy promises to be a powerful tool to study neuronal activity in awake mice (Dombeck et al., 2007; Harvey et al., 2012; Huber et al., 2012). The adaption of complex head-fixed behavior combined with two-photon imaging to the rat will however become increasingly important as rats have already served as a model organism in a multitude of studies of higher cortical functions and decision making (for a review of prefrontal cortical function in rats, see (Uylings et al., 2003)).

The primary somatosensory cortex of the rat (‘barrel cortex’) is one of the best-studied primary sensory areas, ranging from molecular to behavioral investigations (Petersen, 2007). The one-to-one relationship between the vibrissae and the cortical columns

processing the respective tactile input, the large cortical representation of these mechanoreceptors and accessibility on the dorsal part of the neocortex make this structure an ideal candidate for neurophysiological investigations in awake behaving rodents (Curtis and Kleinfeld, 2009; Ferezou et al., 2007; von Heimendahl et al., 2007; Hentschke et al., 2006; De Kock and Sakmann, 2009; Krupa et al., 2004; Stüttgen and Schwarz, 2008).

The aim of this work was to advance methods for combining two-photon calcium imaging with complex behavior in the head-fixed rat. We present psychophysical data from rats trained to perform a two-alternative forced choice (2-AFC) frequency discrimination task as well as the corresponding long-term neurophysiological data recorded with a custom two-photon microscope from barrel cortex neurons during behavior. Two-photon imaging was performed repeatedly over several weeks through a chronic cranial window using a genetically encoded fluorescent calcium indicator. This combination of techniques provides a valuable setting to investigate neuronal correlates of perceptual decision making and learning in the upper layers of neocortex with unsurpassed precision.

## 7.3 Methods

*General*

All experimental and surgical procedures were approved by the local veterinary authorities. Four female Sprague Dawley rats in total, weighing approximately 250 g each, were used in this study. Rats were trained in a discrimination task following head-post implantation. The animals were injected with a recombinant adeno-associated virus (rAAV) mediating the expression of the genetically encoded fluorescent calcium indicator Yellow Cameleon 3.60 (YC3.60) in neurons and were imaged using two-photon microscopy. The rats were housed in group-cages of two animals with food and water *ad libitum*, except for the behavioral training where the animals were subjected to water restriction during five days per week. Body weight was assessed prior to each of the two daily training sessions and additional water was given in the case of a body weight loss of more than 10% compared to the body weight with free access to water. The 12-hour day/night cycle was inverted in order to train the animals during the lights-off phase.

*Virus preparation*

rAAV equipped with YC3.60 (Nagai et al., 2004) under the control of a human synapsin promoter was co-transfected with pDp1, pDp2 (ratio 3:1) helper plasmids into HEK293 cells. Seventy-two hours after transfection, HEK293 cells were harvested and packaged viruses were released by repeated freeze/thaw using a dry ice/ethanol bath. Viruses were initially purified by iodixanol gradient centrifugation and were further purified and concentrated by fast-protein liquid chromatography on heparin affinity columns (Amersham) (Kügler et al., 2007). Infectious virus titers were determined in primary neuron cultures. Viruses were delivered through thin glass pipettes by stereotaxic injection (Cetin et al., 2007) to the principal whisker area as described in the next section.

*Surgical procedure*

Anesthesia was induced and maintained with 1–3% isoflurane adjusted to keep pain reflexes subthreshold. The animal’s rectal temperature was controlled automatically by a feedback circuit composed of a rectal probe and a heating pad set to 36°C (Harvard Apparatus, Holliston, MA, USA). The rats were placed in a stereotaxic apparatus and bucain injections were administered subcutaneously prior to the scalp incision. A

circular area of 4-mm diameter of the skull above the barrel cortex (–3 mm from bregma, 3 mm lateral) was thinned in order to locate D1 whisker representation using intrinsic optical imaging with 630-nm illumination. The thinned skull above the identified D1 barrel position was removed to inject 400 nl of rAAV serotype 2/1 (40 nl/min) carrying the YC3.60 construct at 300-µm depth below the dura. The trepanation was then sealed with black dental cement (Tetric Color; Ivoclar Vivadent AG, Schaan, Principality of Liechtenstein) to mark the position for subsequent optical window implantation. Titanium screws (Modus 1.5, 3-mm length; Medartis, Basel, Switzerland) were placed in the skull to anchor the head-cap. Before applying the bonding agent (Gluma Comfort Bond; Heraeus Kulzer, Hanau, Germany), the skull was cleaned and rinsed with saline. After a drying period of 40 s, the bonding was polymerized using a hand-held light source (600 mW/cm$^2$; Demetron LC, Bioggio, Switzerland). The first layers of the head-cap were then put in place by applying transparent light-curing dental cement (Tetric EvoFlow; Ivoclar Vivadent AG) on top of the bonding. Finally, a large screw (M5x15), turned head-down, was cemented into the head-cap above the cerebellum. This screw was used later for head fixation. Antibiotic ointment was applied to the wound (Nebacetin; Astellas Pharma, Munich, Germany). The open skin was sutured and carefully attached to the implant. After surgery the animals were kept warm and provided with analgesics. Antibiotic treatment (1 ml enrofloxacin (Baytril)/500 ml drinking water; Bayer, Leverkusen, Germany) was given for one week. After two weeks, given good recovery, the animals were handled by the experimenter and systematically desensitized to all experimental procedures including head fixation for a minimum of two weeks. After the animals accepted head fixation without signs of stress, the time of head immobilization was gradually incremented from a few seconds to a maximum of 20 min (minimum one week, two sessions per day). After three weeks of training, two of the four animals were subjected to a window implantation surgery. The aforementioned black dental cement and skull were removed with a dental drill to obtain a trepanation with a diameter of 5 mm. Dura mater was removed and the borders were sealed with silicone (Kwik-Sil; World Precision Instruments, Sarasota, FL, USA). A round coverslip (#1, 4-mm diameter) was lightly pressed on the exposed brain and fixed with dental cement.

*Experimental set-up*

The stimulus was presented with a 5-mm long glass capillary mounted to the tip of a piezo bending actuator (T223-H4CL-303X; Piezo Systems, Woburn, MA, USA; 440-Hz resonant frequency of the piezo element), which was fixed on an articulated arm (Baitella, Zurich, Switzerland) to allow positioning of the stimulator. The movement of the bending actuator was calibrated using an optical laser micrometer (RX 03; Metralight, San Mateo, CA, USA) and strain gauge sensors mounted on the piezo element. The training procedure was conducted in a soundproof box. Additionally, 80-dB white noise was presented with one loudspeaker located 10 cm above the rat’s head to prevent auditory cues. The training box was illuminated with infrared light and two cameras that were located above the piezo elements to ensure that the animal did not pull the whisker out of the glass capillary.

*Behavioral paradigm*

After implantation of the head-post and an initial training to establish the tolerance to head fixation, the water-deprived rats were first trained to detect a target frequency on either a left or right whisker. The left and right D1 whiskers were inserted into the glass capillary such that it was located at a distance of approximately 5 mm to the rat’s face. The stimulus consisted of a 2.5-s long 190-Hz sinusoid with amplitude of approximately 200 µm. In a first step, the rats learned in a prompting procedure to associate the location of the target stimulus with the corresponding waterspout in order to obtain a reward. A motorized mechanical system gently turned the animal’s head to one of two waterspouts – according to the stimulus side – located 20° from the center position.

The head-post was fixed to a holder that allowed head rotation in the horizontal plane (Figure 18). The movement could, however, be restricted to a variable amount of rotation (maximally ± 30° from the center position) with a V-shaped brake that fitted the shape of the head-post holder (Figure 18B). Closing the brake completely brought the animal to a center position with minimal inter-trial repositioning error (micrometer range). Head fixation was released immediately following stimulus presentation. In this way, the animal was allowed to perform a left or right rotation of the head to receive a reward from a waterspout located on either side. By choosing one of the spouts, the animal reported which stimulus it perceived – e.g. a stimulation of the left/right whisker – would lead to a reward from the respective waterspout. The lick response was measured with a piezo sensor that was glued to the drinking spout (LDT0-028K;

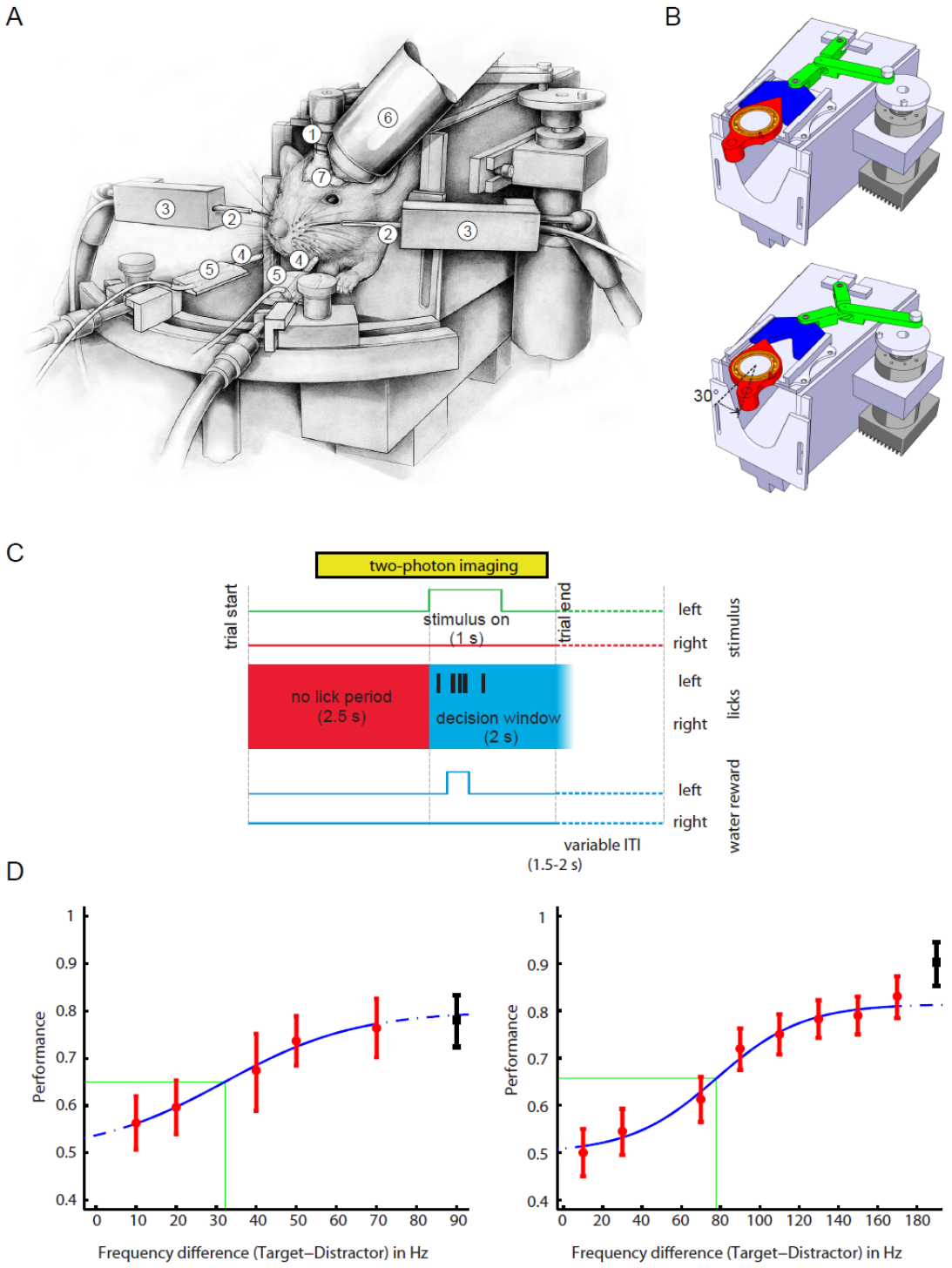


**Figure 18. 2-AFC behavioral apparatus and the head rotation mechanics.**
**(A)** Illustration of a rat in the behavioral apparatus that is connected to the rotation mechanics via an implanted head-post (1). A single whisker is inserted into a glass tube (2) that is glued to a piezo actuator (3) used to deliver the vibration stimuli. The water reward is delivered with two waterspouts (4), which are mounted on a semi-circular rail in front of the animal and equipped with piezo lick sensors (5). The two-photon microscope objective (6) is positioned above the rat’s chronic cranial window (7). **(B)** Head rotation mechanics in the closed center position (upper image). The head-post holder (red) is connected to the animal box (light gray) via a precision ball bearing (orange). The head-post holder is kept in the center position by means of a brake (blue), which is blocked via a toggle lever (green) that can be actuated with a DC motor (dark

gray). Retraction of the brake (blue) allows the head-posted animal to rotate its head to a limited angle (lower image). **(C)** Schematic representation of the time sequence of the behavior paradigm and the two-photon image acquisition (intertrial-interval (ITI)). **(D)** Psychophysical performance of one rat in two different frequency discrimination paradigms. Left graph: Psychometric curve of one animal performing a frequency discrimination based on a pulse-based stimulus (two example stimuli plotted in the inset). The rat had to discriminate between 90 Hz (target frequency, consisting of pulse repetitions taken from a single 120-Hz cosine wave) and lower frequencies (also consisting of pulse repetitions taken from a single 120-Hz cosine wave, for a 40-Hz example). The performance is plotted against the difference of the target pulse repetition frequency to the non-target pulse repetition rate. Right graph: Psychometric curve of the same animal performing frequency discrimination with a target frequency of 190 Hz. The stimulus consisted of sinusoidal vibration applied to a single whisker on each side of the face, as plotted in the inset. The percentage of correct responses is plotted against the difference to the target frequency of the stimulus that was applied simultaneously at the opposite side of the target frequency (distractor frequency).

Measurement Specialities, Hampton, VA, USA). The solenoid (Bürkert, Ingelfingen, Germany) that controlled the water delivery opened only if the first recorded lick was on the correct side. If the rat decided to lick the incorrect spout, no reward was given and the brake was immediately closed to bring the animal back to the center position before starting the next trial. Biases of the animals to lick on a certain side or alternating left/right strategies were prevented using a previously published bias correction algorithm (Knutsen, 2006).

A custom-written LabVIEW program (National Instruments, Austin, TX, USA) in combination with a multifunction data acquisition card (PCI-6229; National Instruments) controlled the behavioral apparatus and recorded the licking responses.

*Two-photon imaging and microscope design*

Imaging was performed using a custom-built two-photon laser-scanning microscope. One passive linear stage (LF 4; Isel, Eichenzell, Germany) and three stepper motor-driven linear stages (LF 6; Isel) with a length of 390 mm were used to move the microscope head in the x-, y- and z-dimension. Rotation of at least ± 90° was achieved by a rotation axis (RDH-S; Isel) that was mounted to the z-linear stage (Figure 19). Each of the motor-driven linear axes carried one mirror mounted at an angle of 45° with respect to the motion direction that deflected the laser beam to the next mirror of the respective axis. The laser beam was then deflected on a mirror located on the z-axis, which aimed at the end of the hollow shaft of the rotation axis mirror. This design allowed translation and rotation of the microscope head with a stable beam position with respect to the galvanometric scanners (6215H; Cambridge Technology, Lexington, MA, USA), scan lens (100-mm focal length), tube lens (200-mm focal length) and the 20× or 40× water immersion microscope objective (0.95, 0.8 NA; Olympus Optical, Tokyo, Japan). The objective was positioned using a piezo motor-driven linear stage with 50-mm travel and a precision of 10 nm (FB05, HR4; Nanomotion, Yokneam, Israel). YC3.60 was excited with a Ti:sapphire laser (870 nm, 140-fs pulses at 80 MHz, Chameleon Ultra II; Coherent, Santa Clara, CA, USA). Emission of YC3.60 was detected with two photomultipliers (H9305-03; Hamamatsu Photonics, Hamamatsu City, Japan) with the following filters: dichroic mirror 515 DCXR, bandpass filter BrightLine HC 542/50 (yellow channel) and bandpass filter BrightLine HC 475/64 (blue channel) (Semrock, Rochester, NY, USA). For scan mirror control and photomultiplier data acquisition, custom-written LabVIEW software was used (Langer and Helmchen, 2009). Functional signals (128 × 128

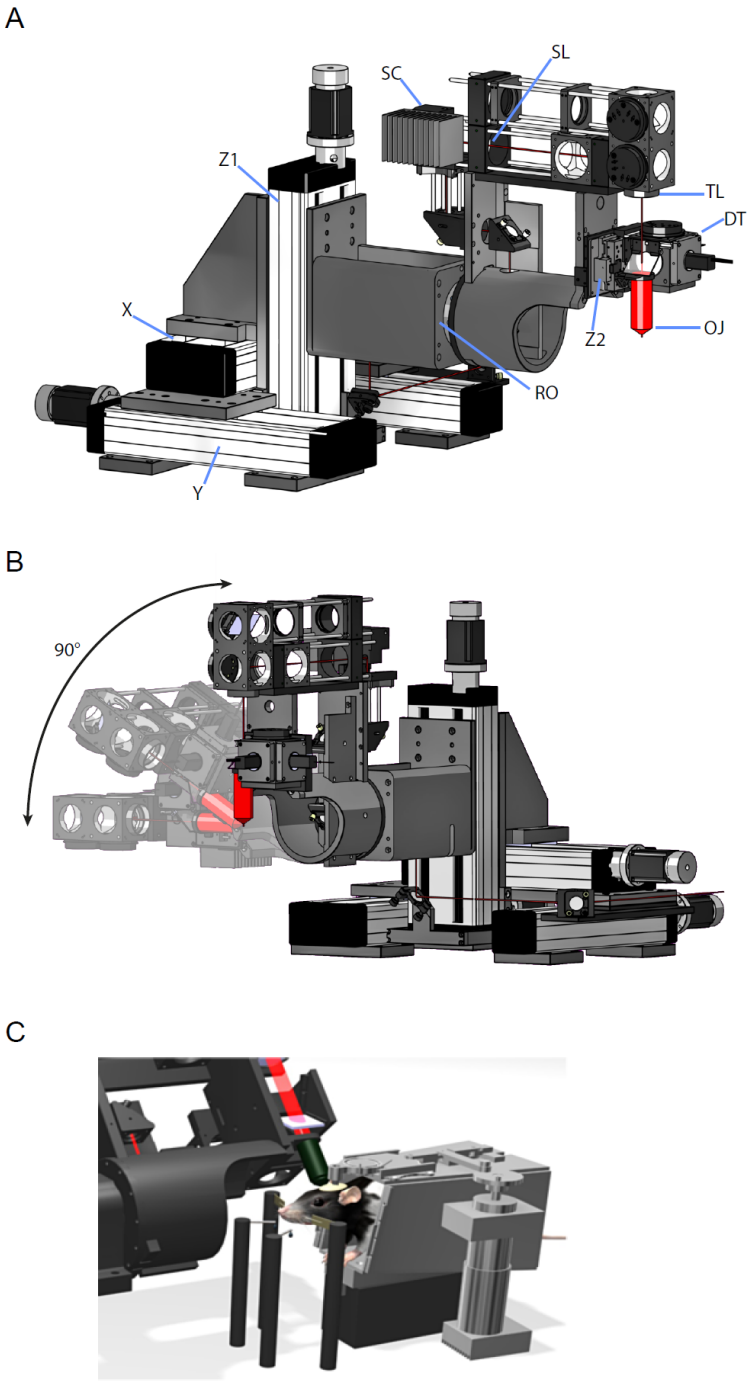


**Figure 19. Two-photon microscope with the behavioral apparatus.**
**(A)** Computer rendering of the two-photon microscope (left perspective). Large x, y and z axes with 13 cm of possible movement (X,Y,Z1). Galvo-scanner (SC), scan lens (SL), tube lens (TL), piezo motor for objective positioning (Z2), 16× objective (OJ; red) and the two-channel PMT detector assembly (DT) are mounted on the rotation axis (RO) and can be tilted around the focus of the objective by ± 90°. **(B)** Computer rendering of the two-photon microscope in the upright, 60° and 90° tilted position (shaded versions for 60° and 90° tilt). **(C)** Rendered image of the microscope head with the objective (green) pointing to the cranial window of a head-fixed rat. The laser beam is colored red.

pixels) were acquired at a frequency of 8 Hz. Anatomical imaging was performed with a resolution of 256 × 256 pixels at 4 Hz.

*Data analysis*

Data analysis and image motion correction were performed using Matlab (MathWorks, Natick, MA, USA). Background subtraction was computed by first finding the minimum pixel value in the whole imaging movie and by subtracting this value from all pixels of the entire movie. This was done for each channel and individual movies separately. Regions of interest (ROIs), encompassing either neuropil areas or single neuronal cell bodies, were drawn manually. Pixel values within each ROI were summed separately for the yellow fluorescent protein (YFP) and cyan fluorescent protein (CFP) photomultiplier channel. The ratio time series (R) were generated by dividing the YFP by CFP photomultiplier channel values for each ROI. The baseline activity (R0) was computed as the mean R value in the 2-s pre-stimulus time interval. Individual ROI **Δ**R/R0 traces were computed with the following formula: (R-R0)/R0. Image motion correction was then performed using a hidden Markov model-based algorithm (Dombeck et al., 2007). Movies containing z-motion and strong distortions due to fast xy-motion were not included in the subsequent data analysis using the following criteria. The correlation value of each ROI in each frame of the individual trial movies had to be larger than the median correlation value minus two times the standard deviation (SD) of the correlation value of all trials within a session. To ensure the presence of the individual cells across trials, the correlation value between the individual ROIs and the respective ROIs of a high-resolution image (256 × 256 pixels) of each imaging area had to be larger than the aforementioned threshold. All correlation thresholds were computed for each imaging session separately. Neurons were included in the final analysis if they had at least 20 trials in the contra- or ipsilateral stimulus condition over all behavioral categories. Classifying neurons as stimulus responsive or non-responsive was conducted in the following way. First, calcium transients of individual neurons that crossed a threshold of one SD (computed from the entire trial) for at least two out of three frames (8-Hz imaging rate) were classified as neuronal events and were used to compute a post-stimulus time histogram (PSTH). Neurons that had an event rate larger than the SD of baseline event rate in the post-stimulus time window were classified as stimulus-responsive cells. The response probability was computed from PSTH event rate in the 0–400-ms time windows after stimulus onset.

Peak activation of each neuron was computed by taking the maximal value of the 0–400-ms post-stimulus time window from the average of the individual **Δ**R/R0 traces from one session for each stimulus condition.

Psychometric curves were obtained by computing the performance for each stimulus pair and plotting it against the difference between distractor and rewarded frequency. The confidence intervals were computed on the basis of a binomial distribution taking a confidence level of 95%. Psychometric functions were fitted using psignifit version 2.5.6 (see http://bootstrap-software.org/psignifit/), a software package that implements the maximum-likelihood method described by Wichmann and Hill (Wichmann and Hill, 2001). A logistic function $\psi(x;\alpha,\beta,\gamma,\lambda) = \gamma + (1-\gamma-\lambda)F(x;\alpha,\beta)$,

where $F(x;\alpha,\beta) = 1 / (1 + \exp[(\alpha - x) / \beta])$

was fitted (fit parameters: $\alpha$, $\beta$, $\gamma$, $\lambda$; $\gamma$ fixed to 0.5 and $\lambda$ constrained between [0 0.2]) to the data points and was used to obtain the discrimination threshold and slopes. The discrimination threshold was defined as the frequency difference between distractor and target frequency at which the logistic fit reached 50% of its cumulative value.

*Statistics*

Statistical errors are standard errors of the mean unless otherwise stated. Wilcoxon signed-rank tests and Mann-Whitney U-tests (Matlab implementations) were used to statistically test differences between two dependent or between two independent groups of observations, respectively. Correlations were analyzed using Pearson's correlation coefficient.

## 7.4 Results

*Behavioral apparatus*

The goal of this work was to combine a 2-AFC paradigm for head-fixed rats with functional two-photon imaging. The presented apparatus allows the animal to perform a large number of trials in a tactile frequency discrimination paradigm. We furthermore developed a two-photon microscope that has a high degree of positioning freedom such that dorsal and lateral areas of neocortex can be easily accessed and imaged during behavior. The basis of this head-fixed 2-AFC is a behavioral box equipped with a head rotation mechanics that can be fixed during stimulus delivery and released to allow a left and right horizontal rotation of the animal’s head in order to access two waterspouts for reward delivery (Figure 18A). The counterpart used to secure the implanted head-post is connected to the behavioral box with a ball bearing that allows rotation around the vertical axis (Figure 18B). This rotation mechanism can be blocked with a brake (Figure 18B). Retracting this brake allows a variable range of head rotation angles depending on how far this DC motor-controlled brake is retracted. The repositioning error had a SD of 3.5 µm in the x-dimension and 1.6 µm in the y-dimension, measured directly at the head-implant of an awake rat performing the discrimination task (n=15 trials).

*Two-photon microscope design*

The presented two-photon microscope has been designed to allow a high degree of positioning flexibility without the need to move or rotate the animal and the components necessary to control and record the animal’s behavior during the 2-AFC discrimination task. The use of three large linear stages and one rotation stage allows objective movement of 13 cm in x, y, z and rotation of more than ± 90° such that most dorsal and lateral parts of the rodent brain can be easily targeted and imaged (Figure 19). The rotation axis lies within the focal point of the objective, allowing structures in the middle of the imaging area to be kept in focus while rotating the microscope head. One additional fast linear piezo stage was used to position the objective with a precision of 10 nm (travel range of 50 mm). This device allows rapid retraction of the microscope objective to avoid collision with the implant when the animal is allowed to rotate its head in order to retrieve a reward, and subsequent repositioning of the objective when the rat’s head is locked in the center position for stimulus delivery. This feature can be

useful in experiments where imaging occurs during the first learning phase when the head motion is important to prevent unwanted impulsive licking behavior. However, after an initial training with head rotation, rats were also able to perform the task without head rotation while solely using their tongues to reach one of the two waterspouts. Therefore, the objective was kept in a fixed position during the whole imaging session.

*2-AFC task and psychophysical performance*

Rats first learned to associate the reward location in a simple detection task where a whisker vibration composed of a 190-Hz sinusoidal vibration (peak velocity 1000°/s) was randomly presented on one whisker on either the left or the right side (Figure 18C). After two weeks of detection training, an additional lower frequency vibration was presented simultaneously on the opposite side of the target stimulus, ranging from 10 to 180 Hz with the same amplitude as the target stimulus (Supplementary movie S1). Psychophysical performance was also assessed in a second task where the peak velocity was kept constant (790°/s) and the frequency of pulses – taken from a single 120-Hz cosine wave – was varied from 5 to 85 Hz for the non-target and 90 Hz for the target frequency. The licking response of the animals was recorded and served to discern which side they chose. The animals were able to perform more than 200 trials in one session every day in this 2-AFC tactile discrimination task.

The performance of the animal increased as a function of stimulus frequency difference and hence of the peak velocities applied to the whiskers (Figure 18D). Rats were able to detect a difference of 78 Hz to the 190-Hz target frequency ($p<0.05$ in one animal) in the paradigm where the animal had to discriminate different sinusoidal stimuli. In the paradigm where the peak velocity was kept constant by varying the repetition rate of a prototype pulse, rats had a threshold of approximately 50 Hz.

*Two-photon imaging of tactile responses during behavior*

We combined the aforementioned behavioral task with two-photon imaging of neuronal calcium activity in the barrel cortex with the presented novel microscope design (Figure 19; n=4 animals). The rat’s head was left in a comfortable upright position during the task while the rotation axis of the microscope was moved such that the objective was perpendicular to the surface of the primary somatosensory cortex (barrel cortex). YC3.60 was introduced into neurons via infection with a rAAV injected into the representation of the whisker D1, which has been identified with intrinsic optical

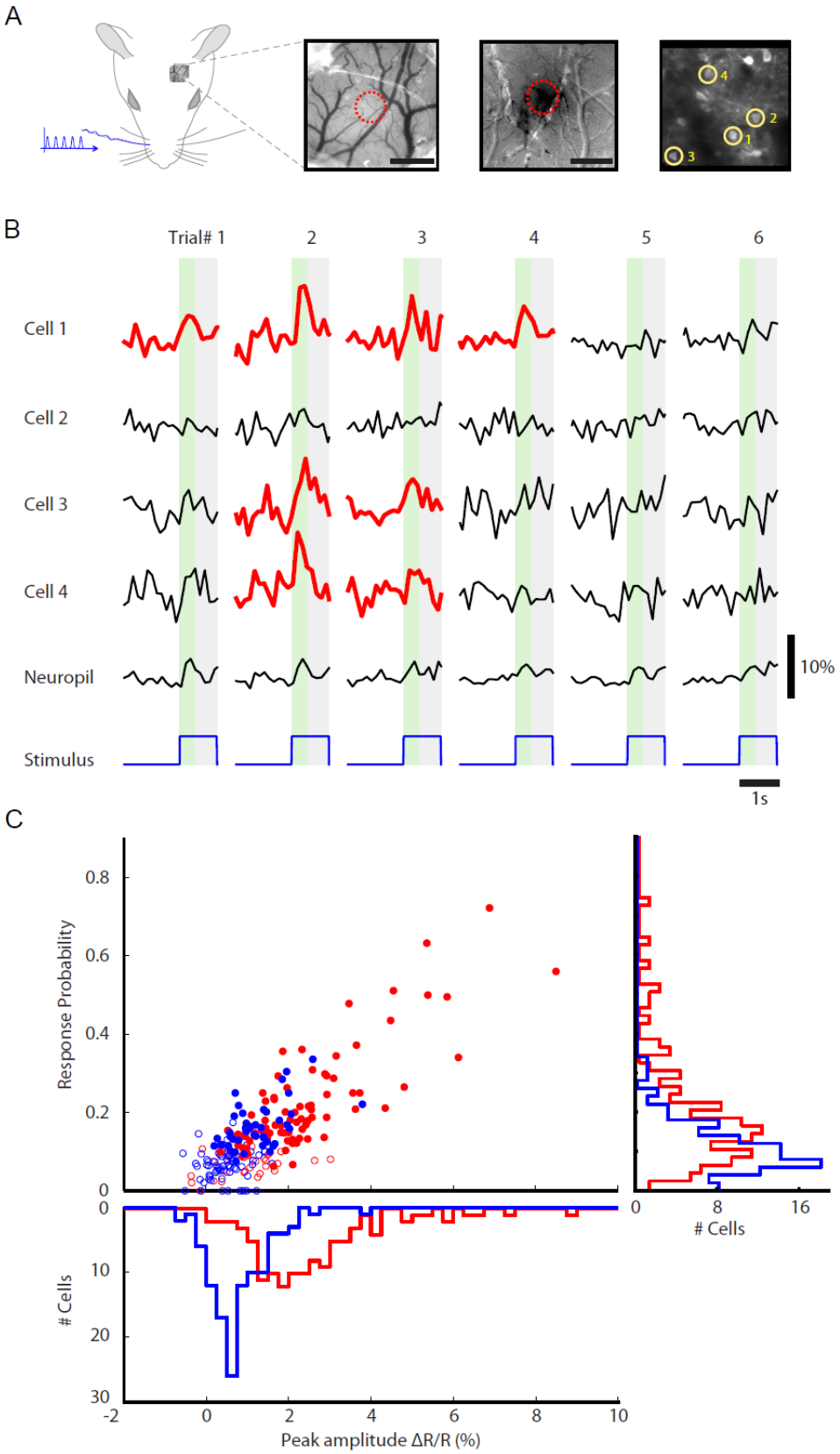


**Figure 20. Single trial activity and population activity of neurons and the neuropil of an awake rat performing a detection task.**

**(A)** Left schematic drawing: Stimulation and imaging configuration. Surface vessel image taken with 570-nm illumination (left image). Intrinsic optical imaging map of single whisker stimulation under anesthesia (middle image). The dark area represents the single whisker activation region. Red dashed circle indicates the virus injection and two-

photon imaging site. Right image: Two-photon image of neurons expressing the genetically encoded fluorescent calcium indicator YC 3.60 in the area indicated by the red dashed circle in the left and middle images. Regions of interest used to compute the calcium transients in panel b are depicted by yellow circles. **(B)** Single cell, consecutive single trial ΔR/R calcium traces of an awake rat performing a detection task (190-Hz sinusoidal stimulus applied on either the left or right side of the face). Red traces indicate single trials that were classified as responses to the contralateral stimulus. **(C)** Population scatter plot of the response probability versus peak calcium responses for all rats (n=4). Closed circles are cells that were classified as responders to the stimulus (red: contralateral stimulation; blue: ipsilateral stimulation). Right subpanel: Population histogram of the response probabilities plotted in the left subpanel. Lower subpanel: Population histogram of the peak of the average calcium transients (color code same as in the upper left subpanel).

imaging of the somatosensory cortex prior to the optical window implantation (Figure 20A). The vessel pattern (Figure 20A) acquired during the intrinsic optical imaging session served as a reference to navigate the two-photon microscope to the center of the D1 whisker representation expressing YC 3.60 in neurons of the upper layer of neocortex.

The average timespan of functional two-photon imaging was approximately 50 days (maximum timespan was 118 days for one animal). The maximum timespan covered with functional imaging of the same imaging area in one animal was 57 days. The average imaging area had a size of 130 × 130 µm and was located at an average depth of 140 µm (range of 30–200 µm). We were typically able to image the activity of approximately 16 cells per imaging area in 2–6 imaging areas per animal (range of 6–29 cells and a total of 242 cells in four rats).

Tactile stimulation produced calcium transients in neuronal cell bodies, reflected in the increase of the ratio taken from the yellow and cyan fluorescence emitted from YC 3.60. The use of this ratiometric calcium indicator in combination with the offline motion correction algorithm allowed single trial fluorescence traces of individual cells and the neuropil to be obtained during the behavioral task (Figure 20B). On average, 20% of the trials were rejected from analysis due to image artifacts caused by movement of the animal mainly during the licking/reward phase of a trial. Single whisker stimulation on the contralateral or ipsilateral side of the imaging site elicited responses in 76% and 36% of neurons, respectively (contralateral, n=112 cells; ipsilateral, n=109 cells; see methods section for the definition of responsive cells) (Figure 20B). Only a small fraction of neurons responded with a high response probability and large peak calcium responses (median response probability for contralateral stimulation: 0.148, SD 0.130 and for ipsilateral stimulation: 0.094, SD 0.067; median peak of calcium transients contralateral: 0.017, SD 0.015 and ipsilateral: 0.007, SD 0.007) (Figure 20C). Neurons with a high response probability for contralateral and ipsilateral stimulation also showed a large peak in the calcium transients and, therefore, high correlation coefficients (contralateral: $r=0.80$ $p<0.001$, n=82 cells; ipsilateral: $r=0.52$ $p<0.001$, n=43 cells) (Figure 20C). Average peak calcium responses during the discrimination task were larger when the animals were engaged in the task (correct and error responses) compared to the situation where the animals did not respond to the presented stimuli (miss trials) (Figure 21A; $p<0.001$, n=42 cells). However, we did not observe a difference in the peak calcium

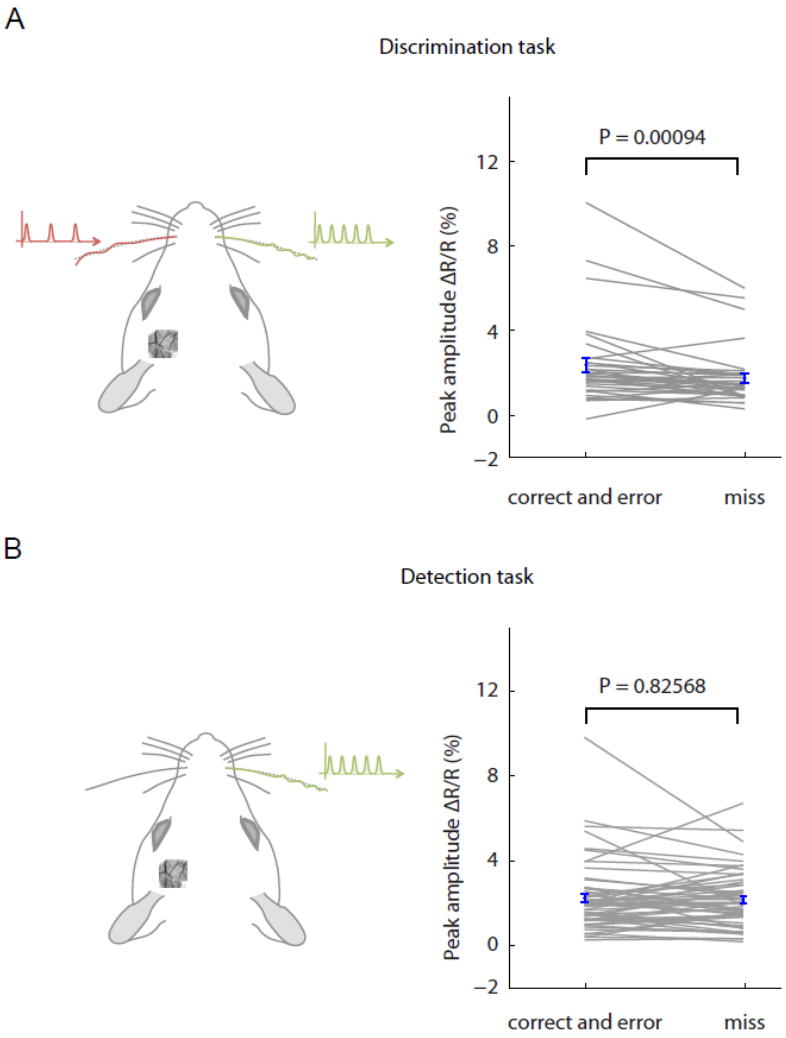


**Figure 21. Behavioral state dependent neuronal responses.**
**(A)** Averaged neuronal activity for individual cells of all animals (n=4) performing a frequency discrimination task. Left schematic drawing: Stimulation and imaging configuration. Right graph: Cell-wise peak of calcium transients during correct/error responses and missed trials. **(B)** Averaged neuronal activity for individual cells of all animals (n=4) performing a detection task. Left schematic drawing: Stimulation and imaging configuration. Right graph: Cell-wise peak of calcium transients during correct/error responses and missed trials.

response amplitude between the correct/error and miss trials in the population of imaged neurons in the detection task (Figure 21B; p=0.83, n=56 cells).

*Long-term two-photon imaging with the durectomized rat cranial window preparation*

The dura mater of rats is opaque and does not allow two-photon imaging of neuronal activity at a cellular level. We developed a chronic window preparation where the dura is removed and regrowth is prevented with silicone (Supplementary Figure S 8). We were able to image neuronal activity for more than three months after the chronic window implantation and the expression of YC 3.60. Images of the surface vessels at different days are shown in Supplementary Figure S 8. Two-photon images (Figure 22A, Supplementary Figure S 8) and the activity (Figure 22B) of the same neurons in one imaging area were recorded for several days. Neuronal and neuropil responses to a contralateral whisker stimulus in a detection task were visible up to four months after injection of the virus carrying YC 3.60. The stability of the individual cell calcium responses was quantified by correlating the peak calcium trace activity from one imaging session with the peak calcium trace activity of the same cells from the previous session. The correlation was high for the pooled data of all cells (contralateral stimulation: $r=0.71$ $p<0.001$, n=54 cells; ipsilateral stimulation: $r=0.35$ $p<0.01$, n=27 cells). Hence, we could observe stability of responses of layer 2/3 neurons to contralateral stimulation over days.

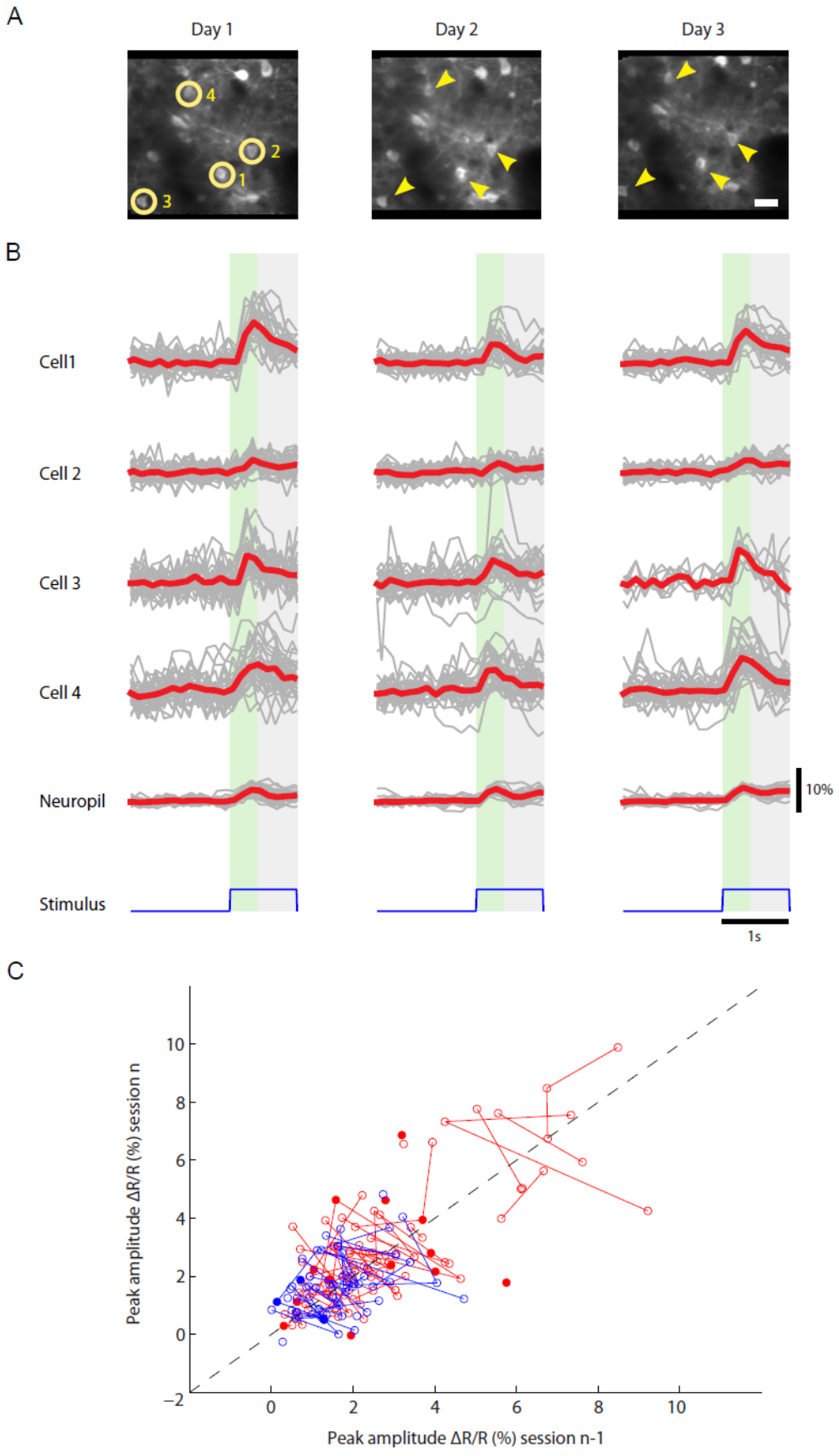


**Figure 22. Single trial activity of single neurons and the neuropil over days of an awake behaving rat performing the behavioral task.**

**(A)** Two-photon image of layer 2/3 neurons expressing YC 3.60 in the left cortical hemisphere. Regions of interest used to compute the average calcium transients in

panel b are depicted by yellow circles and arrowheads. **(B)** Single trial (gray) and averaged (red) ΔR/R calcium transients from four neurons and the neuropil (top to bottom traces). **(C)** Correlation of peak of calcium transients from one session with the previous session (n=4 rats; closed circles: single cell activity from one session plotted against the previous session with at least a 72-hour time difference. Lines connecting data points: session pairs of the same cell. Red: contralateral stimulation; blue: ipsilateral stimulation).

## 7.5 Discussion

We have developed a 2-AFC task and a two-photon microscope that in combination allowed us to record neuronal activity during complex discriminative behavior. We furthermore developed a chronic cranial window with removed dura for rats that remained clear and stable for several months after implantation. Neuronal signals from the genetically encoded fluorescent calcium indicator YC3.60 could be recorded throughout this time.

We combined the advantages of the head-fixed preparation with the amenity of the behaviorally well-controlled 2-AFC paradigm. The animal has to discriminate two frequencies presented at the same time to one specific whisker on the left and right side. The rat reports its decision in this perceptually rather demanding task by turning its head in an intuitive fashion towards the side where the stimulus indicates the reward location. Therefore, the head rotation itself is a report of the perceived stimulus. This is very akin to the long-standing standard of head-fixed primate experiments where the monkey reports the percept, for example, by activating one of two possible levers. Head-fixed rodent experiments, however, were typically conducted in a go/no-go manner (Stüttgen and Schwarz, 2008; Stüttgen et al., 2006; Welsh, 1998). The 2-AFC task is a popular method in human and monkey psychophysics and has several advantages compared to the go/no-go paradigm. Thirsty water-deprived animals have a natural tendency to lick irrespective of the stimuli presented, making it difficult to condition them to report what they perceived. This impulsive behavior can only be controlled with punishing measures. On the other hand, it is also difficult to interpret the animals’ behavior when they do not respond by licking, which could be due to a lack of thirst and motivation or alternatively because they did not perceive the stimulus. These difficulties can be avoided with 2-AFC tasks where the licking response is not the primary indicator of the percept. The presented task gives the animals the possibility to respond in three ways. They either choose one of two reward locations or indicate that they are not engaged in the task by not turning their heads to one of the two waterspouts. Using these clearly defined behavioral response categories allowed us to compare response properties of layer 2/3 neurons in the respective conditions. We observed larger responses for the condition where the animal was engaged (correct and

error responses) compared to the situation where the animal did not respond to the stimulus (miss condition).

Using YC3.60 we were able to record neuronal activity in layer 2/3 of the neocortex during complex discriminative behavior. The presented behavioral paradigm is furthermore well suited to investigate inter-hemispheric interactions that occur in the primary somatosensory cortex as the animal has to discriminate two frequencies applied simultaneously on the right and left side of the snout. We observed stimulation-driven activity in the hemisphere ipsilateral to the side of the whisker vibration. Ipsilateral responses were, however, smaller and less common than contralateral responses in layer 2/3 neurons (Figure 20C).

Neuronal activity in the upper layer 2 was, however, sparse. Few cells were highly active during tactile stimulation. This phenomenon has been reported in two-photon imaging, whole-cell patch-clamp and extracellular studies in anesthetized and awake animals (Crochet and Petersen, 2006; Kerr et al., 2007; De Kock and Sakmann, 2009).

The presented fully motorized microscope has several advantages concerning the flexibility of positioning the objective. The precision of the linear and rotation axes enables quick automatized repositioning from animal to animal and would also be suited to repositioning within an experimental session such that multiple locations within one cranial window or several cranial windows would be attainable. The large rotation angle also allows the imaging of areas located more laterally such as the auditory cortex or the secondary somatosensory cortex. 3D scanning strategies that have recently been developed to record the activity from hundreds of neurons in a volume (Gobel and Helmchen, 2007) could be combined with the presented microscope design as the large linear axes used in this design easily allow additional loads to be carried by the microscope.

The genetically encoded ratiometric calcium indicator YC3.60 exhibits stable expression over months without signs of cytotoxicity such as fluorescent cell nuclei that can be observed, for example, with the genetically encoded calcium indicator GCaMP3 (Tian et al., 2009). The stability over time of the cranial window preparation and YC3.60 is, therefore, well suited for long-term experiments where the activity of a specific neuronal population can be followed during the learning phase of a behavioral task. Future experiments will take advantage of these features to track changes in response patterns as the animal is learning the tactile discrimination task. The presented work has

been performed with rats. However, we have also successfully adapted the paradigm for mice in combination with the two-photon microscope design (data not shown here). Mice are presently the most elaborate mammalian genetic model organism. Transgenic mouse driver lines that express Cre recombinase in specific cell types (Luo et al., 2008; O’Connor et al., 2009) can then be used to target genetically encoded calcium indicators or subtypes of neurons. These recent developments will enable the recording and interference of the activity of specific neuronal subsets during complex behavior, which will help to elucidate their contribution to perception and decision-making processes.

In summary, the novel 2-AFC task in combination with the genetically encoded fluorescent calcium indicator YC3.60 and the microscope design provide an ideal framework to perform simultaneous psychophysical and neurophysiological measurements in the neocortex. The presented method is certainly not limited to the tactile modality and could be easily adapted for visual, auditory or olfactory stimulation.

## 7.6 Acknowledgements

We thank Stefan Weber for technical assistance. This work was funded by the NEUROCHOICE project of SystemsX.ch (FHe, BW), the EU-FP7 program (BRAIN-I-NETS project 243914 to FHa and FHe, and BrainScales project 269921 to FHa and FHe) and the Swiss National Science Foundation (grant #PP00B-110751/1 to FHa and BW). We also thank Peter Roth for the illustrations.

# 8 Discussion

*Frequency discrimination versus single whisker deflection*

In our task setting we used temporally extended stimuli on both sides of the animal's snout. Pulsatile stimuli of 1 sec duration with different repetition rates were delivered to individual whiskers (Figure 5). Such streams of inputs may occur when the rodents are running in tunnels and their macro-vibrissae are touching the walls and the ground. Do animals use the vibrotactile information generated in this situation for their navigation when visual cues are less informative or simply cannot be perceived? Here, we showed that rodents (mice and rats) were able to discriminate different frequencies in the range of 10 – 90 Hz. These frequencies can be related to the physical properties of a surface, since rough surfaces induce more fast whisker deflections (so called stick-slip events) than smooth surfaces (Wolfe et al., 2008). Hence, rodents could use this frequency information for orientation in their environment and decisions of memorized food locations. Such streams of successive stick-slip events can be considered as one extreme stimulus conditions. Another extreme stimulus condition is a single and strong whisker deflection on one side of the animal's snout. It has been shown that mice can reliably detect brief and strong whisker deflections (Sachidhanandam et al., 2013). The somatosensory processing of these two extreme stimulus condition may be very different. For single brief whisker deflections, it was shown that corpus callosum-mediated reduction of a contralaterally presented deflection occurred when an ipsilateral deflection preceded the contralateral deflection (Shuler et al., 2001). In the hind paw region of the somatosensory cortex, a similar interhemispheric inhibition mediated by $GABA_B$ receptors was identified (Palmer et al., 2012). In contrast, we saw a weak ipsilateral modulation which showed a net excitatory component (Figure S 6). It remains open if these two effects rely on two distinct processing mechanisms (circuits) or on the fact that the processing of one hemisphere is distributed to (continued on) the other (Palmer et al., 2012; Petreanu et al., 2007).

At this point, it is unclear if the stimulus feature (frequency) used in this study is meaningful for the animal. Barrel cortex neurons show strong adaptation (Khatri, 2004; Melzer et al., 2006), which suggests the whisker system is more tuned for detecting changes in a constant stream of vibrotactile input rather than extracting a certain stimulus feature (like frequency). This would also explain the poor "Weber-fraction" of

about 0.5 in our task setting (Figure 7). The direction of whisker deflection activates distinct neuronal populations (Andermann and Moore, 2006; Kremer et al., 2011; Tsytsarev et al., 2010), but there is no clear behavioral evidence that rodents can use this feature to solve a task. It would be beneficial to investigate whether rodents can better differentiate vibrotactile stimuli (e.g. different directions, different whiskers, different accelerations), which have a more distinct neuronal representation / processing compared to the vibrotactile pulsatile stimuli used here (Figure 14).

*Long learning phase*

With our training procedure it took an average of 14 days for the animal to reach a high and stable level during the detection paradigm (Figure 8). When we compare this to simple detection of a whisker deflection in a Go/NoGo setting (~7 days), this seems to be surprisingly long (Sachidhanandam et al., 2013). Similarly, in a pole detection paradigm (Go/NoGo), mice were able learn the task within 6 days to a sufficiently high level (Huber et al., 2012). The most reasonable explanation is that it takes the animals much longer to associate the rewarded stimuli with two drinking spouts in the 2AFC setting (i.e. the complexity of the task). When presenting the animals with difficult frequency pairs (e.g. 90 Hz versus 80 Hz) we also had to take care that enough easy frequency pairs (e.g. 90 Hz versus 10 Hz) are presented in between to keep the animal motivated (i.e. a reasonable level of difficulty). Another important point is that different laboratories use different experimental procedures in training animals. For example, a higher deprivation level of the animal can lead to more performed trials per day (own observation) and therefore to a learning within fewer sessions. Since animal law differs over countries laboratories could exploit this fact to different degrees and by that pushing the trial numbers.

*Relating a stable psychophysics to a stable percept – is it a flaw?*

The measurement of a psychophysical curve of a certain stimulus feature enables us to characterize objectively the sensibility of a sensory system in differentiating the strength of a stimulus feature (e.g. frequency of tones, whisker vibrations). In more technical terms, this is a black box approach: a defined input leads to a measureable output which can be described by a receiver operator characteristic (ROC) (Stüttgen et al., 2011). Animals were trained twice a day over months, resulting in over-training as indicated by a stable discrimination performance for the presented frequency pairs (Figure 16). This can be a desired result for relating neuronal responses (e.g. neurometric) to

psychophysics (Stüttgen, 2010) or studying behavior induced and not learning induced changes in sensory processing, since learning may also effect primary sensory cortex in this kind of task (Siucinska and Kossut, 1996, 2004; Yotsumoto et al., 2008). The similar psychophysical curves and thresholds across animals speak for a similar sensory processing across animals, which should be a prerequisite for studying the common neuronal mechanisms in perceptual decision making (Figure 7). We deduced from the stable psychophysics (i.e. ROC) that the percept should be preserved, but this does not need to be the case. It could well be that the animal had already a stable percept at the beginning of the training. The stability of the responses (Figure 15, Figure 16) suggests that the sensory percept of different stimulation frequencies is stable, but the association of the different frequencies within the task setting has to be learned by the animal. One way out of this dilemma would be to define a stable percept by a constant psychophysics or stable performance. This of course does not solve the last mentioned problem but could at least help us the grasp this ill-defined expression on a more experimental basis.

*Behavioral modulation of stimulus processing*

The presented 2AFC task allowed us to differentiate three well distinguishable behavioral categories (see also Introduction). We observed larger $Ca^{2+}$ responses for the condition where the animal was engaged (correct and error condition) compared to the situation where the animal did not respond to the stimulus (miss condition) (Figure 21). This suggests during the engaged condition there was an enhanced representation of repeated or temporally extended stimuli (less response adaptation; (Castro-Alamancos, 2004; Harris and Thiele, 2011)). For example, barrel cortex neurons show less response adaptation to repetitive single whisker deflection when going from an anesthetized state to an awake state (own observations and personal communication with Simon Musall and Wolfger von der Behrens; (Castro-Alamancos, 2004)).

*Why is the sparse coding scheme so appealing to us?*

The reason for a sparse coding in cortex remains unclear. However, there are some potential advantages of this coding strategy (see also Introduction). First, if only a subset of neurons fire action potentials a large amount of energy (Adenosintriphosphate (ATP)) is conserved. Action potential firing uses approximately a third of the signal transmission and 13% of the total neuronal energy budget (Lennie, 2003). Second, if only a few neurons are activated for a certain stimulus feature (here, repeated whisker deflections)

the storage capacity is increased. Third, related to the point before, a certain stimulus feature becomes more explicit because it is represented in a distinct subpopulation of neurons and can be read out from a neuron or population of neurons down-stream. Forth, depending on the influence of this sparse population on neurons down-stream, a small shift or change in firing (e.g. silencing one neuron) could have a drastic effect on that neuron(s). This could allow the system to adapt rapidly to changed stimulus conditions (Margolis et al., 2012) or enable an association with a different modality (fear conditioning). Back propagating action potential firing and dendritic disinhibition could be powerful neuronal mechanisms establishing this link (Larkum, 2013; Letzkus et al., 2011).

*Weak bilateral interaction in the supragranular layers*

The presented behavioral paradigm is well suited to investigate inter-hemispheric interactions that occur in the primary somatosensory cortex as the animal must discriminate between two frequencies applied simultaneously on the right and left side of the snout. We observed stimulation-driven activity in the hemisphere ipsilateral to the side of the whisker vibration. Ipsilateral responses were smaller and less common than contralateral responses in layer 2/3 neurons (Figure 20, see also Figure S 6). In contrast, previous reports for layer 5 in the rat showed that ipsilateral induced responses were comparable to the contralateral responses (Shuler et al., 2001; Wiest, 2005). Furthermore, Channelrhodopsin-2–assisted circuit mapping of long-range callosal projections showed stronger layer 2/3 to layer 5 projections compared to layer 2/3 to layer 2/3 projections (Petreanu et al., 2007). Therefore, bilateral integration of vibrotactile stimuli is layer dependent and the presented study should be extended to deeper layers of cortex.

*General methodological considerations*

The presented physiological results are restricted to the supragranular layers of the barrel cortex because of methodological reasons. However, there are differences between layers reflected by the composition of different neurons types and the connectivity within the barrel column and with other areas. Therefore, this study can only be a partial description of stable sensory processing in the whisker system.

Intracellular calcium changes are necessary to cause different forms of cellular plasticity. Since $Ca^{2+}$ has to bind at a GECI to change its fluorescence properties and report changes in intracellular $Ca^{2+}$, it also acts as an artificial $Ca^{2+}$ buffer. It has been

hypothesized that GECIs can lead to impaired plasticity. For GCaMP3, no perturbation of long-term potentiation in hippocampal brain slices was reported (Huber et al., 2012) and also YC3.60 expressing neurons show normal and reversible plasticity effects (Margolis et al., 2012), which speaks for unaffected plasticity in neurons expressing GECIs. Furthermore, the genetically encoded ratiometric calcium indicator YC3.60 exhibited stable expression over months and animals trained in discriminating pairs of vibrotactile frequencies showed normal psychophysics.

Since 80% of neurons are excitatory and 20% are inhibitory, there is a systematic sampling bias which puts a focus on excitatory cells (but this holds for all recording techniques). For future studies this could be circumvented by expressing the GECI only in GABAergic neurons using a corresponding Cre mouse line.

An obstacle in $Ca^{2+}$ imaging is that positive firing rate changes have a greater influence (increase) on the calculated ratiometric signal compared to inhibition phases (decrease). Therefore, it is difficult to identify neurons which are inhibited. For example, some neurons become silent upon stimulus presentation, which manifests as decreased firing rates compared to spontaneous activity (Simons, 1978). One way to partly circumvent this could be to calculate the inverse ratio and put a focus on decreases in the $Ca^{2+}$ signal.

The amplitude and the area below the neuronal $Ca^{2+}$ transient can be related to the number of action potentials fired in a defined time span. Hence, firing rate changes are well described by $Ca^{2+}$ transients (Bathellier et al., 2012; Kerr et al., 2007; Lütcke, 2010; Niessing and Friedrich, 2010). The temporal resolution of individual action potential detection in $Ca^{2+}$ imaging is limited by two factors. First, by the cellular $Ca^{2+}$ dynamics: a fast rise in intracellular $Ca^{2+}$ caused by voltage gated calcium channels is followed by slower decay established through removal of $Ca^{2+}$ via sodium-calcium exchangers and plasma membrane calcium ATPases. Second, the $Ca^{2+}$ dissociation kinematic of the dye molecule: high-affinity indicators (low dissociation constant (Kd)) report within a delay (YC-Nano 15: Kd = 15 - 50 nM, $\tau_{decay}$ = 2.5 s) the change in the free cytosolic $Ca^{2+}$ concentration (Grienberger and Konnerth, 2012; Helmchen et al., 1997). Therefore, even with very high scan speed, single action potential resolution on a millisecond basis (< 10 ms) is not practical with $Ca^{2+}$ imaging. Although, the temporal occurrence of individual action potentials can be recovered when the firing rate is not too high and potential motion artifacts can be excluded or compensated (Grewe et al., 2010).

When imaging head fixed animals, motion artifacts interfering with the measured $Ca^{2+}$ signal can occur. Motor movements, heartbeat, and breathing are the main source for fast movements and the strength may also depend on the rodent species used (own observation between rats and mice). If the animal is engaged in task reward retrieval, imaging is accompanied by licking (Chen et al., 2013a; Mayrhofer et al., 2013; O'Connor et al., 2010b). During licking or when the animal struggles, a relative motion between the brain and the objective can occur. When working in the frame scan mode, displacement parallel to the imaging plane can be corrected by offline motion correction. Depending on the scan speed, either rigid registration of the entire frame (>15 Hz) or single line registration can be sufficient to correct for motion artifacts (Dombeck et al., 2007; Greenberg and Kerr, 2009). As soon as the imaging plane changes its depth, no offline correction can be applied. Here, only an online motion correction can help to recover the original imaging plane (Chen et al., 2013b; Laffray et al., 2011). Another possibility would be to change the paradigm in a way that reward retrieval is shifted a few seconds after stimulus presentation and motor movements are punished by shifting the reward window backwards. It is important to note that a change in task timing can have an influence on the task involved brain structures and may not be desired.

*What's next and where is the decision made?*

We found that the stability of neuronal activity elicited by different frequencies in the very active neurons reflected the stable psychophysics seen in trained animals. Is this sparse neural activity also causally linked to the behavior of the animals? There are several lines of research which point in this direction. For a simple detection of a brief whisker deflection, inhibition of S1 activity impaired the animal's detection performance (Sachidhanandam et al., 2013). In mice trained to detect a photostimulus (light activation of channelrhodopsin-2 expressed in layer 2/3 neurons), only a small subset of neurons (< 1%) was sufficient to drive a reliable behavior (Huber et al., 2008), causally linking the sparse activity in layer 2/3 to perceptual decisions and learning. However, rats with a lesioned S1 did not show impairment in the detection of frequency change induced by an air stream (Hutson and Masterton, 1986). Since lesioning leads to permanent and strong rewiring in the brain, this study demonstrates more the brain's flexibility to adjust to new conditions and shows that depending on the availability of the cortex it may be involved or other structures will take over in simple task settings

(e.g. Go/NoGo). However, in more complex tasks (e.g. 2AFC) the cortex is needed or even necessary (Diamond and Arabzadeh, 2012), so there is good evidence from previous studies that S1 activity is needed to solve the presented task.

The sparseness seen in the supragranular layers seems partly to be of cortical origin, since firing rates in layer 4 are generally higher compared to the upper layers and also the infragranular layers are less sparse (Barth and Poulet, 2012). Furthermore, the stable and sparse representations are dependent on a stable thalamocortical input (Margolis et al., 2012). The subpopulation of very active neurons we observed are likely to form a strong interconnected subnetwork within a barrel (Yassin et al., 2010). The frequency information from such an ensemble could be conveyed to a subset of layer 5 neurons (sitting in S1 or S2; (Chen et al., 2013a)) which also could receive input from different interconnected subnetworks in a different barrel (creating a hierarchical order) (Kampa et al., 2006). The integrated frequency information could then be sent to different cortical areas involved in the decision making process. There is growing evidence from human neuroimaging and monkey single-neuron physiology that suggests parietal and frontal cortices form an essential brain system for temporal accumulation of evidence from sensory input and categorical choice formation in perceptual decision making (Wang, 2008). Also the striatum may be a good candidate as a next station in the decision circuit. In a tone discrimination task rats showed a strong cortical-striatum projection dependency (Znamenskiy and Zador, 2013).

With the help of new methodological tools we hope to identify the decision circuits in more detail in future studies. This will enable us to also better understand mal-functioning decision making / circuits as they are thought to occur in depression and other mental disorders – linking basic neuroscience to clinics (Murphy et al., 2001).

*Technical outlook*

With the combination of a chronic window preparation in rats and mice and the availability of GECIs, it is now possible to perform long term monitoring of cortical neurons and to study stability and changes in cortical circuits. Additionally, mice and rats can be trained to tolerate head fixation and in this setting learn to perform a complex perceptual decision making task. This not only facilitates the study of neuronal correlates during decision making, but also neuronal changes during learning (behavior induced map plasticity on single neurons or the population level) (Lütcke et al., 2013).

Another advantage of using GECIs is that they can be specifically expressed in neuronal subtypes using Cre mouse lines. Hence, cell-type specific monitoring of activity could be easily implemented to investigate whether the small subpopulation of highly active neurons observed in this study could be assigned to a subclass of excitatory projecting neurons.

Another future direction would be an extension of the investigation to deeper and different layers. New emerging red-shifted GECIs are potential candidates for imaging deep in cortex. Also, a microprism can be used to monitor the activity over different layers to study sensory processing (Chia and Levene, 2009). This would allow expanding the investigation of stability in sensory processing over multiple layers: is the sparse and stable processing of vibrotactile stimuli unique to the supragranular layers? Interaction of the different layers during sensory processing and decision making could be studied in populations of neurons over weeks.

A completely different approach to study neuronal correlates of behavior is to manipulate the brain activity during the behavior of the animal. A classical paradigm would be to locally activate many neurons by micro stimulation with electrodes or single cell stimulation with glass pipettes (Houweling and Brecht, 2007; Romo et al., 1998). Since there is direct control of the input one can create a neuronal bottleneck (Stüttgen et al., 2011) where a well-defined drive of cortical activity leads to the motor output or behavior of the animal. It is also possible to use light-gated ion channels to depolarize (activate; e.g. channelrhodopsins: non-specific cation channels) or hyperpolarize neurons (de-activate; e.g. halorhodopsins: light-driven ion pumps, specific for chloride ions). These proteins can be expressed in all neurons via viral transfection and neuron specific promoters or in a subclass of neurons (GABAergic neurons) using Cre-dependent mouse lines. This allows dissection of the circuitry in even greater detail in the awake, behaving animal. For example, one could stimulate the end-fibers of projecting neurons to manipulate the activity in the target region and to try to understand the influence of the projecting area during behavior.

Another potential future direction is to combine chronic imaging techniques with optical stimulation. One possibility is to have diffuse optical stimulation in a subset of neurons and monitor the neuronal network activity elicited within the population. For example, general recurrent inhibition could be reduced by expressing halorhodopsins in GABAergic neurons and examining whether the sparse stimulus processing is changed or

even lost. Another interesting line of research would be to stimulate cortex projection cholinergic end fibers through expression of channelrhodopsins in cholinergic neurons and optical activation in the cortex. Cholinergic modulation can lead to a disinhibition of pyramidal neurons which could be used to temporarily modulate sparseness and in turn allow map plasticity and stimulus association.

At the moment, a more technically challenging option would be to activate single or defined sets of neurons with optical stimulation (Prakash et al., 2012). This would allow stimulation of a small subset of neurons in a stereotypic way and could indicate if the stable neuronal representation we observed was causally linked to the stable percept. With this method it would also be theoretically possible to find out if attractor-like activation is implemented in the cortex by stimulating a subset of the active (attractor) neurons and mimicking their response.

Last, but not least, the task setting allows relatively easy to use classical electrophysiological recording techniques for studying neuronal correlates of perceptual stability. They still have the advantage of clear activity readouts, manifested in high temporal resolution, high signal-to-noise ratio and fidelity of spike detection. They also allow recording from deep layers, subcortical structures and optically less accessible areas (e.g. ventral tegmental area or frontal cortices).

# 9 References

Adibi, M., Diamond, M.E., and Arabzadeh, E. (2012). Behavioral study of whisker-mediated vibration sensation in rats. Proc. Natl. Acad. Sci. *109*, 971–976.

Ahissar, E., Sosnik, R., Bagdasarian, K., and Haidarliu, S. (2001). Temporal frequency of whisker movement. II. Laminar organization of cortical representations. J. Neurophysiol. *86*, 354–367.

Alloway, K.D. (2007). Information Processing Streams in Rodent Barrel Cortex: The Differential Functions of Barrel and Septal Circuits. Cereb. Cortex *18*, 979–989.

Andermann, M.L. (2010). Chronic cellular imaging of mouse visual cortex during operant behavior and passive viewing. Front. Cellullar Neurosci.

Andermann, M.L., and Moore, C.I. (2006). A somatotopic map of vibrissa motion direction within a barrel column. Nat. Neurosci. *9*, 543–551.

Andermann, M.L., Ritt, J., Neimark, M.A., and Moore, C.I. (2004). Neural Correlates of Vibrissa Resonance-Band-Pass and Somatotopic Representation of High-Frequency Stimuli. Neuron *42*, 451–464.

Angelaki, D.E., McHenry, M.Q., Dickman, J.D., Newlands, S.D., and Hess, B.J. (1999). Computation of inertial motion: neural strategies to resolve ambiguous otolith information. J. Neurosci. *19*, 316–327.

Arabzadeh, E., Petersen, R.S., and Diamond, M.E. (2003). Encoding of whisker vibration by rat barrel cortex neurons: implications for texture discrimination. J. Neurosci. *23*, 9146–9154.

Aronoff, R., Matyas, F., Mateo, C., Ciron, C., Schneider, B., and Petersen, C.C.H. (2010). Long-range connectivity of mouse primary somatosensory barrel cortex. Eur. J. Neurosci. *31*, 2221–2233.

Attwell, D., and Laughlin, S.B. (2001). An energy budget for signaling in the grey matter of the brain. J. Cereb. Blood Flow Metab. *21*, 1133–1145.

Barnes, D.C., Hofacer, R.D., Zaman, A.R., Rennaker, R.L., and Wilson, D.A. (2008). Olfactory perceptual stability and discrimination. Nat. Neurosci. *11*, 1378–1380.

Barth, A.L., and Poulet, J.F.A. (2012). Experimental evidence for sparse firing in the neocortex. Trends Neurosci. *35*, 345–355.

Bathellier, B., Ushakova, L., and Rumpel, S. (2012). Discrete Neocortical Dynamics Predict Behavioral Categorization of Sounds. Neuron *76*, 435–449.

Beaton, R., and Miller, J.M. (1975). Single cell activity in the auditory cortex of the unanesthetized, behaving monkey: Correlation with stimulus controlled behavior* 1. Brain Res. *100*, 543–562.

Boitier, F., Godard, A., Rosencher, E., and Fabre, C. (2009). Measuring photon bunching at ultrashort timescale by two-photon absorption in semiconductors. Nat. Phys. *5*, 267–270.

Bosman, L.W.J., Houweling, A.R., Owens, C.B., Tanke, N., Shevchouk, O.T., Rahmati, N., Teunissen, W.H.T., Ju, C., Gong, W., Koekkoek, S.K.E., et al. (2011). Anatomical Pathways Involved in Generating and Sensing Rhythmic Whisker Movements. Front. Integr. Neurosci. *5*.

Boulnois, J.-L. (1986). Photophysical processes in recent medical laser developments: A review. Lasers Med. Sci. *1*, 47–66.

Brodmann, K. (1909). Vergleichende Lokalisationslehre der Grosshirnrinde in ihren Prinzipien dargestellt auf Grund des Zellenbaues.

Bruno, R.M. (2006). Cortex Is Driven by Weak but Synchronously Active Thalamocortical Synapses. Science *312*, 1622–1627.

Carpenter, R.H.S., and Williams, M.L.L. (1995). Neural computation of log likelihood in control of saccadic eye movements. Nature *377*, 59–62.

Carvell, G., and Simons, D. (1990). Biometric analyses of vibrissal tactile discrimination in the rat. J. Neurosci. *10*, 2638 –2648.

Carvell, G.E., and Simons, D.J. (1987). Thalamic and corticocortical connections of the second somatic sensory area of the mouse. J. Comp. Neurol. *265*, 409–427.

Carvell, G.E., and Simons, D.J. (1995). Task- and subject-related differences in sensorimotor behavior during active touch. Somatosens. Mot. Res. *12*, 1–9.

Castro-Alamancos, M.A. (2004). Absence of rapid sensory adaptation in neocortex during information processing states. Neuron *41*, 455–464.

Cetin, A., Komai, S., Eliava, M., Seeburg, P.H., and Osten, P. (2007). Stereotaxic gene delivery in the rodent brain. Nat. Protoc. *1*, 3166–3173.

Chang, C.-C., and Lin, C.-J. (2011). LIBSVM: a library for support vector machines. ACM Trans. Intell. Syst. Technol. TIST *2*, 27.

Chen, J.L., Carta, S., Soldado-Magraner, J., Schneider, B.L., and Helmchen, F. (2013a). Behaviour-dependent recruitment of long-range projection neurons in somatosensory cortex. Nature.

Chen, J.L., Pfaffli, O.A., Voigt, F.F., Margolis, D.J., and Helmchen, F. (2013b). Online correction of licking-induced brain motion during two-photon imaging with a tunable lens. J. Physiol.

Chia, T.H., and Levene, M.J. (2009). In vivo Imaging of Deep Cortical Layers using a Microprism. J. Vis. Exp.

Da Costa, N.M., and Martin, K.A.C. (2010). Whose cortical column would that be? Front. Neuroanat.

Crochet, S., and Petersen, C.C.H. (2006). Correlating whisker behavior with membrane potential in barrel cortex of awake mice. Nat. Neurosci. *9*, 608–610.

Crochet, S., Poulet, J.F.A., Kremer, Y., and Petersen, C.C.H. (2011). Synaptic Mechanisms Underlying Sparse Coding of Active Touch. Neuron *69*, 1160–1175.

Curtis, J.C., and Kleinfeld, D. (2009). Phase-to-rate transformations encode touch in cortical neurons of a scanning sensorimotor system. Nat. Neurosci. *12*, 492–501.

Cybulska-Klosowicz, A., and Kossut, M. (2000). Mice can learn roughness discrimination with vibrissae in a jump stand apparatus. Acta Neurobiol. Exp. (Warsz.) *61*, 73–76.

Debowska, W., Liguz-Lecznar, M., and Kossut, M. (2011). Bilateral Plasticity of Vibrissae SII Representation Induced by Classical Conditioning in Mice. J. Neurosci. *31*, 5447–5453.

Decharms, R.C., and Zador, A. (2000). Neural representation and the cortical code. Annu. Rev. Neurosci. *23*, 613–647.

DeFelipe, J. (2010). From the Connectome to the Synaptome: An Epic Love Story. Science *330*, 1198–1201.

Denk, W., Strickler, J.H., and Webb, W.W. (1990). Two-Photon Laser Scanning Fluorescence Microscopy. Sel. Pap. Confocal Microsc. *131*, 411.

Diamond, M.E., and Arabzadeh, E. (2012). Whisker sensory system - From receptor to decision. Prog. Neurobiol.

Diamond, M.E., Huang, W., and Ebner, F.F. (1994). Laminar comparison of somatosensory cortical plasticity. Science *265*, 1885–1888.

Diamond, M.E., von Heimendahl, M., Knutsen, P.M., Kleinfeld, D., and Ahissar, E. (2008). “Where” and “what” in the whisker sensorimotor system. Nat. Rev. Neurosci. *9*, 601–612.

Dombeck, D.A., Khabbaz, A.N., Collman, F., Adelman, T.L., and Tank, D.W. (2007). Imaging Large-Scale Neural Activity with Cellular Resolution in Awake, Mobile Mice. Neuron *56*, 43–57.

Dombeck, D.A., Harvey, C.D., Tian, L., Looger, L.L., and Tank, D.W. (2010). Functional imaging of hippocampal place cells at cellular resolution during virtual navigation. Nat. Neurosci. *13*, 1433–1440.

Douglas, R.J., and Martin, K.A.C. (2004). NEURONAL CIRCUITS OF THE NEOCORTEX. Annu. Rev. Neurosci. *27*, 419–451.

Drake, R.L. (2010). Gray’s anatomy for students (Philadelphia, PA: Churchill Livingstone/Elsevier).

Durelli, L., Schmidt, E.M., McIntosh, J.S., and Bak, M.J. (1978). Single-unit chronic recordings from the sensorimotor cortex of unrestrained cats during locomotion. Exp. Neurol. *62*, 580–594.

Ebara, S., Kumamoto, K., Matsuura, T., Mazurkiewicz, J.E., and Rice, F.L. (2002). Similarities and differences in the innervation of mystacial vibrissal follicle-sinus complexes in the rat and cat: a confocal microscopic study. J. Comp. Neurol. *449*, 103–119.

Erlich, J.C., Bialek, M., and Brody, C.D. (2011). A cortical substrate for memory-guided orienting in the rat. Neuron *72*, 330–343.

Ewert, T.A.S., Vahle-Hinz, C., and Engel, A.K. (2008). High-Frequency Whisker Vibration Is Encoded by Phase-Locked Responses of Neurons in the Rat's Barrel Cortex. J. Neurosci. *28*, 5359–5368.

Fechner, G.T. (1860). Elementeder Psychophysik (Leipzig: Breitkopf).

Feldman, D.E. (2005). Map Plasticity in Somatosensory Cortex. Science *310*, 810–815.

Feldmeyer, D. (2012). Excitatory neuronal connectivity in the barrel cortex. Front. Neuroanat. *6*.

Feldmeyer, D., Lübke, J., Silver, R.A., and Sakmann, B. (2002). Synaptic connections between layer 4 spiny neurone-layer 2/3 pyramidal cell pairs in juvenile rat barrel cortex: physiology and anatomy of interlaminar signalling within a cortical column. J. Physiol. *538*, 803–822.

Feldmeyer, D., Brecht, M., Helmchen, F., Petersen, C.C.H., Poulet, J.F.A., Staiger, J.F., Luhmann, H.J., and Schwarz, C. (2012). Barrel cortex function. Prog. Neurobiol.

Fenno, L., Yizhar, O., and Deisseroth, K. (2011). The Development and Application of Optogenetics. Annu. Rev. Neurosci. *34*, 389–412.

Ferezou, I., Haiss, F., Gentet, L.J., Aronoff, R., Weber, B., and Petersen, C.C.H. (2007). Spatiotemporal Dynamics of Cortical Sensorimotor Integration in Behaving Mice. Neuron *56*, 907–923.

Fox, K. (2008). Barrel cortex (Cambridge ; New York: Cambridge University Press).

Freedman, D.J. (2001). Categorical Representation of Visual Stimuli in the Primate Prefrontal Cortex. Science *291*, 312–316.

Froemke, R.C., Merzenich, M.M., and Schreiner, C.E. (2007). A synaptic memory trace for cortical receptive field plasticity. Nature *450*, 425–429.

Garaschuk, O., Milos, R.-I., Grienberger, C., Marandi, N., Adelsberger, H., and Konnerth, A. (2006). Optical monitoring of brain function in vivo: from neurons to networks. Pflügers Arch. - Eur. J. Physiol. *453*, 385–396.

Gentet, L.J., Avermann, M., Matyas, F., Staiger, J.F., and Petersen, C.C.H. (2010). Membrane Potential Dynamics of GABAergic Neurons in the Barrel Cortex of Behaving Mice. Neuron *65*, 422–435.

Gerdjikov, T.V., Bergner, C.G., Stüttgen, M.C., Waiblinger, C., and Schwarz, C. (2010). Discrimination of Vibrotactile Stimuli in the Rat Whisker System: Behavior and Neurometrics. Neuron *65*, 530–540.

Gilbert, C.D., and Sigman, M. (2007). Brain States: Top-Down Influences in Sensory Processing. Neuron *54*, 677–696.

Gobel, W., and Helmchen, F. (2007). In Vivo Calcium Imaging of Neural Network Function. Physiology *22*, 358–365.

Greenberg, D.S., and Kerr, J.N.D. (2009). Automated correction of fast motion artifacts for two-photon imaging of awake animals. J. Neurosci. Methods *176*, 1–15.

Grewe, B.F., and Helmchen, F. (2009). Optical probing of neuronal ensemble activity. Curr. Opin. Neurobiol. *19*, 520–529.

Grewe, B.F., Langer, D., Kasper, H., Kampa, B.M., and Helmchen, F. (2010). High-speed in vivo calcium imaging reveals neuronal network activity with near-millisecond precision. Nat. Methods *7*, 399–405.

Grienberger, C., and Konnerth, A. (2012). Imaging Calcium in Neurons. Neuron *73*, 862–885.

Hahnloser, R.H.R., Kozhevnikov, A.A., and Fee, M.S. (2002). An ultra-sparse code underlies the generation of neural sequences in a songbird. Nature *419*, 65–70.

Haiss, F., Jolivet, R., Wyss, M.T., Reichold, J., Braham, N.B., Scheffold, F., Krafft, M.P., and Weber, B. (2009). Improved in vivo two-photon imaging after blood replacement by perfluorocarbon. J. Physiol. *587*, 3153–3158.

Harris, K.D. (2005). Neural signatures of cell assembly organization. Nat. Rev. Neurosci. *6*, 399–407.

Harris, K.D., and Thiele, A. (2011). Cortical state and attention. Nat. Rev. Neurosci. *12*, 509–523.

Harris, J.A., Harris, I.M., and Diamond, M.E. (2001). The Topography of Tactile Working Memory. J. Neurosci. *21*, 8262 –8269.

Harvey, C.D., Coen, P., and Tank, D.W. (2012). Choice-specific sequences in parietal cortex during a virtual-navigation decision task. Nature *484*, 62–68.

Hasselmo, M.E. (1999). Neuromodulation: acetylcholine and memory consolidation. Trends Cogn. Sci. *3*, 351–359.

Hebb, D.O. (2002). The organization of behavior: a neuropsychological theory (Mahwah, N.J: L. Erlbaum Associates).

Von Heimendahl, M., Itskov, P.M., Arabzadeh, E., and Diamond, M.E. (2007). Neuronal Activity in Rat Barrel Cortex Underlying Texture Discrimination. PLoS Biol. *5*, e305.

Helmchen, F., and Denk, W. (2005). Deep tissue two-photon microscopy. Nat. Methods *2*, 932–940.

Helmchen, F., Borst, J.G., and Sakmann, B. (1997). Calcium dynamics associated with a single action potential in a CNS presynaptic terminal. Biophys. J. *72*, 1458–1471.

Hentschke, H., Haiss, F., and Schwarz, C. (2006). Central Signals Rapidly Switch Tactile Processing in Rat Barrel Cortex during Whisker Movements. Cereb. Cortex *16*, 1142 –1156.

Hernández, A., Salinas, E., García, R., and Romo, R. (1997). Discrimination in the Sense of Flutter: New Psychophysical Measurements in Monkeys. J. Neurosci. *17*, 6391 –6400.

Hernández, A., Zainos, A., and Romo, R. (2000). Neuronal correlates of sensory discrimination in the somatosensory cortex. Proc. Natl. Acad. Sci. *97*, 6191–6196.

Holtmaat, A., Bonhoeffer, T., Chow, D.K., Chuckowree, J., De Paola, V., Hofer, S.B., Hübener, M., Keck, T., Knott, G., Lee, W.-C.A., et al. (2009). Long-term, high-resolution imaging in the mouse neocortex through a chronic cranial window. Nat. Protoc. *4*, 1128–1144.

Houweling, A.R., and Brecht, M. (2007). Behavioural report of single neuron stimulation in somatosensory cortex. Nature *451*, 65–68.

Hromádka, T., DeWeese, M.R., and Zador, A.M. (2008). Sparse representation of sounds in the unanesthetized auditory cortex. PLoS Biol. *6*, e16.

Hubel, D.H., and Wiesel, T.N. (1968). Receptive fields and functional architecture of monkey striate cortex. J. Physiol. *195*, 215–243.

Hubel, D.H., Henson, C.O., Rupert, A., and Galambos, R. (1959). " Attention" Units in the Auditory Cortex. Science *129*, 1279.

Huber, D., Petreanu, L., Ghitani, N., Ranade, S., Hromádka, T., Mainen, Z., and Svoboda, K. (2008). Sparse optical microstimulation in barrel cortex drives learned behaviour in freely moving mice. Nature *451*, 61–64.

Huber, D., Gutnisky, D.A., Peron, S., O'Connor, D.H., Wiegert, J.S., Tian, L., Oertner, T.G., Looger, L.L., and Svoboda, K. (2012). Multiple dynamic representations in the motor cortex during sensorimotor learning. Nature *484*, 473–478.

Hutson, K.A., and Masterton, R.B. (1986). The sensory contribution of a single vibrissa's cortical barrel. J. Neurophysiol. *56*, 1196 –1223.

Jadhav, S.P., Wolfe, J., and Feldman, D.E. (2009). Sparse temporal coding of elementary tactile features during active whisker sensation. Nat. Neurosci. *12*, 792–800.

Jenkinson, E.W., and Glickstein, M. (2000). Whiskers, Barrels, and Cortical Efferent Pathways in Gap Crossing by Rats. J. Neurophysiol. *84*, 1781 –1789.

Kampa, B.M., Letzkus, J.J., and Stuart, G.J. (2006). Cortical feed-forward networks for binding different streams of sensory information. Nat. Neurosci. *9*, 1472–1473.

Kandel, E.R. (2000). Principles of neural science (New York: McGraw-Hill, Health Professions Division).

Kerr, J.N.D., de Kock, C.P.J., Greenberg, D.S., Bruno, R.M., Sakmann, B., and Helmchen, F. (2007). Spatial Organization of Neuronal Population Responses in Layer 2/3 of Rat Barrel Cortex. J. Neurosci. *27*, 13316–13328.

Khatri, V. (2004). Adaptation in Thalamic Barreloid and Cortical Barrel Neurons to Periodic Whisker Deflections Varying in Frequency and Velocity. J. Neurophysiol. *92*, 3244–3254.

Kleinfeld, D., Ahissar, E., and Diamond, M.E. (2006). Active sensation: insights from the rodent vibrissa sensorimotor system. Curr. Opin. Neurobiol. *16*, 435–444.

Knutsen, P.M. (2006). Haptic Object Localization in the Vibrissal System: Behavior and Performance. J. Neurosci. *26*, 8451–8464.

De Kock, C.P.J., and Sakmann, B. (2008). High frequency action potential bursts (>= 100 Hz) in L2/3 and L5B thick tufted neurons in anaesthetized and awake rat primary somatosensory cortex. J. Physiol. *586*, 3353–3364.

De Kock, C.P.J., and Sakmann, B. (2009). Spiking in primary somatosensory cortex during natural whisking in awake head-restrained rats is cell-type specific. Proc. Natl. Acad. Sci. *106*, 16446–16450.

König, P., Engel, A.K., and Singer, W. (1996). Integrator or coincidence detector? The role of the cortical neuron revisited. Trends Neurosci. *19*, 130–137.

Kremer, Y., Leger, J.-F., Goodman, D., Brette, R., and Bourdieu, L. (2011). Late Emergence of the Vibrissa Direction Selectivity Map in the Rat Barrel Cortex. J. Neurosci. *31*, 10689–10700.

Krupa, D.J., Matell, M.S., Brisben, A.J., Oliveira, L.M., and Nicolelis, M.A.. (2001). Behavioral properties of the trigeminal somatosensory system in rats performing whisker-dependent tactile discriminations. J. Neurosci. *21*, 5752.

Krupa, D.J., Wiest, M.C., Shuler, M.G., Laubach, M., and Nicolelis, M.A.L. (2004). Layer-specific somatosensory cortical activation during active tactile discrimination. Science *304*, 1989–1992.

Kügler, S., Hahnewald, R., Garrido, M., and Reiss, J. (2007). Long-term rescue of a lethal inherited disease by adeno-associated virus-mediated gene transfer in a mouse model of molybdenum-cofactor deficiency. Am. J. Hum. Genet. *80*, 291–297.

Laffray, S., Pagès, S., Dufour, H., De Koninck, P., De Koninck, Y., and Côté, D. (2011). Adaptive Movement Compensation for In Vivo Imaging of Fast Cellular Dynamics within a Moving Tissue. PLoS ONE *6*, e19928.

LaMotte, R.H., and Mountcastle, V.B. (1975). Capacities of humans and monkeys to discriminate vibratory stimuli of different frequency and amplitude: a correlation between neural events and psychological measurements. J. Neurophysiol. *38*, 539 –559.

Langer, D., van 't Hoff, M., Keller, A.J., Nagaraja, C., Pfäffli, O.A., Göldi, M., Kasper, H., and Helmchen, F. (2013). HelioScan: A software framework for controlling in vivo microscopy setups with high hardware flexibility, functional diversity and extendibility. J. Neurosci. Methods *215*, 38–52.

Larkum, M. (2013). A cellular mechanism for cortical associations: an organizing principle for the cerebral cortex. Trends Neurosci. *36*, 141–151.

Lee, S.-H., and Dan, Y. (2012). Neuromodulation of Brain States. Neuron *76*, 209–222.

Lefort, S., Tomm, C., Floyd Sarria, J.-C., and Petersen, C.C.H. (2009). The Excitatory Neuronal Network of the C2 Barrel Column in Mouse Primary Somatosensory Cortex. Neuron *61*, 301–316.

Lennie, P. (2003). The cost of cortical computation. Curr. Biol. *13*, 493–497.

Letzkus, J.J., Wolff, S.B.E., Meyer, E.M.M., Tovote, P., Courtin, J., Herry, C., and Lüthi, A. (2011). A disinhibitory microcircuit for associative fear learning in the auditory cortex. Nature *480*, 331–335.

Leutgeb, J.K., Leutgeb, S., Moser, M.-B., and Moser, E.I. (2007). Pattern Separation in the Dentate Gyrus and CA3 of the Hippocampus. Science *315*, 961–966.

Lottem, E., and Azouz, R. (2009). Mechanisms of Tactile Information Transmission through Whisker Vibrations. J. Neurosci. *29*, 11686–11697.

Luna, R., Hernández, A., Brody, C.D., and Romo, R. (2005). Neural codes for perceptual discrimination in primary somatosensory cortex. Nat. Neurosci. *8*, 1210–1219.

Luo, L., Callaway, E.M., and Svoboda, K. (2008). Genetic dissection of neural circuits. Neuron *57*, 634–660.

Lütcke, H. (2010). Optical recording of neuronal activity with a genetically-encoded calcium indicator in anesthetized and freely moving mice. Front. Neural Circuits.

Lütcke, H., Margolis, D.J., and Helmchen, F. (2013). Steady or changing? Long-term monitoring of neuronal population activity. Trends Neurosci.

Margolis, D.J., Lütcke, H., Schulz, K., Haiss, F., Weber, B., Kügler, S., Hasan, M.T., and Helmchen, F. (2012). Reorganization of cortical population activity imaged throughout long-term sensory deprivation. Nat. Neurosci. *15*, 1539–1546.

Masino, S.A., and Frostig, R.D. (1996). Quantitative long-term imaging of the functional representation of a whisker in rat barrel cortex. Proc. Natl. Acad. Sci. *93*, 4942–4947.

Mayrhofer, J.M., Skreb, V., von der Behrens, W., Musall, S., Weber, B., and Haiss, F. (2013). Novel two-alternative forced choice paradigm for bilateral vibrotactile whisker frequency discrimination in head-fixed mice and rats. J. Neurophysiol. *109*, 273–284.

Mehta, S.B., Whitmer, D., Figueroa, R., Williams, B.A., and Kleinfeld, D. (2007). Active spatial perception in the vibrissa scanning sensorimotor system. PLoS Biol. *5*, e15.

Melzer, P., Sachdev, R.N.S., Jenkinson, N., and Ebner, F.F. (2006). Stimulus Frequency Processing in Awake Rat Barrel Cortex. J. Neurosci. *26*, 12198–12205.

Minderer, M., Liu, W., Sumanovski, L.T., Kügler, S., Helmchen, F., and Margolis, D.J. (2011). Chronic imaging of cortical sensory map dynamics using a genetically encoded calcium indicator. J. Physiol. no–no.

Moore, C.I. (2004). Frequency-Dependent Processing in the Vibrissa Sensory System. J. Neurophysiol. *91*, 2390–2399.

Morita, T., Kang, H., Wolfe, J., Jadhav, S.P., and Feldman, D.E. (2011). Psychometric Curve and Behavioral Strategies for Whisker-Based Texture Discrimination in Rats. PLoS ONE *6*, e20437.

Mountcastle, V.B. (1957). Modality and topographic properties of single neurons of cat's somatic sensory cortex. J Neurophysiol *20*, 408–434.

Mountcastle, V.B. (1997). The columnar organization of the neocortex. Brain *120*, 701–722.

Mountcastle, V., Steinmetz, M., and Romo, R. (1990). Frequency discrimination in the sense of flutter: psychophysical measurements correlated with postcentral events in behaving monkeys. J. Neurosci. *10*, 3032 –3044.

Munk, H. (1880). Uber die Funktionen der Großhirnrinde gesammelte Mitteilungen aus den Jahren 1877 - 80 (Saarbrücken: VDM Verlag Dr. Müller).

Murphy, F.C., Rubinsztein, J.S., Michael, A., Rogers, R.D., Robbins, T.W., Paykel, E.S., and Sahakian, B.J. (2001). Decision-making cognition in mania and depression. Psychol. Med. *31*, 679–693.

Nagai, T., Yamada, S., Tominaga, T., Ichikawa, M., and Miyawaki, A. (2004). Expanded dynamic range of fluorescent indicators for Ca2+ by circularly permuted yellow fluorescent proteins. Proc. Natl. Acad. Sci. U. S. A. *101*, 10554–10559.

Niessing, J., and Friedrich, R.W. (2010). Olfactory pattern classification by discrete neuronal network states. Nature *465*, 47–52.

O'Connor, D.H., Huber, D., and Svoboda, K. (2009). Reverse engineering the mouse brain. Nature *461*, 923–929.

O'Connor, D.H., Peron, S.P., Huber, D., and Svoboda, K. (2010a). Neural Activity in Barrel Cortex Underlying Vibrissa-Based Object Localization in Mice. Neuron *67*, 1048–1061.

O'Connor, D.H., Clack, N.G., Huber, D., Komiyama, T., Myers, E.W., and Svoboda, K. (2010b). Vibrissa-Based Object Localization in Head-Fixed Mice. J. Neurosci. *30*, 1947–1967.

O'Connor, D.H., Hires, S.A., Guo, Z.V., Li, N., Yu, J., Sun, Q.-Q., Huber, D., and Svoboda, K. (2013). Neural coding during active somatosensation revealed using illusory touch. Nat. Neurosci. *16*, 958–965.

O'Reilly, R.C., and McClelland, J.L. (1994). Hippocampal conjunctive encoding, storage, and recall: avoiding a trade-off. Hippocampus *4*, 661–682.

Olshausen, B., and Field, D. (2004). Sparse coding of sensory inputs. Curr. Opin. Neurobiol. *14*, 481–487.

Orbach, H.S., Cohen, L.B., and Grinvald, A. (1985). Optical mapping of electrical activity in rat somatosensory and visual cortex. J. Neurosci. *5*, 1886–1895.

Palmer, L.M., Schulz, J.M., Murphy, S.C., Ledergerber, D., Murayama, M., and Larkum, M.E. (2012). The Cellular Basis of GABAB-Mediated Interhemispheric Inhibition. Science *335*, 989–993.

Parker, A.J., and Newsome, W.T. (1998). SENSE AND THE SINGLE NEURON: Probing the Physiology of Perception. Annu. Rev. Neurosci. *21*, 227–277.

Petersen, C.C.H. (2007). The Functional Organization of the Barrel Cortex. Neuron *56*, 339–355.

Petersen, C.C.H., and Crochet, S. (2013). Synaptic Computation and Sensory Processing in Neocortical Layer 2/3. Neuron *78*, 28–48.

Petreanu, L., Huber, D., Sobczyk, A., and Svoboda, K. (2007). Channelrhodopsin-2–assisted circuit mapping of long-range callosal projections. Nat. Neurosci. *10*, 663–668.

Petreanu, L., Gutnisky, D.A., Huber, D., Xu, N., O'Connor, D.H., Tian, L., Looger, L., and Svoboda, K. (2012). Activity in motor–sensory projections reveals distributed coding in somatosensation. Nature *489*, 299–303.

Pologruto, T.A., Sabatini, B.L., and Svoboda, K. (2003). ScanImage: flexible software for operating laser scanning microscopes. Biomed Eng Online *2*, 13.

Prakash, R., Yizhar, O., Grewe, B., Ramakrishnan, C., Wang, N., Goshen, I., Packer, A.M., Peterka, D.S., Yuste, R., Schnitzer, M.J., et al. (2012). Two-photon optogenetic toolbox for fast inhibition, excitation and bistable modulation. Nat. Methods *9*, 1171–1179.

Prigg, T., Goldreich, D., Carvell, G.E., and Simons, D.J. (2002). Texture discrimination and unit recordings in the rat whisker/barrel system. Physiol. Behav. *77*, 671–675.

Rice, F.L., Mance, A., and Munger, B.L. (1986). A comparative light microscopic analysis of the sensory innervation of the mystacial pad. I. Innervation of vibrissal follicle-sinus complexes. J. Comp. Neurol. *252*, 154–174.

Roesch, M.R., Calu, D.J., and Schoenbaum, G. (2007). Dopamine neurons encode the better option in rats deciding between differently delayed or sized rewards. Nat. Neurosci. *10*, 1615–1624.

Romo, R., and de Lafuente, V. (2013). Conversion of sensory signals into perceptual decisions. Prog. Neurobiol. *103*, 41–75.

Romo, R., Hernández, A., Zainos, A., and Salinas, E. (1998). Somatosensory discrimination based on cortical microstimulation. Nature *392*, 387–390.

Roth, G., and Dicke, U. (2005). Evolution of the brain and intelligence. Trends Cogn. Sci. *9*, 250–257.

Sachidhanandam, S., Sreenivasan, V., Kyriakatos, A., Kremer, Y., and Petersen, C.C.H. (2013). Membrane potential correlates of sensory perception in mouse barrel cortex. Nat. Neurosci.

Safaai, H., von Heimendahl, M., Sorando, J.M., Diamond, M.E., and Maravall, M. (2013). Coordinated Population Activity Underlying Texture Discrimination in Rat Barrel Cortex. J. Neurosci. *33*, 5843–5855.

Salinas, E., Hernandez, A., Zainos, A., and Romo, R. (2000). Periodicity and firing rate as candidate neural codes for the frequency of vibrotactile stimuli. J. Neurosci. *20*, 5503–5515.

Schwarz, C., Hentschke, H., Butovas, S., Haiss, F., Stüttgen, M.C., Gerdjikov, T.V., Bergner, C.G., and Waiblinger, C. (2010). The head-fixed behaving rat—Procedures and pitfalls. Somatosens. Mot. Res. *27*, 131–148.

Shadlen, M.N., and Newsome, W.T. (1994). Noise, neural codes and cortical organization. Curr. Opin. Neurobiol. *4*, 569–579.

Shuler, M.G., Krupa, D.J., and Nicolelis, M.A.L. (2001). Bilateral integration of whisker information in the primary somatosensory cortex of rats. J. Neurosci. *21*, 5251–5261.

Simons, D.J. (1978). Response properties of vibrissa units in rat SI somatosensory neocortex. J. Neurophysiol. *41*, 798–820.

Siucinska, E., and Kossut, M. (1996). Short-lasting classical conditioning induces reversible changes of representational maps of vibrissae in mouse SI cortex—a 2DG study. Cereb. Cortex *6*, 506–513.

Siucinska, E., and Kossut, M. (2004). Experience-dependent changes in cortical whisker representation in the adult mouse: A 2-deoxyglucose study. Neuroscience *127*, 961–971.

Srivastava, V., Parker, D.J., and Edwards, S.F. (2008). The nervous system might “orthogonalize” to discriminate. J. Theor. Biol. *253*, 514–517.

Stüttgen, M.C. (2010). Toward Behavioral Benchmarks for Whisker-Related Sensory Processing. J. Neurosci. *30*, 4827 –4829.

Stüttgen, M.C., and Schwarz, C. (2008). Psychophysical and neurometric detection performance under stimulus uncertainty. Nat. Neurosci. *11*, 1091–1099.

Stüttgen, M.C., and Schwarz, C. (2010). Integration of Vibrotactile Signals for Whisker-Related Perception in Rats Is Governed by Short Time Constants: Comparison of Neurometric and Psychometric Detection Performance. J. Neurosci. *30*, 2060 –2069.

Stüttgen, M.C., Rüter, J., and Schwarz, C. (2006). Two Psychophysical Channels of Whisker Deflection in Rats Align with Two Neuronal Classes of Primary Afferents. J. Neurosci. *26*, 7933 –7941.

Stüttgen, M.C., Schwarz, C., and Jäkel, F. (2011). Mapping spikes to sensations. Front. Neurosci. *5*.

Svoboda, K., and Yasuda, R. (2006). Principles of Two-Photon Excitation Microscopy and Its Applications to Neuroscience. Neuron *50*, 823–839.

Taube, J.S., Muller, R.U., and Ranck, J.B., Jr (1990). Head-direction cells recorded from the postsubiculum in freely moving rats. II. Effects of environmental manipulations. J. Neurosci. Off. J. Soc. Neurosci. *10*, 436–447.

Thompson, L.T., and Best, P.J. (1990). Long-term stability of the place-field activity of single units recorded from the dorsal hippocampus of freely behaving rats. Brain Res. *509*, 299–308.

Tian, L., Hires, S.A., Mao, T., Huber, D., Chiappe, M.E., Chalasani, S.H., Petreanu, L., Akerboom, J., McKinney, S.A., Schreiter, E.R., et al. (2009). Imaging neural activity in worms, flies and mice with improved GCaMP calcium indicators. Nat. Methods *6*, 875–881.

Tsytsarev, V., Pope, D., Pumbo, E., Yablonskii, A., and Hofmann, M. (2010). Study of the cortical representation of whisker directional deflection using voltage-sensitive dye optical imaging. NeuroImage *53*, 233–238.

Uylings, H.B.M., Groenewegen, H.J., and Kolb, B. (2003). Do rats have a prefrontal cortex? Behav. Brain Res. *146*, 3–17.

Wang, X.-J. (2008). Decision Making in Recurrent Neuronal Circuits. Neuron *60*, 215–234.

Welsh, J.P. (1998). Systemic harmaline blocks associative and motor learning by the actions of the inferior olive. Eur. J. Neurosci. *10*, 3307–3320.

Wichmann, F.A., and Hill, N.J. (2001). The psychometric function: I. Fitting, sampling, and goodness of fit. Percept. Psychophys. *63*, 1293.

Wick, S.D., Wiechert, M.T., Friedrich, R.W., and Riecke, H. (2009). Pattern orthogonalization via channel decorrelation by adaptive networks. J. Comput. Neurosci. *28*, 29–45.

Wickelgren, W.A. (1977). Speed-accuracy tradeoff and information processing dynamics. Acta Psychol. (Amst.) *41*, 67–85.

Wiest, M.C. (2005). Heterogeneous Integration of Bilateral Whisker Signals by Neurons in Primary Somatosensory Cortex of Awake Rats. J. Neurophysiol. *93*, 2966–2973.

Wills, T.J., Lever, C., Cacucci, F., Burgess, N., and O'Keefe, J. (2005). Attractor dynamics in the hippocampal representation of the local environment. Science *308*, 873–876.

Wolfe, J., Hill, D.N., Pahlavan, S., Drew, P.J., Kleinfeld, D., and Feldman, D.E. (2008). Texture Coding in the Rat Whisker System: Slip-Stick Versus Differential Resonance. PLoS Biol. *6*, e215.

Woolsey, T.A., and Van der Loos, H. (1970). The structural organization of layer IV in the somatosensory region (SI) of mouse cerebral cortex. The description of a cortical field composed of discrete cytoarchitectonic units. Brain Res. *17*, 205–242.

Wurtz, R.H. (1968). Visual cortex neurons: response to stimuli during rapid eye movements. Science *162*, 1148–1150.

Yang, Y., and Zador, A.M. (2012). Differences in Sensitivity to Neural Timing among Cortical Areas. J. Neurosci. *32*, 15142–15147.

Yassin, L., Benedetti, B.L., Jouhanneau, J.-S., Wen, J.A., Poulet, J.F.A., and Barth, A.L. (2010). An Embedded Subnetwork of Highly Active Neurons in the Neocortex. Neuron *68*, 1043–1050.

Yizhar, O., Fenno, L.E., Davidson, T.J., Mogri, M., and Deisseroth, K. (2011). Optogenetics in Neural Systems. Neuron *71*, 9–34.

Yotsumoto, Y., Watanabe, T., and Sasaki, Y. (2008). Different Dynamics of Performance and Brain Activation in the Time Course of Perceptual Learning. Neuron *57*, 827–833.

Zariwala, H.A., Madisen, L., Ahrens, K.F., Bernard, A., Lein, E.S., Jones, A.R., and Zeng, H. (2011). Visual tuning properties of genetically identified layer 2/3 neuronal types in the primary visual cortex of cre-transgenic mice. Front. Syst. Neurosci. *4*, 162.

Znamenskiy, P., and Zador, A.M. (2013). Corticostriatal neurons in auditory cortex drive decisions during auditory discrimination. Nature *497*, 482–485.

Zucker, R.S. (1999). Calcium- and activity-dependent synaptic plasticity. Curr. Opin. Neurobiol. *9*, 305–313.

# 10 Appendix

## 10.1 Supplemental Figures

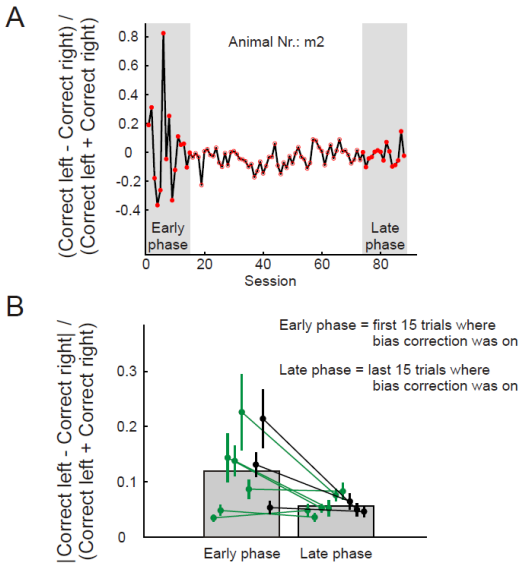


**Figure S 1. Influence of bias correction algorithm.**
To capture the animals bias a "bias index" was computed: (% correct left side - % correct right side) / (% correct left side + % correct right side) over sessions **(A)** an example of the 'bias index' over the entire training phase, where the bias correction was switched on. Grey shaded areas correspond to early (first 15 sessions) and late phase (last 15 sessions) in the training. **(B)** the absolute bias index for all animals is shown. Note only for animals having a bias in the early training phase the bias is reduced over time. When we compared the first 15 sessions with the last 15 sessions where the bias correction mode was switched on we saw a significant decrease of the bias in 4/9 animals (Kruskal-Wallis test, $p<0.05$). Thus, the "bias correction mode" helps to reduce the bias of animals more rapidly in the cases where a bias exists.

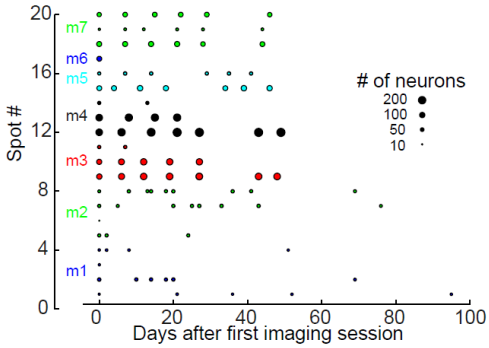


**Figure S 2. Overview of all spots imaged.**
Area of the circle corresponds to number of neurons imaged. Number of individual animals is shown on the left.

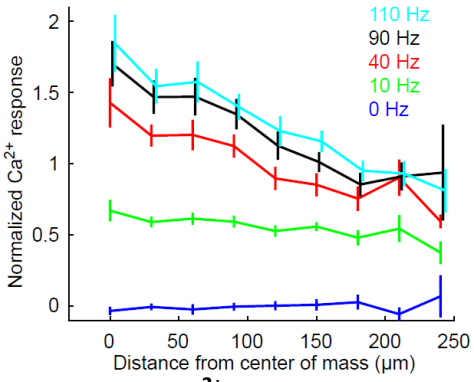


**Figure S 3. Spatial distribution of $Ca^{2+}$ responses.**
The average $Ca^{2+}$ response over distance measured from the center of mass of activity in a given field of view is plotted. The center of mass for activity was computed for each session individually (SD of center of mass for activity over sessions for X = 8.9 ± 1.2 µm and Y = 9.4 ± 1.3 µm, n = 17 spots in 6 mice). Increased stimulation frequency increases the activity distribution in a homogeneous way (n = 20 spots in 7 mice).

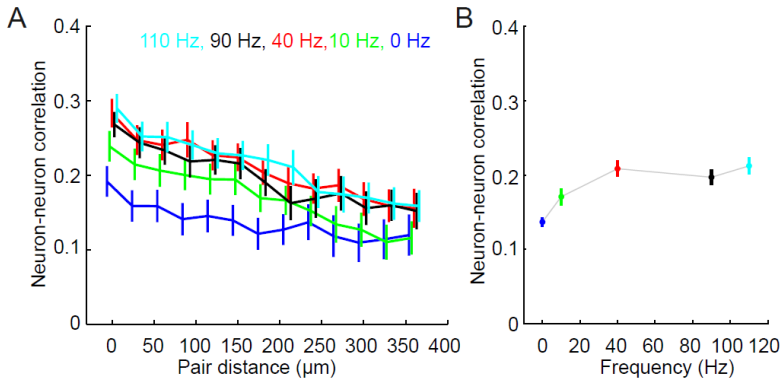


**Figure S 4. Neuron-to-neuron correlation.**
**(A)** Neuron-to-neuron correlation is plotted over the pair distance (n = 20 spots in 7 mice). Stimulus evoked responses of neurons in the same spot were correlated with each other. Neurons which are further apart show a smaller correlation than close by neurons. With increased stimulation strength a stronger pair-correlation is seen **(B)**. Plots and values are mean ± SEM.

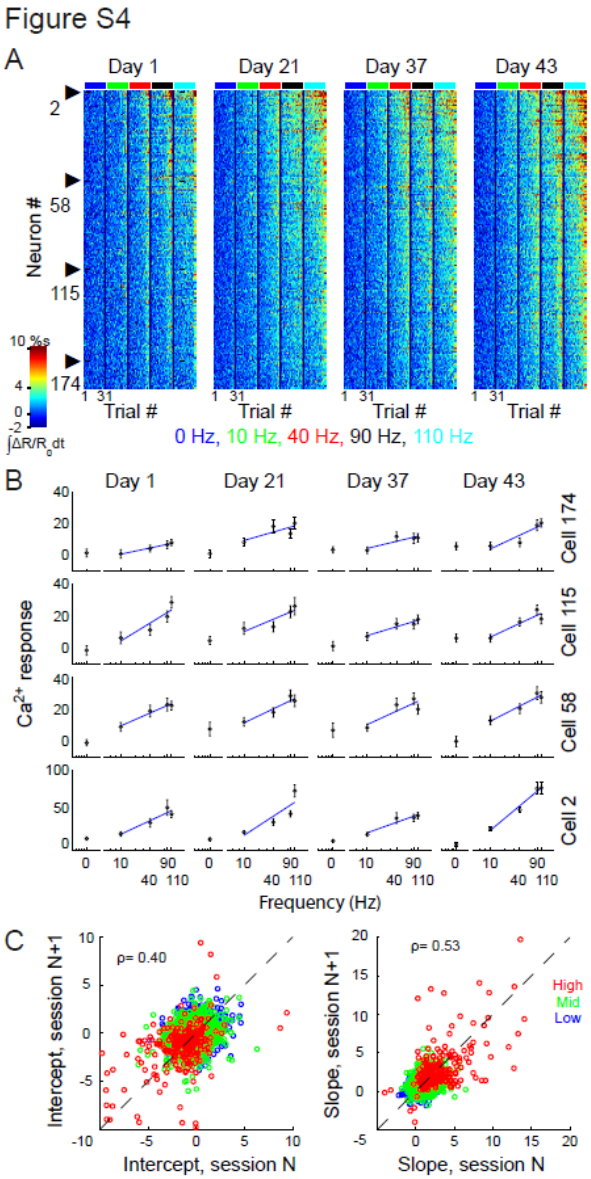


**Figure S 5. Individual stimulus response are in general conserved.**

**(A)** Example population activity matrix for 0 (spontaneous activity), 10, 40, 90 and 110 Hz stimulation from the same imaging location over different experimental days: rows correspond to neuron ID and columns to trial ID. 31 trials per stimulus frequency are presented. Trials were sorted for each stimulus frequency according to the mean response amplitude of the population. Neurons were sorted with respect to their mean response amplitude over all trials, experiments and stimulus frequency. **(B)** Examples of neuronal tuning curves from neurons depicted in **(A)** over different experimental days. The blue lines are fits of the form y(x) = S*log(x) + I for x > 0. **(C)** Correlation of intercept and slope of the tuning curve fits of individual neurons from one experimental day with previous day for all neurons (n = 1431 neurons in 6 mice). Color codes are according to the three response categories in Figure 13A. Not all data are shown in **(C)**: for intercept 10 points and for slope 6 points. Statistical analysis: Pearson's correlation.

In this example, the high activity neurons do not turn into low activity neurons from one session to the next and vice versa indicating a low session-to-session variability of the population activity distribution. Since most barrel cortex neurons show adaptation to repeated stimuli firing rate increases logarithmically with frequency (Melzer et al., 2006). To quantify the stability of individual neuronal frequency responses the function y(x) = S*log(x) + I was fitted to the average response magnitude of the different stimulus

frequencies (> 0 Hz) over imaging sessions (**(B)**shows four example neurons depicted in **(A)**; mean ± SD of $R^2$ for fits of 4 neurons and 4 sessions: 0.84 ± 0.11). The fit parameters S and I (slope and intercept) derived from the individual sessions (mean ± SD of $R^2$ for fits of 1431 neurons: 0.62 ± 0.31) were correlated from one session with the following session **(C)**. Perfectly stable neuronal frequency responses would align along the diagonals. The average correlation over sessions is significant which indicates that the individual stimulus response are in general conserved (n = 1431 neurons in 6 mice, Intercept: ρ = 0.40, p < 0.01; Slope: ρ = 0.53, p < 0.01). The data were divided into three categories: high, mid and low, which are based on the average response magnitude to the contralateral stimuli (see above for definition of categories). Highly responsive neurons showed on average a steeper tuning towards higher frequencies over days (**(C)**, right panel).

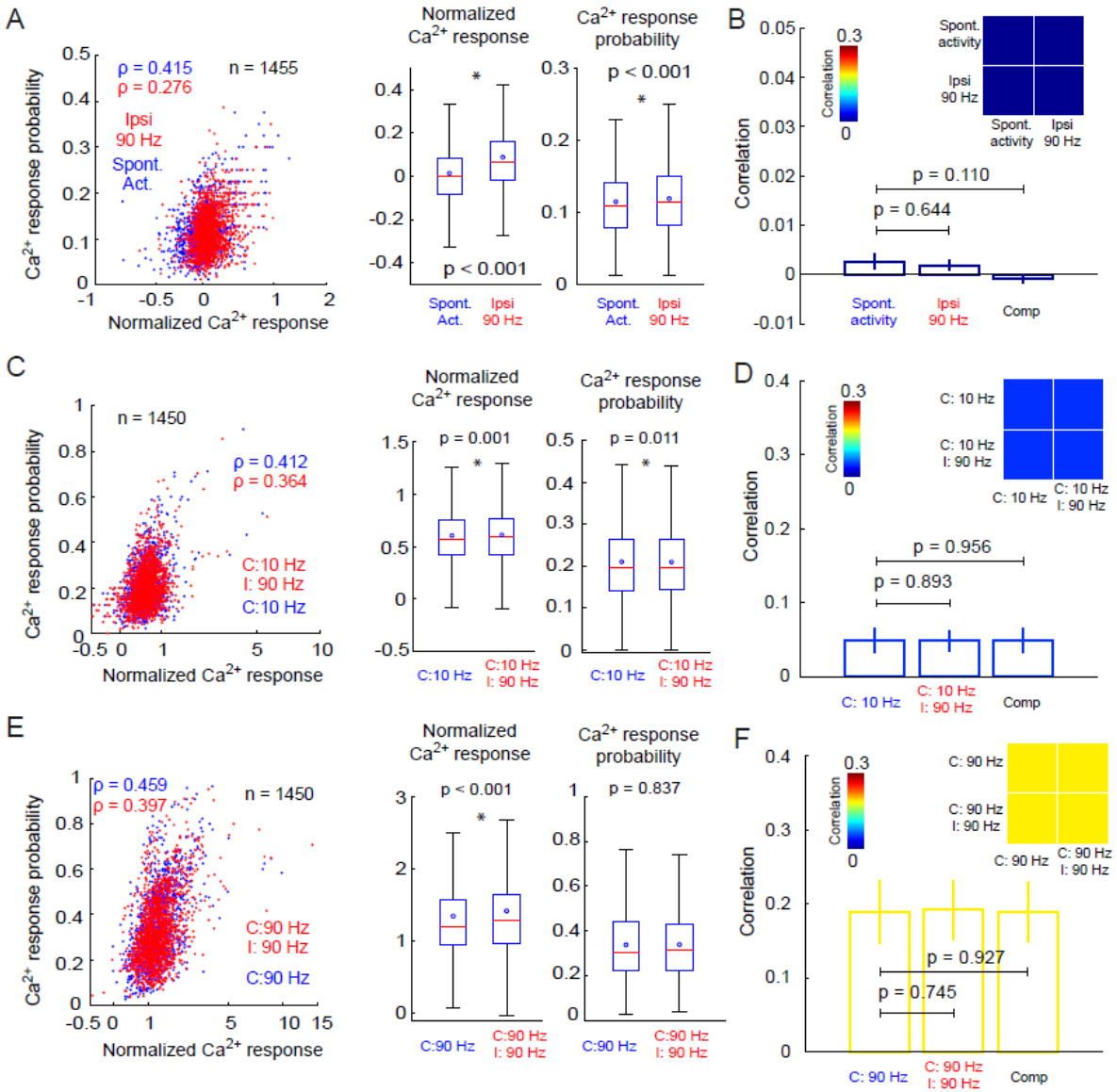


**Figure S 6. Weak ipsilateral response and modulation.**

**(A)** $Ca^{2+}$ response probability over response amplitude for ipsilateral 90 Hz pulsatile stimulation (red) compared to spontaneous activity (blue) (left panel). Center and right panel show the boxplot of the response amplitude and the $Ca^{2+}$ response probability for ipsilateral stimulation and spontaneous activity (n = 1455 neurons in 7 mice). **(B)** Trial-

to-trial correlation of population activity for spontaneous activity and for 90 Hz ipsilateral stimulation (reliability). The comparison of the trial-to-trial correlation between categories (similarity) is displayed as the third bar. The inset shows the similarity matrix (n = 20 spots in 7 mice). **(C)** $Ca^{2+}$ response probability over response amplitude for contralateral 10 Hz pulsatile stimulation (blue) compared to bilateral stimulation with 10 Hz contralateral and 90 Hz ipsilateral (red) with respect to the imaging location. Center and right panel show the boxplot of the response amplitude and the $Ca^{2+}$ response probability for the two stimulus categories (n = 1450 neurons in 7 mice). **(D)** same as in **(B)** for: pure contralateral 10 Hz stimulus versus 10 Hz contralateral plus 90 Hz ipsilateral stimulation. **(E)** $Ca^{2+}$ response probability over response amplitude for contralateral 90 Hz pulsatile stimulation (blue) compared to bilateral stimulation with 90 Hz contra and 90 Hz ipsilateral (red). Right panel shows the boxplot of the response amplitude and the $Ca^{2+}$ response probability for the two stimulus categories (n = 1450 neurons in 7 mice). **(F)** same as in **(B)** and for pure contralateral 90 Hz stimulus versus 90 Hz contralateral plus 90 Hz ipsilateral stimulation (n = 19 spots in 7 mice). Note that the x- axis of the left panel was logarithmically scaled in **(A)**, **(C)** and **(E)**. In all box plots the mean is shown as blue circle and the median as a red line. Boxplot whiskers are drawn as 1.5 interquartile ranges otherwise mean ± SEM. Outliers are not shown. Statistical analysis: Wilcoxon signed rank and Student's t test. $p < 0.05$ (*).

The barrel cortex receives input from the ipsilateral whisker pad through the corpus callosum. We addressed the question whether ipsilateral stimulation evokes a neuronal response in cortical layers I-III. This Figure shows the average response for individual neurons to a 90 Hz ipsilateral stimulation. The correlation between the $Ca^{2+}$ response probability and the mean response amplitude of individual neurons **(B)** demonstrates that neurons with higher response amplitude reach more often a measureable activation. The boxplots (right panels) summarize the population data for the response amplitude and the $Ca^{2+}$ response probability. The ipsilateral stimulation showed only a subtle but significant $Ca^{2+}$-response in comparison to spontaneous activity for both the response amplitude and the $Ca^{2+}$ response probability (n = 1455 neurons in 7 mice, $p < 0.001$ and $p < 0.001$). The ipsilateral stimulation did not evoke a reliable population response and is not significant different from spontaneous activity **(D)**. To investigate a possible modulatory effect of an ipsilateral input on the contralateral stimulus a 10 Hz contralateral stimulus was presented simultaneously with a 90 Hz ipsilateral stimulus. Such a bilateral stimulation led to a small increase of the $Ca^{2+}$-response amplitudes and $Ca^{2+}$ response probability compared to a solely contralateral 10 Hz stimulation (**(C)**, n = 1450 neurons in 7 mice, $p = 0.001$ and $p = 0.011$). A pairing of a 90 Hz contralateral and 90 Hz ipsilateral stimulus yielded the same effect: a weak increase in the average $Ca^{2+}$-response compared to the purely contralateral stimulation (**(E)**, n = 1450 neurons in 7 mice, $p < 0.001$ and $p = 0.837$). The response $Ca^{2+}$ response probability was not changed. On the population level the additional ipsilateral stimulation did not activate a different set of neurons compared to the sole contralateral stimulation (**(D)** and **(F)**).

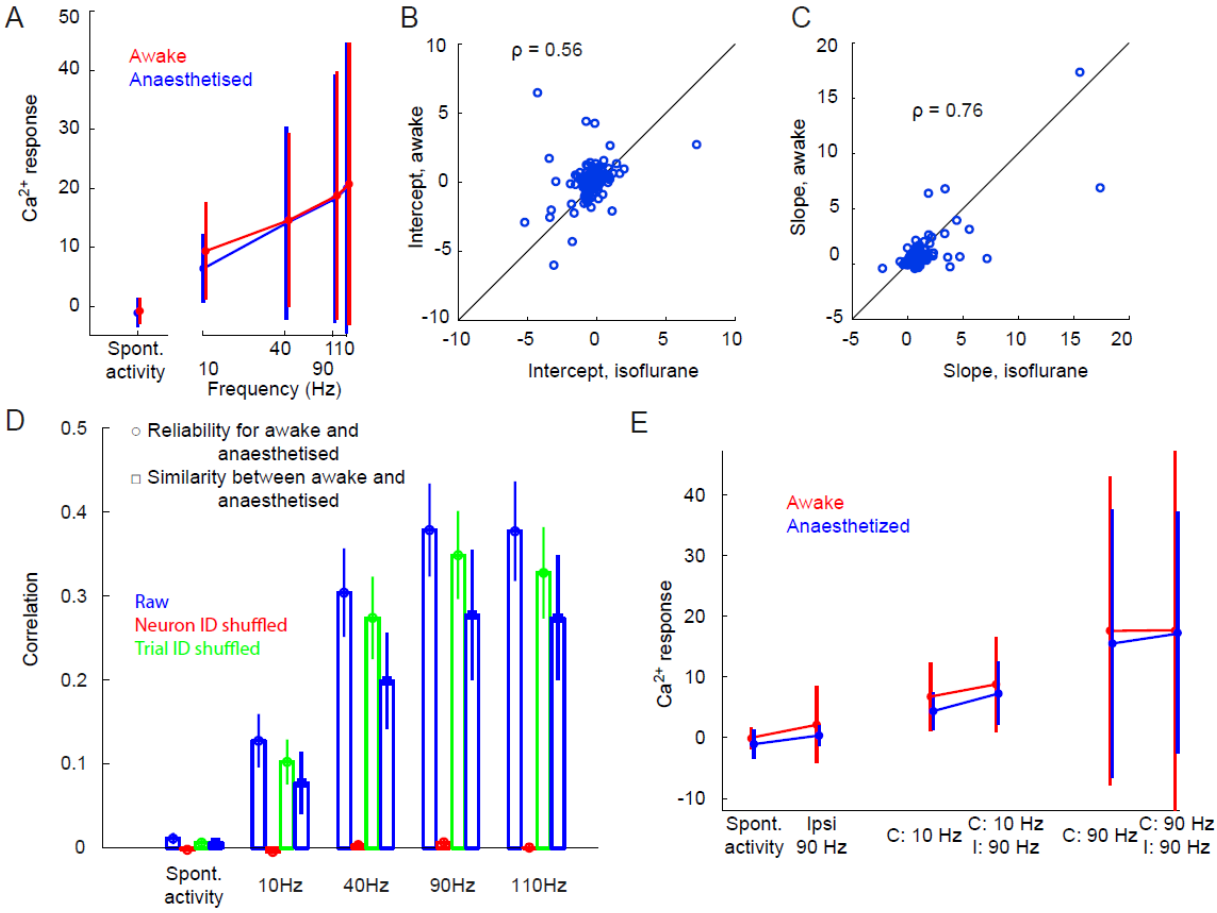


**Figure S 7. Responses in the awake state are similar to anaesthetized state.**
**(A)** Response amplitude for different stimulation frequencies and spontaneous activity shown in the anaesthetized state (n = 249 neurons in 7 spots and 2 mice, mean ± SD) and awake state (n = 264 neurons in 7 spots and 2 mice, mean ± SD). **(B)** and **(C)** Correlation of intercept and slope of the tuning curves fits of individual neurons from one experimental awake session with previous anaesthetized session for all neurons (n = 144 cells in 5 spots and 2 mice). **(D)** compares the reliability values for anaesthetized and awake state to the similarity between these two for the different stimulation frequencies and the control case in which the trial ID or the neuron ID was shuffled (n = 5 spots in 2 mice, mean ± SEM). **(E)** displays the ipsilateral response and modulation in the awake and in the anaesthetized state (n = 61 neurons and N= 68 neurons in 3 spots and 2 mice, mean ± SD).

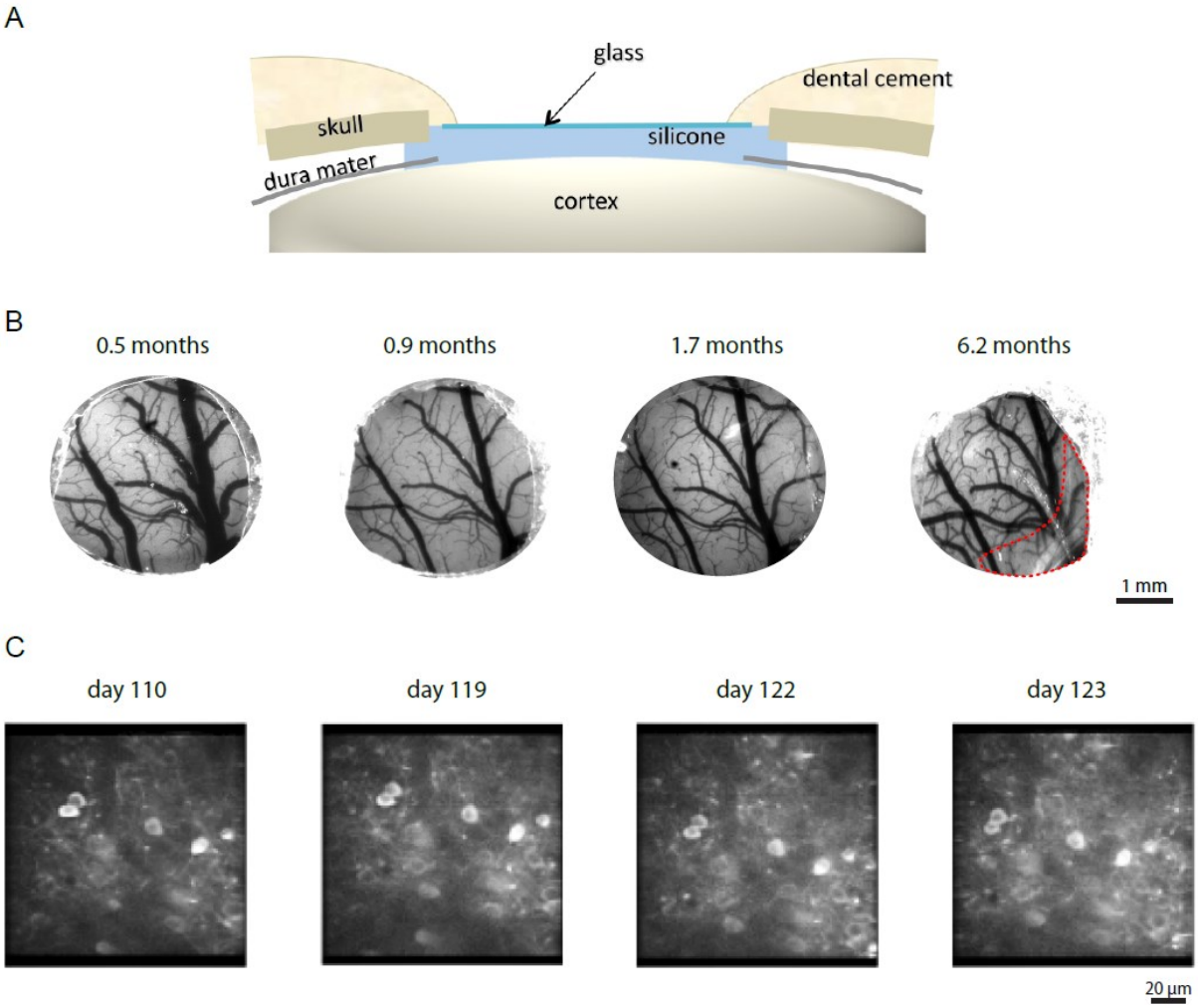


**Figure S 8. Long-term stability of the cranial window and the genetically encoded fluorescent calcium indicator.**

**(A)** Schematic of the cranial window with durectomy. **(B)** Images taken through the cranial window at 570-nm illumination 0.5, 0.9, 1.7 and 6.2 months after implantation (left to right). Red dashed line indicates a region where dura regrowth was visible. **(C)** Two-photon images of infected neurons expressing YC3.60 in the left cortical hemisphere at a depth of 175 µm from the brain surface. Images were taken 3.6, 3.9, 4 and 4.03 months after injection of the virus carrying YC3.60 (left to right). The cranial window was implanted two months after virus injection.

## 10.2 Supplemental Experimental Procedures

*Headpost implantation, virus injection and cranial window implantation*

The animals were anesthetized with isoflurane (1–3%; Abbott, USA). The depth of anesthesia was checked on the basis of hind paw withdrawal and corneal reflexes. The animal's temperature was maintained at 37°C by a feedback controlled heating pad in combination with a rectal temperature probe (Harvard Apparatus, Holliston, USA). To protect the eyes from desiccation an ointment was applied (vitamin A eye cream; Bausch & Lomb, Switzerland). A stereotaxic apparatus was used to fix the animal. Once the skull was cleaned, it was moistened with water based gel (Ultrasonic gel, Skintact, Leonhard Lang GmbH, Austria) and window was placed at the estimated region of the barrel cortex (1 mm caudal and 3 mm lateral from Bregma) to perform IOI. After functionally identifying the barrel cortex a bonding agent (Gluma Comfort Bond; Heraeus Kulzer, Germany) was applied to the cleaned skull and polymerized (blue light, 600 mW/cm$^2$; Demetron LC, Switzerland. On top of the bonding layer several layers of transparent light-curing dental cement (Tetric EvoFlow; Ivoclar Vivadent AG, Liechtenstein) were put to sculpt the headcap. The area of the left barrel cortex was spared for the later virus injection and window implantation. A custom-made aluminum headpost was attached (2 mm caudal to lambda) with additional dental cement. After washing the wound with saline, an antibiotic ointment was applied (Cicatrex; Janssen-Cilag AG, Switzerland). The open skin was sutured and attached to the implant with acrylic glue (Histoacryl, B. Braun, Germany). In a second surgery a craniotomy above the left barrel cortex was done (approx. 4x4 mm). Virus was injected through thin glass pipettes (Cetin et al., 2007) to the principal whisker area identified by IOI. 150 nl of rAAV hybrid serotype 2/1 (40 nl/min) carrying the Yellow Cameleon 3.60 (YC3.60, under human synapsin promoter) construct diluted 1:2 with Mannitol (Mannitol 20%, B. Braun, Switzerland) was injected at 300 µm depth below the dura mater. A square cover slip (3x3 mm, UQG Optics Ltd, UK) was lightly pressed on the exposed brain and fixed with dental cement to the headcap. After surgeries the animals were kept warm and provided with analgesics (Novaminsulfon; 50%; Sintetica, Switzerland). In the first week of recovery an antibiotic was added to the drinking water (Baytril (enrofloxacin); 200 mg/l drinking water; Bayer, Germany).

*Two-photon imaging settings*

A 20x water immersion microscope objective was used (W Plan-Apochromat 20x/1,0 DIC VIS-IR, Zeiss, Germany). The genetically encoded $Ca^{2+}$ indicator YC3.60 was excited with a Ti:sapphire laser (870 nm, 140-fs pulses at 80 MHz, Chameleon Ultra II; Coherent, USA). Emission of YC3.60 was detected with two GaAsP photomultipliers (H10770PA-40; Hamamatsu Photonics, Japan) with the following filters settings: dichroic mirror 515 DCXR, band pass filter BrightLine HC 542/50 (yellow channel), band pass filter BrightLine HC 475/64 (cyan channel) (Semrock, Rochester, USA) and short pass filters BrightLine 750/sp for each channel. The two-photon laser-scanning microscope was controlled by a custom-written LabVIEW software (Langer et al., 2013) or Scanimage (Pologruto et al., 2003).

*Awake two-photon imaging*

Mice were habituated to head-fixation before awake imaging was performed. Animals were repeatedly head-fixed in 3 - 4 sessions a day for time spans lasting from a few minutes up to 30 minutes. As soon as mice tolerated the head-fixed situation for as long as 30 minutes two-photon imaging was performed. The same setup and stimulus paradigm as for the anaesthetized experiments was used.

*Analysis of awake imaging data*

Movies containing z-motion and strong distortions due to fast xy-motion induced by the movement of the animal were not included in the subsequent data analysis using the following criteria (~5.4% of all trials). To ensure the presence of the individual cells across trials, the correlation value between the individual ROIs and the respective ROIs of a high-resolution image (e.g. 256×256 pixels) of each imaging area had to be larger than a certain correlation threshold. This threshold computed as follows: the correlation value of each ROI in each frame of the individual trial movies had to be larger than the median correlation value minus two times the standard deviation (SD) of the correlation value of all trials within a session. All correlation thresholds were computed for each imaging session separately.

# 11 Publications

## 11.1 During PhD

**Mayrhofer JM***, Skreb V*, von der Behrens W, Musall S, Weber B, Haiss F. Novel two-alternative forced choice paradigm for bilateral vibrotactile whisker frequency discrimination in head-fixed mice and rats, J Neurophysiol. 2013 January

**Mayrhofer JM**, Haiss F, Helmchen F, Weber B. Sparse, reliable and persistent frequency representation in the mouse barrel cortex, in preparation

Haiss F*, **Mayrhofer JM***, Scheidegger M*, Olini N, Margolis DJ, Langer D, Kügler S, Hasan MT, Helmchen F, Weber B. Two-photon calcium imaging of neuronal population activity during complex discriminative behavior in the head-fixed rat, in preparation

## 11.2 Before PhD

Zillich RE, **Mayrhofer JM**, Chin SA. Extrapolated high-order propagators for path integral Monte Carlo simulations, J Chem Phys. 2010 January

**Mayrhofer JM**. Condensate fraction of liquid helium-4 droplets, Diploma thesis, JKU Linz, Supervisors: Prof. Dr. Eckhard Krotscheck, Dr. Robert E. Zillich. 2008

# 12 Talks and poster presentations

## 12.1 Talks

Bilateral vibrotactile whisker frequency processing in rodents: behavior and neuronal population coding in somatosensory cortex, Synapses and Circuits Seminar, EPFL, Lausanne, March 2013

Long term two-photon calcium imaging during complex behavior in the head-fixed rat, ZNZ Symposium, Zürich, September 2010

A barrel full of magic potion, INI / HIFO Symposium, Zürich, July 2010

Neuronal response of the awake behaving rat during decision making, Brain-i-Nets kick-off-meeting, Graz, February 2010

## 12.2 Poster presentations

**Mayrhofer J**, von der Behrens W, Musall S, Helmchen F., Haiss F, Weber B (2013) Long-term bilateral vibrotactile whisker frequency representation in neuronal populations of the mouse somatosensory cortex, SfN meeting, San Diego, USA

**Mayrhofer J**, Skreb V, von der Behrens W, Musall S, Kügler S, Haiss F, Weber B (2012) Bilateral vibrotactile whisker frequency discrimination in head-fixed mice and rats: behavior, psychophysical performance and two-photon imaging of neuronal ensembles, FENS meeting, Barcelona, Spain

**Mayrhofer J**, Haiss F, Margolis D, Hasan MT, Kügler S, Helmchen F, Weber B (2010) Long term repeated two-photon calcium imaging during complex discriminative behavior in barrel cortex of the head fixed rat, SfN meeting, San Diego, USA

**Mayrhofer J**, Haiss F, Margolis D, Hasan MT, Kügler S, Helmchen F, Weber B (2010) Two-photon calcium imaging during complex discriminative behavior in barrel cortex of the

head fixed rat, Summer school on cognition and action: systems neuroscience approaches to understanding complex behavior, Dubrovnik, Croatia

**Mayrhofer J**, Haiss F, Weber B (2010) Tactile frequency discrimination in the head fixed rat performing a two alternative forced choice task, SSN meeting, Lausanne

**Mayrhofer J**, Haiss F, Margolis D, Hasan MT, Helmchen F, Weber B (2009) Neuronal response of the awake, behaving rat during decision making, ZNZ meeting, Zürich

# 13 Curriculum Vitae

**Personal Details**

**Name:** Johannes Maria Mayrhofer

**Place & Date of birth:** Linz, Austria, 2nd of February, 1983

**Citizenship:** Austrian

**Education**

| | |
|---|---|
| Since 03/2009 | PhD program in neuroscience at University of Zürich, Switzerland; Supervisor: Prof. Bruno Weber; Steering committee: Prof. Fritjof Helmchen, Prof. Richard Hahnloser |
| 08/2008 - 01/2009 | Research assistant at department for theoretical physics, Johannes Kepler University of Linz, Austria |
| 10/2002 - 07/2008 | Diploma in technical physics at the Johannes Kepler University of Linz, Austria; Diploma thesis: Condensate Fraction of Liquid Helium-4 Droplets; Supervisor: Prof. Dr. Eckhard Krotscheck, Dr. Robert E. Zillich |
| 01/2006 - 07/2006 | Exchange stay (Erasmus) in Lancaster, England |
| 06/2002 | Matura in mechanical engineering at HTL2 Linz (Linzer Technikum) in Linz, Austria |

# 14 Danksagung

An erster Stelle möchte ich ganz herzlich Bruno Weber danken. Er gab mir die Möglichkeit in seiner Arbeitsgruppe in einem spannenden Forschungsgebiet mitzuarbeiten und unterstützte mich dabei während meiner gesamten Doktorarbeit. Ein besonderer Dank gilt auch Florent Haiss, welcher mich vor allem zu Beginn meiner Doktorates tatkräftig unterstützte.

Vielmals danken möchte ich auch meinen Kollegen Wolfger von der Behrens, Renaud Jolivet, Matthias Wyss, Simon Musall, Novella Calcinaghi, Anand Singh, Vida Skreb, Phillip Mächler und Jill Stobart, welche mich mit Rat und Tat unterstützten und für ein gutes Arbeitsklima sorgten.

Für die spannenden Diskussionen und Anregungen möchte ich Wolfger von der Behrens und Simon Musall im Speziellen danken. Zusätzlich möchte ich Wolfger von der Behrens wie auch Jill Stobart für das Korrekturlesen meiner Doktorarbeit vielmals danken.

Natürlich möchte ich auch dem Promotionskomitee Fritjof Helmchen, Bruno Weber und Richard Hahnloser danken.

Ein grosser Dank gebührt auch Stefan Weber und Markus Küpfer, welche mir mit ihrem technischen Wissen und Können zur Verfügung standen.

Besonderen Dank gebührt meiner Familie und meinen Freunden, die mir immer einen willkommenen Ausgleich schenkten und mich dadurch mit neuer Energie an meiner Doktorarbeit weitermachen liessen. Ein grosses Merci gilt dabei Sandra Wipf, die mich mit ihrer Liebe und ihrem Zuspruch in den schwierigen Phasen meines Doktorats ganz besonders unterstützte.